

REPORT NUMBER 163

NOVEMBER 1965

PRELIMINARY FLUTTER ANALYSIS

VOLUME II EMPENNAGE

XV-5A

LIFT FAN FLIGHT RESEARCH AIRCRAFT PROGRAM

CONTRACT NUMBER DA44-177-TC-715

GENERAL  ELECTRIC

163 3000

NASA Scientific and Technical Information Facility

operated for the National Aeronautics and Space Administration by Documentation Incorporated

Post Office Box 33
College Park, Md. 20740

Telephone | Area Code 301
779-2121

FACILITY CONTROL NO. 32904

DATE 5/31/66

ATTACHED IS A DOCUMENT ON LOAN

FROM: NASA Scientific and Technical Information Facility

TO: Defense Documentation Center
Attn: DDC-IRC (Control Branch)
Cameron Station
Alexandria, Va. 22314

In accordance with the NASA-DOD Cooperative AD Number Assignment Agreement it is requested that an AD number be assigned to the attached report.

As this is our only available copy the return of the document (with AD number and any applicable distribution limitations) to the address below is essential.

This document may be retained by DDC. If retained, please indicate AD number and any applicable distribution limitations on the reproduced copy of the title page and return to the address below.

Return Address: NASA Scientific and Technical Information Facility
Attention: INPUT BRANCH
P. O. Box 33
College Park, Maryland 20740

Report Number 163

**PRELIMINARY FLUTTER ANALYSIS
VOLUME II - EMPENNAGE**

**XV-5A Lift Fan
Flight Research Aircraft
Contract DA 44-177-TC-715**

December 1965

**ADVANCED ENGINE & TECHNOLOGY DEPARTMENT
GENERAL ELECTRIC COMPANY
CINCINNATI, OHIO 45215**

ACCESSION for	
CFSTI	WHITE SECTION <input checked="" type="checkbox"/>
DDC	DIFF SECTION <input type="checkbox"/>
UNCLASSIFIED	<input type="checkbox"/>
CLASSIFICATION	
Y	
DISTRIBUTION/AVAILABILITY CODES	
DIST.	AVAIL. and/or SPECIAL
1	

OK for CFSTI per telecon Mr. Spooner 1 June 66 *made*

32904

DDC
 JUN 1 1966
 E W

CONTENTS

SECTION	PAGE
1.0 SUMMARY	1
2.0 INTRODUCTION	3
3.0 METHOD OF APPROACH	5
3.1 Lagrange's Equations of Motion	5
3.1.1 Generalized Mass Matrix	7
3.1.2 Generalized Stiffness Matrix	18
3.1.3 Generalized Aerodynamic Matrix	20
3.2 Symmetric Flutter Analysis	26
3.2.1 Cantilevered	26
3.2.1.1 Generalized Mass Matrix	26
3.2.1.2 Generalized Aerodynamic Matrix	27
3.2.2 Free-Free	28
3.2.2.1 Generalized Mass Matrix	28
3.2.2.2 Generalized Aerodynamic Matrix	30
3.3 Antisymmetric Flutter Analysis	30
3.3.1 Cantilevered	30
3.3.1.1 Generalized Mass Matrix	31
3.3.1.2 Generalized Aerodynamic Matrix	32
3.3.2 Free-Free	32
3.3.2.1 Modal Coupling	33
3.3.2.2 Flutter Analysis	36

CONTENTS (Continued)

SECTION	PAGE
4.0 DISCUSSION AND RESULTS	39
4.1 Idealization of Aircraft	39
4.1.1 Structural Representation	39
4.1.1.1 Horizontal Stabilizer - Elevator	39
4.1.1.2 Vertical Stabilizer - Rudder	40
4.1.1.3 Fuselage	40
4.1.2 Aerodynamic Representation	40
4.1.2.1 Empennage	40
4.1.3 Mass Representation	41
4.1.3.1 Symmetric Analysis	41
4.1.3.2 Antisymmetric Analysis	41
4.2 Modal Functions	42
4.2.1 Symmetric Analysis	42
4.2.1.1 Cantilevered	42
4.2.1.2 Free-Free	42
4.2.2 Antisymmetric Analysis	42
4.2.2.1 Cantilevered	43
4.2.2.2 Free-Free	43
4.3 Flutter Analysis	43
4.3.1 Symmetric	44
4.3.1.1 Cantilevered Analysis	44
4.3.1.2 Free-Free Analysis	46
4.3.2 Antisymmetric	46
4.3.2.1 Cantilevered Analysis	46
4.3.2.2 Free-Free Analysis	47

CONTENTS (Continued)

SECTION	PAGE
5.0 CONCLUSIONS	
5.1 Symmetric Analysis - Cantilevered Condition	49
5.2 Symmetric Analysis - Free-Free Condition	50
5.3 Antisymmetric Analysis - Cantilevered Condition	51
5.4 Antisymmetric Analysis - Free-Free Condition	51
5.5 Overall Evaluation	51
6.0 APPENDIX	
6.1 List of References	53
6.2 Tables	54
6.3 Figures 6 through 69	65

LIST OF FIGURES

FIGURE		PAGE
1	i^{th} Section - Lifting Surface	7
2	Elastic Axis Coordinate System	10
3	Control Surface Coordinate System	15
4	i^{th} Strip Aerodynamic Simulation	21
5	Plot of Function G	24
6	Planform Horizontal Tail	65
7	Planform Vertical Tail	66
8	Stiffness Distribution - Horizontal Stabilizer	67
9	Stiffness Distribution - Vertical Stabilizer	68
10	Stiffness Distribution - Fuselage	68
11	Mode Shapes - Horizontal Stabilizer - Symmetric Analysis (Mode 1 - $f = 29.5$ cps)	69
12	Mode Shapes - Horizontal Stabilizer - Symmetric Analysis (Mode 2 - $f = 91.4$ cps)	69
13	Mode Shapes - Horizontal Stabilizer - Symmetric Analysis (Mode 3 - $f = 110.9$ cps)	70
14	Mode Shapes - Fuselage - Symmetric Analysis (Mode 1, $f = 8.2$ cps - Mode 2, $f = 15.2$ cps)	70
15	Mode Shapes - Fuselage - Symmetric Analysis (Mode 3, $f = 23.2$ cps - Mode 4, $f = 33.0$ cps)	71
16	Mode Shapes - Horizontal Stabilizer - Antisymmetric Analysis (Mode 1 - $f = 29.4$ cps)	71
17	Mode Shapes - Horizontal Stabilizer - Antisymmetric Analysis (Mode 2 - $f = 90.2$ cps)	72
18	Mode Shapes - Horizontal Stabilizer - Antisymmetric Analysis (Mode 3 - $f = 111.0$ cps)	72
19	Mode Shapes - Vertical Stabilizer - Antisymmetric Analysis (Mode 1 - $f = 10.7$ cps)	73
20	Mode Shapes - Vertical Stabilizer - Antisymmetric Analysis (Mode 2 - $f = 21.6$ cps)	73
21	Mode Shapes - Vertical Stabilizer - Antisymmetric Analysis (Mode 3 - $f = 27.9$ cps)	74
22	Mode Shapes - Fuselage - Antisymmetric Analysis (Mode 1, $f = 5.6$ cps - Mode 2, $f = 13.6$ cps)	74
23	Mode Shapes - Fuselage Antisymmetric Analysis (Mode 3, $f = 20.6$ cps - Mode 4, $f = 26.2$ cps)	75
24	Mode Shapes - Fuselage - Antisymmetric Analysis (Mode 1, $f = 13.9$ cps - Mode 2, $f = 19.0$ cps)	75

BLANK PAGE

25	Mode Shapes - Fuselage - Antisymmetric Analysis (Mode 3, f = 29.0 cps - Mode 4, f = 51.9 cps)	76
26	Symmetric Analysis - Cantilevered Condition	77
27	Symmetric Analysis - Cantilevered Condition	78
28	Symmetric Analysis - Cantilevered Condition	79
29	Symmetric Analysis - Cantilevered Condition	80
30	Symmetric Analysis - Cantilevered Condition	81
31	Symmetric Analysis - Cantilevered Condition	82
32	Symmetric Analysis - Cantilevered Condition	83
33	Symmetric Analysis - Cantilevered Condition	84
34	Symmetric Analysis - Cantilevered Condition	85
35	Symmetric Analysis - Cantilevered Condition	86
36	Symmetric Analysis - Cantilevered Condition	87
37	Symmetric Analysis - Cantilevered Condition	88
38	Symmetric Analysis - Cantilevered Condition	89
39	Symmetric Analysis - Cantilevered Condition	90
40	Symmetric Analysis - Cantilevered Condition	91
41	Symmetric Analysis - Cantilevered Condition	92
42	Symmetric Analysis - Cantilevered Condition	93
43	Symmetric Analysis - Cantilevered Condition	94
44	Symmetric Analysis - Cantilevered Condition - Parameter Effects	95
45	Symmetric Analysis - Cantilevered Condition - Modal Coupling	96
46	Symmetric Analysis - Cantilevered Condition	97
47	Symmetric Analysis - Cantilevered Condition	98
48	Symmetric Analysis - Cantilevered Condition	99
49	Symmetric Analysis - Cantilevered Condition	100
50	Symmetric Analysis - Cantilevered Condition	101
51	Symmetric Analysis - Cantilevered Condition	102
52	Symmetric Analysis - Cantilevered Condition	103
53	Symmetric Analysis - Cantilevered Condition	104
54	Symmetric Analysis - Cantilevered Condition	105
55	Symmetric Analysis - Cantilevered Condition	106
56	Symmetric Analysis - Cantilevered Condition	107
57	Symmetric Analysis - Cantilevered Condition	108
58	Symmetric Analysis - Cantilevered Condition - Mach Number Effects	109
59	Symmetric Analysis - Free-Free Condition	110
60	Symmetric Analysis - Free-Free Condition	111
61	Symmetric Analysis - Free-Free Condition	112
62	Symmetric Analysis - Free-Free Condition	113
63	Symmetric Analysis - Free-Free Condition	114
64	Symmetric Analysis - Free-Free Condition	115

65	Symmetric Analysis - Free-Free Condition - Parameter Effects	116
66	Antisymmetric Analysis - Cantilevered Condition	117
67	Antisymmetric Analysis - Cantilevered Condition	118
68	Antisymmetric Analysis - Free-Free Condition	119
69	Antisymmetric Analysis - Free-Free Condition	120

TABLES

TABLE		PAGE
1	Mass and Inertia Distribution - Horizontal Tail ~Symmetric Analysis	54
2	Mass and Inertia Distribution - Fuselage ~ Symmetric Analysis	55
3	Mass and Inertia Distribution - Horizontal Tail ~ Antisymmetric Analysis	56
4	Mass and Inertia Distribution - Vertical Tail ~ Antisymmetric Analysis	57
5	Mass and Inertia Distribution - Fuselage ~ Antisymmetric Analysis	58
6	Modal Data - Horizontal Stabilizer ~ Symmetric Analysis	60
7	Modal Data - Fuselage ~ Symmetric Analysis	61
8	Modal Data - Horizontal Stabilizer ~ Antisymmetric Analysis	62
9	Modal Data - Vertical Stabilizer ~ Antisymmetric Analysis	63
10	Modal Data - Fuselage ~ Antisymmetric Analysis	64

SYMBOLS AND AXES

SYMBOLS

T	-	Kinetic Energy
U	-	Potential Energy
D	-	Dissipation Function
Q	-	Generalized force
q	-	Generalized coordinate
t	-	Time
g	-	Structural damping coefficient
ω	-	Frequency of oscillation - radians per second
f	-	Frequency of oscillation - cycles per second
i	-	Imaginary number, $\sqrt{-1}$
Ω	-	Eigenvalue, $\frac{1}{\omega^2} (1 + ig)$; $1/\omega^2$
$\delta_X, \delta_Y, \delta_Z$	-	Deflection in the X, Y, Z directions
$\bar{\delta}_X, \bar{\delta}_Y, \bar{\delta}_Z$	-	Angular deflections about the X, Y, Z axes
$\bar{\delta}_u, \bar{\delta}_v, \bar{\delta}_w$	-	Angular deflections about the u, v, w axes
u, v, w	-	Total deflection in the X, Y, Z directions respectively
dm	-	Element of mass
m	-	Mass
S	-	Mass-unbalance about an appropriate axis
I	-	Mass inertia about an appropriate axis
P	-	Mass product of inertia about appropriate axes

SYMBOLS AND AXES (Continued)

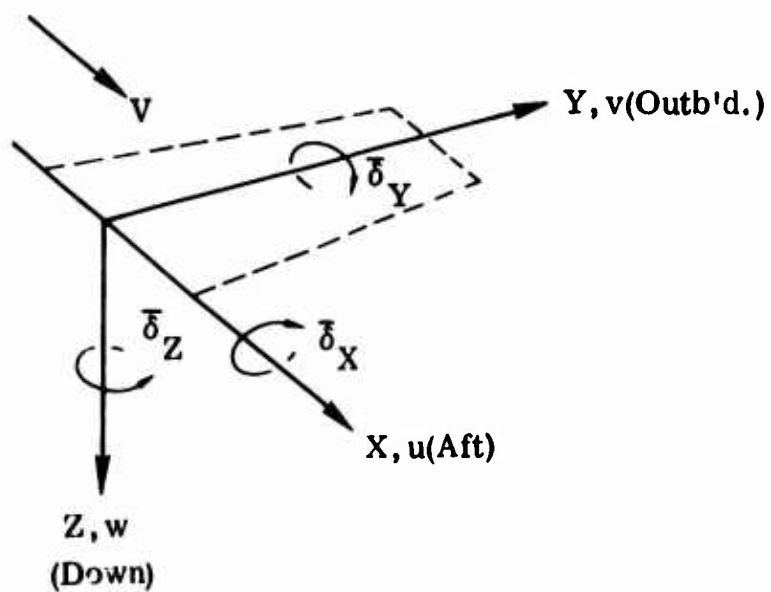
$\psi_{e.a.}$	- Sweep back angle of the elastic-axis
ψ_{H_L}	- Sweep back angle of the control surface hinge-line
$\psi_{c/4}$	- Sweep back angle of the quarter-chord
ϕ_{ij}	- Element of the ϕ matrix; column matrices relating displacements $\delta_X, \delta_Y, \delta_Z$, etc. to the j^{th} generalized coordinate
L'	- Aerodynamic lift
M'	- Aerodynamic moment
T'	- Aerodynamic hinge-moment
b	- Half-chord
h	- Displacement of quarter-chord point
α	- Angular rotation of the surface about a line parallel to the Y-axis through quarter-chord point
β	- Angular rotation of the control surface about a line parallel to the Y-axis through the control surface hinge-line, measured relative to the basic surface
ρ	- Atmospheric density
$L_{hh}, L_{h\alpha}$, etc.	- Oscillatory coefficients
δW	- Virtual work
$\delta \frac{h}{b}, \delta \alpha, \delta \beta, \delta q$	- Virtual displacement
l	- Semi-span
F_F	- Finite-span factor
a	- Streamwise distance from quarter-chord to elastic-axis
H.T.	- Horizontal Tail

SYMBOLS AND AXES (Continued)

V.T.	-	Vertical Tail
F	-	Fuselage
φ	-	Normalized bending displacement
θ	-	Normalized torsional displacement
EI	-	Bending stiffness
GJ	-	Torsional stiffness
AG	-	Shear effects
<u>M</u>	-	Generalized mass matrix
<u>K</u>	-	Generalized stiffness matrix
<u>A</u>	-	Generalized aerodynamic matrix
<u>J</u>	-	Mass matrix
<u>δ</u>	-	Displacement matrix
<u>Δ</u>	-	Total displacement matrix
<u>B</u>	-	Matrix of arbitrary distances along X, Y, Z axes
<u>T</u>	-	Transformation matrix defined by Equation 15.0
<u>φ</u>	-	Generalized displacement matrix
<u>K</u>	-	Stiffness influence coefficient matrix
<u>F</u>	-	Force matrix
<u>$T^{(1)}$</u> , <u>$T^{(2)}$</u>	-	Transformation matrices for aerodynamic purposes - Equations 37.0 and 38.0

AXES

SYMBOLS AND AXIS (Continued)



1.0 SUMMARY

The overall preliminary theoretical flutter analysis of the Ryan XV-5A Lift Fan Aircraft is presented in three volumes. This is Volume II, which reports the investigation of the flutter characteristics of the empennage. Volumes I and III detail the analysis of the wing and control surfaces, respectively.

Results of the empennage flutter analysis indicate a possible flutter situation existing within the design flight envelope of the XV-5A aircraft. The flutter mode is characterized by horizontal tail pitch coupled with basically symmetric horizontal tail bending for low values of pitch frequencies (40 cps) and for pitch coupled with horizontal tail torsion at pitch frequencies greater than 40 cps. The required pitch frequency would be of the order of approximately 55 cps for a flutter velocity margin of 15% of the design limit dive speed at sea-level, which is the critical altitude. Establishment of the actual pitch frequency through experimental methods is required for definite determination of flutter margins. The analyses presented in this report should be taken as a preliminary evaluation of the empennage of the XV-5A aircraft. Subsequent analytical and experimental investigations should then be directed toward finalization of the actual flutter characteristics of the XV-5A aircraft, with due regard for the findings of the studies presented in this report.

2.0 INTRODUCTION

This report presents the results of the preliminary empennage flutter analysis of the U. S. Army XV-5A Lift Fan Research Aircraft, illustrated in Figure 1.0 of Reference 1. The XV-5A is a V/STOL aircraft designed for research flight testing of the General Electric X-353-S Lift Fan Propulsion System.

The XV-5A aircraft is characterized by the existence of a T-tail with manual type, conventional aerodynamic control surfaces (elevator and rudder). Such tails are prone to exhibit flutter instabilities, unless extreme care is taken during the design stages to insure a flutter-free structure. Further difficulties are presented due to the fact that the horizontal tail is pivoted to provide for longitudinal trim and is powered by an irreversible jackscrew with power applied to the jackscrew through hydraulic circuits.

The analysis of the empennage was facilitated by the use of simple beam idealization of the horizontal and vertical stabilizers and fuselage. Aerodynamic representation was accomplished through the use of two-dimensional strip theory. Parametric investigations of important items such as the horizontal tail pitch frequency, elevator and rudder rotational frequency, and horizontal tail rigid body yaw and roll were carried out for establishment of critical areas.

3.0 METHOD OF APPROACH

The method of approach followed in the flutter analysis of the empennage is that of the Rayleigh-Ritz approach, or what might be termed the modal approach to the flutter problem. In this approach the equations of motion are formulated in terms of carefully chosen modal functions. The modal functions chosen to represent the deformation of the structure are the calculated normal modes of vibration of the particular component, i.e., horizontal and vertical stabilizers and fuselage.

3.1 LAGRANGE'S EQUATIONS OF MOTION

In applying the modal approach to the flutter problem, Lagrange's equations of motion are convenient for obtaining the equations of motion necessary for a flutter solution. In general, Lagrange's equations may be expressed as,

$$\frac{d}{dt} \frac{\partial T}{\partial \dot{q}_j} + \frac{\partial U}{\partial q_j} + \frac{\partial D}{\partial \dot{q}_j} = Q_j \quad (1)$$

where:

\dot{q}_j is the j^{th} generalized coordinate

T is the kinetic energy of the system

U is the potential energy (internal strain energy) of the system

D is a dissipation function and is composed of damping forces in the structure

Q_j is the generalized force applied to the system in the j^{th} coordinate.

The kinetic energy expression T may be written as,

$$T = \frac{1}{2} \dot{\underline{q}}' \underline{M} \dot{\underline{q}} \quad (2)$$

where \underline{M} is termed the generalized mass matrix and is composed of terms which are products of the lumped masses and/or mass-inertias and the chosen modal functions.

The potential energy expression U may be written as

$$U = \frac{1}{2} \underline{q}' \bar{\underline{K}} \underline{q} \quad (3)$$

where $\bar{\underline{K}}$ is termed the generalized stiffness matrix and is composed of terms which are products of the frequency of oscillation squared of a particular mode and its appropriate generalized mass.

The dissipation function D is due to the damping forces acting in the structure. These may be considered as forces in phase with the velocity and proportional to the restoring forces acting in the structure. Therefore,

$$D = - \frac{g}{2\omega} \dot{\underline{q}}' \bar{\underline{K}} \dot{\underline{q}} \quad (4)$$

where g is the coefficient of structural damping and ω is the frequency of oscillation.

The generalized force Q_j is due to the oscillatory aerodynamics acting on the structure and, for all force components j , Q_j may be written as,

$$\underline{Q} = \omega^2 \underline{A} \underline{q} \quad (5)$$

where \underline{A} is called the generalized aerodynamic matrix.

Applying Equation 1 to Equations 2, 3, 4, and 5, and assuming harmonic motion ($\underline{q} = \underline{q}_0 e^{i\omega t}$), the equations of motion for a flutter solution are,

$$-\omega^2 \underline{M} \underline{q} + \bar{\underline{K}} \underline{q} + ig \bar{\underline{K}} \underline{q} = \omega^2 \underline{A} \underline{q}$$

or

$$\underline{M} \underline{q} - \frac{1}{\omega^2} \bar{\underline{K}} \underline{q} - \frac{ig}{\omega^2} \bar{\underline{K}} \underline{q} = - \underline{A} \underline{q}$$

Rearranging,

$$\left(\underline{M} + \underline{A} - \frac{1}{\omega^2} (1 + ig) \bar{\underline{K}} \right) \underline{q} = \underline{0}$$

or

$$(\underline{M} + \underline{A} - \Omega \underline{\bar{K}}) \underline{q} = \underline{o} \quad (6)$$

where $\Omega = 1/\omega^2 (1 + ig)$.

For a solution to exist, the determinant of the matrix of Equation 6 must be equal to zero, i. e.,

$$|\underline{M} + \underline{A} - \Omega \underline{\bar{K}}| = 0 \quad (7)$$

Solution of Equation 7 by standard means yields the required complex eigenvalues from which the flutter speed, frequency and damping values are determined.

3.1.1 Generalized Mass Matrix

This section is devoted to the derivation of the generalized mass matrix in a general sense to which particulars are applied in subsequent sections.

Assume a given element of mass dm , as shown in Figure 1, which represents a portion of the i^{th} section of a lifting surface. A rectangular cartesian coordinate system is fixed to the surface at point i , which represents a point on the elastic axis of the surface.

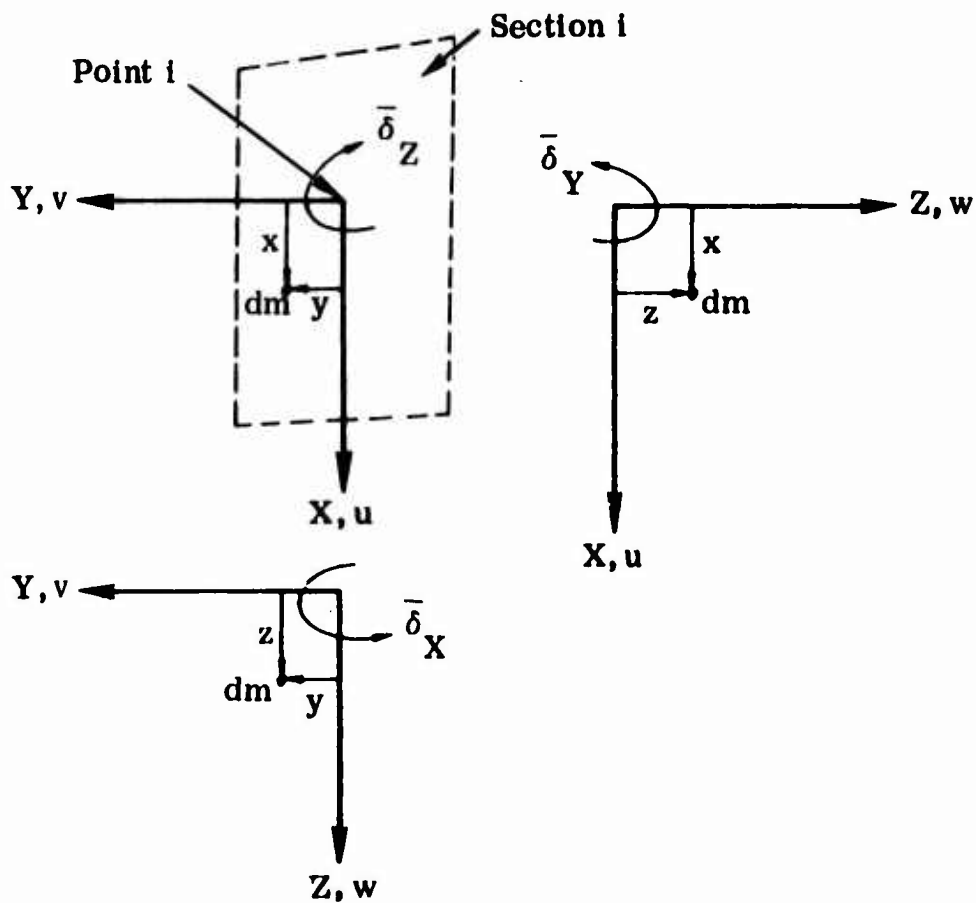


Figure 1 i^{th} Section - Lifting Surface

The displacement of the element dm , in terms of displacements of point i , may be written as,

$$u = \delta_X - \bar{\delta}_Y z - \bar{\delta}_Z y \quad (8)$$

$$v = \delta_Y - \bar{\delta}_X z + \bar{\delta}_Z x \quad (9)$$

$$w = \delta_Z + \bar{\delta}_X y + \bar{\delta}_Y x \quad (10)$$

Equations 8, 9, and 10 may be written in matrix form as

$$\begin{Bmatrix} u \\ v \\ w \end{Bmatrix} = \begin{bmatrix} 1.0 & 0 & 0 & 0 & -z & -y \\ 0 & 1.0 & 0 & -z & 0 & x \\ 0 & 0 & 1.0 & y & x & 0 \end{bmatrix} \begin{Bmatrix} \delta_X \\ \delta_Y \\ \delta_Z \\ \bar{\delta}_X \\ \bar{\delta}_Y \\ \bar{\delta}_Z \end{Bmatrix}$$

or

$$\underline{\Delta} = \underline{B} \underline{\delta}^{(1)} \quad (11)$$

The kinetic energy of the i^{th} section is

$$2T = \int_{\text{Section}} \underline{L} \begin{Bmatrix} \dot{u} \\ \dot{v} \\ \dot{w} \end{Bmatrix} dm \quad (12)$$

And by substituting Equation 11,

$$\begin{aligned} 2T &= \int_{\text{Section}} \underline{\delta}^{(1)'} \underline{B}' \underline{B} \underline{\delta}^{(1)} dm \\ &= \underline{\delta}^{(1)'} \int_{\text{Section}} \underline{B}' \underline{B} dm \underline{\delta}^{(1)} \end{aligned} \quad (13)$$

Multiplying out the matrix product $\underline{B}' \underline{B}$ yields,

$$\begin{bmatrix} 1.0 & 0 & 0 & 0 & -z & -y \\ 0 & 1.0 & 0 & -z & 0 & x \\ 0 & 0 & 1.0 & y & x & 0 \\ 0 & -z & y & y^2 + z^2 & xy & -xz \\ -z & 0 & x & xy & x^2 + z^2 & yz \\ -y & x & 0 & -xz & yz & x^2 + y^2 \end{bmatrix}$$

Therefore, the kinetic energy expression may be written as

$$2T = \underline{\dot{\delta}}^{(1)'} \int_{\text{Section}} \begin{bmatrix} 1.0 & 0 & 0 & 0 & -z & -y \\ 0 & 1.0 & 0 & -z & 0 & x \\ 0 & 0 & 1.0 & y & x & 0 \\ 0 & -z & y & y^2 + z^2 & xy & -xz \\ -z & 0 & x & xy & x^2 + z^2 & yz \\ -y & x & 0 & -xz & yz & x^2 + y^2 \end{bmatrix} dm \underline{\dot{\delta}}^{(1)}$$

Integrating over the i^{th} section results in the following expression for the kinetic energy of the lumped parameter system of the i^{th} section,

$$2T = \underline{\dot{\delta}}^{(1)'} \begin{bmatrix} m & 0 & 0 & 0 & -S_{YZ} & -S_{ZY} \\ 0 & m & 0 & -S_{XZ} & 0 & S_{ZX} \\ 0 & 0 & m & S_{XY} & S_{YX} & 0 \\ 0 & -S_{XZ} & S_{XY} & I_X & P_{XY} & -P_{XZ} \\ -S_{YZ} & 0 & S_{YX} & P_{XY} & I_Y & P_{YZ} \\ -S_{ZY} & S_{ZX} & 0 & -P_{XZ} & P_{YZ} & I_Z \end{bmatrix} \underline{\dot{\delta}}^{(1)}$$

or

$$2T = \underline{\dot{\delta}}^{(1)'} \underline{J}^{(1)} \underline{\dot{\delta}}^{(1)} \quad (14)$$

where

- m is the mass of section i lumped at station i
- I_X, I_Y, I_Z is the mass moment of inertia of section i about the X, Y, Z axes, respectively
- P_{XY}, P_{XZ}, P_{YZ} is the mass product of inertia of section i about the X - Y, X - $Z, and Y$ - Z axes, respectively
- S_{X_Y}, S_{X_Z} is the static mass moment of section i about the X -axis, with distances measured along the Y and Z axes, respectively
- S_{Y_X}, S_{Y_Z} is the static mass moment of section i about the Y -axis, with distances measured along the X and Z axes, respectively
- S_{Z_X}, S_{Z_Y} is the static mass moment of section i about the Z -axis, with distances measured along the X and Y axes, respectively.

Normally, the surface to be analyzed is swept; therefore a coordinate transformation is required, since the analysis is based upon elastic-axis displacements. Consider the coordinate system shown in Figure 2, where $\psi_{e.a.}$ is the sweep back angle of the elastic-axis of the surface.

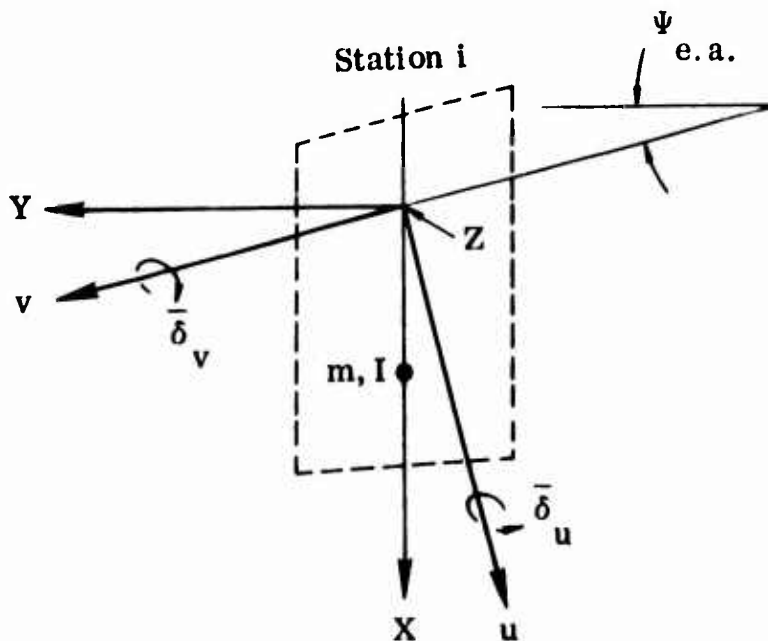


Figure 2 Elastic Axis Coordinate System

The displacements $\underline{\delta}^{(1)}$ given in Equation 14 may be written in terms of elastic-axis displacements as follows:

$$\begin{Bmatrix} \delta_X \\ \delta_Y \\ \delta_Z \\ \bar{\delta}_X \\ \bar{\delta}_Y \\ \bar{\delta}_Z \end{Bmatrix} = \begin{bmatrix} 1.0 & 0 & 0 & 0 & 0 & 0 \\ 0 & 1.0 & 0 & 0 & 0 & 0 \\ 0 & 0 & 1.0 & 0 & 0 & 0 \\ 0 & 0 & 0 & \cos \Psi_{e.a.} & -\sin \Psi_{e.a.} & 0 \\ 0 & 0 & 0 & \sin \Psi_{e.a.} & \cos \Psi_{e.a.} & 0 \\ 0 & 0 & 0 & 0 & 0 & 1.0 \end{bmatrix} \begin{Bmatrix} \delta_X \\ \delta_Y \\ \delta_Z \\ \bar{\delta}_u \\ \bar{\delta}_v \\ \bar{\delta}_Z \end{Bmatrix}$$

or

$$\underline{\delta}^{(1)} = \underline{T} \underline{\delta}^{(2)} \quad (15)$$

Substituting Equation 15 into Equation 14 and performing the required matrix multiplication,

$$2T = \underline{\delta}^{(2)'} \underline{T}' \underline{J}^{(1)} \underline{T} \underline{\delta}^{(2)}$$

or

$$2T = \underline{\delta}^{(2)'} \begin{bmatrix} m & 0 & 0 & -S_{YZ} \sin \psi_{e.a.} & -S_{YZ} \cos \psi_{e.a.} & -S_{ZY} \\ 0 & m & 0 & -S_{XZ} \cos \psi_{e.a.} & S_{XZ} \sin \psi_{e.a.} & S_{ZX} \\ & & & S_{XY} \cos \psi_{e.a.} & -S_{XY} \sin \psi_{e.a.} & \\ 0 & 0 & m & +S_{YX} \sin \psi_{e.a.} & +S_{YX} \cos \psi_{e.a.} & 0 \\ & & & S_{XY} \cos \psi_{e.a.} & I_X \cos^2 \psi_{e.a.} + I_Y \sin^2 \psi_{e.a.} & (I_Y - I_X) \cos \psi_{e.a.} \sin \psi_{e.a.} & -P_{XZ} \cos \psi_{e.a.} \\ -S_{YZ} \sin \psi_{e.a.} & -S_{XZ} \cos \psi_{e.a.} & +S_{YX} \sin \psi_{e.a.} & +2P_{XY} \sin \psi_{e.a.} \cos \psi_{e.a.} & +(\cos^2 \psi - \sin^2 \psi) P_{XY} & +P_{YZ} \sin \psi_{e.a.} \\ & & & -S_{XY} \sin \psi_{e.a.} & (I_Y - I_X) \cos \psi_{e.a.} \sin \psi_{e.a.} & I_X \sin^2 \psi_{e.a.} + I_Y \cos^2 \psi_{e.a.} & P_{XZ} \sin \psi_{e.a.} \\ -S_{YZ} \cos \psi_{e.a.} & S_{XZ} \sin \psi_{e.a.} & +S_{YX} \cos \psi_{e.a.} & +(\cos^2 \psi - \sin^2 \psi) P_{XY} & -2P_{XY} \sin \psi_{e.a.} \cos \psi_{e.a.} & +P_{YZ} \cos \psi_{e.a.} \\ & & & -P_{XZ} \cos \psi_{e.a.} & P_{XZ} \sin \psi_{e.a.} & \\ -S_{ZY} & S_{ZX} & 0 & +P_{YZ} \sin \psi_{e.a.} & +P_{YZ} \cos \psi_{e.a.} & I_Z \end{bmatrix} \underline{\delta}^{(2)} \quad (16)$$

Since

$$I_u = I_X \cos^2 \psi_{e.a.} + I_Y \sin^2 \psi_{e.a.} + 2 P_{XY} \sin \psi_{e.a.} \cos \psi_{e.a.}$$

$$I_v = I_X \sin^2 \psi_{e.a.} + I_Y \cos^2 \psi_{e.a.} - 2 P_{XY} \sin \psi_{e.a.} \cos \psi_{e.a.}$$

$$P_{uv} = (I_Y - I_X) \sin \psi_{e.a.} \cos \psi_{e.a.} + P_{XY} (\cos^2 \psi_{e.a.} - \sin^2 \psi_{e.a.})$$

$$S_u = S_{X_Y} \cos \psi_{e.a.} + S_{Y_X} \sin \psi_{e.a.}$$

$$S_v = S_{Y_X} \cos \psi_{e.a.} - S_{X_Y} \sin \psi_{e.a.}$$

Equation 16 may be written as

$$2T = \underline{\delta}^{(2)'} \left[\begin{array}{cccccc} m & 0 & 0 & -S_{Y_Z} \sin \psi_{e.a.} & -S_{Y_Z} \cos \psi_{e.a.} & -S_{Z_Y} \\ 0 & m & 0 & -S_{X_Z} \cos \psi_{e.a.} & S_{X_Z} \sin \psi_{e.a.} & S_{Z_X} \\ 0 & 0 & m & S_u & S_v & 0 \\ -S_{Y_Z} \sin \psi_{e.a.} & -S_{X_Z} \cos \psi_{e.a.} & S_u & I_u & P_{uv} & -P_{XZ} \cos \psi_{e.a.} \\ -S_{Y_Z} \cos \psi_{e.a.} & S_{X_Z} \sin \psi_{e.a.} & S_v & P_{uv} & I_v & +P_{YZ} \sin \psi_{e.a.} \\ -S_{Z_Y} & S_{Z_X} & 0 & -P_{XZ} \cos \psi_{e.a.} & P_{XZ} \sin \psi_{e.a.} & +P_{YZ} \cos \psi_{e.a.} \\ & & & +P_{YZ} \sin \psi_{e.a.} & +P_{YZ} \cos \psi_{e.a.} & I_Z \end{array} \right] \underline{\delta}^{(2)}$$

Since we are dealing with surfaces lying mainly in the X-Y plane (X-Z plane in the case of the vertical stabilizer), all distances in the Z direction are small compared to X and Y distances, and the mass properties involving these distances may therefore be set equal to zero.

Equation 17 therefore reduces to the following:

$$2T = \underline{\dot{\delta}}^{(2)'} \begin{bmatrix} m & 0 & 0 & 0 & 0 & -S_{Z_Y} \\ 0 & m & 0 & 0 & 0 & S_{Z_X} \\ 0 & 0 & m & S_u & S_v & 0 \\ 0 & 0 & S_u & I_u & P_{uv} & 0 \\ 0 & 0 & S_v & P_{uv} & I_v & 0 \\ -S_{Z_Y} & S_{Z_X} & 0 & 0 & 0 & I_Z \end{bmatrix} \underline{\dot{\delta}}^{(2)} \quad (18)$$

With the mass distribution taken as in Figure 2, i.e., streamwise strips, the following may be substituted for the static moment off-diagonal terms in Equation 18:

$$S_{Z_Y} = 0$$

$$S_{Z_X} = S_u \sin \psi_{e.a.} + S_v \cos \psi_{e.a.}$$

Equation 18 therefore takes the following form:

$$2T = \underline{\dot{\delta}}^{(2)'} \begin{bmatrix} m & 0 & 0 & 0 & 0 & 0 \\ 0 & m & 0 & 0 & 0 & S_u \sin \psi_{e.a.} \\ 0 & 0 & m & S_u & S_v & +S_v \cos \psi_{e.a.} \\ 0 & 0 & S_u & I_u & P_{uv} & 0 \\ 0 & 0 & S_v & P_{uv} & I_v & 0 \\ S_u \sin \psi_{e.a.} & +S_v \cos \psi_{e.a.} & 0 & 0 & 0 & I_Z \end{bmatrix} \underline{\dot{\delta}}^{(2)}$$

or

$$2T = \underline{\dot{\delta}}^{(2)'} \underline{J}^{(2)} \underline{\dot{\delta}}^{(2)} \quad (19)$$

For mass distributions taken perpendicular or nearly perpendicular to the elastic-axis, various terms of the mass matrix $\underline{J}^{(2)}$ take on the following values:

$$S_u = 0$$

$$P_{uv} = 0$$

$$S_{Z_Y} = -S_v \sin \Psi_{e.a.}$$

$$S_{Z_X} = S_v \cos \Psi_{e.a.}$$

Equation 18 therefore reduces to the following form:

$$2T = \underline{\dot{\delta}}^{(2)'} \begin{bmatrix} m & 0 & 0 & 0 & 0 & S_v \sin \Psi_{e.a.} \\ 0 & m & 0 & 0 & 0 & S_v \cos \Psi_{e.a.} \\ 0 & 0 & m & 0 & S_v & 0 \\ 0 & 0 & 0 & I_u & 0 & 0 \\ 0 & 0 & S_v & 0 & I_v & 0 \\ S_v \sin \Psi_{e.a.} & S_v \cos \Psi_{e.a.} & 0 & 0 & 0 & I_z \end{bmatrix} \underline{\dot{\delta}}^{(2)}$$

or

$$2T = \underline{\dot{\delta}}^{(2)'} \underline{J}^{(3)} \underline{\dot{\delta}}^{(2)} \quad (20)$$

Equations 19 and 20 are written for motion of the basic surface; for inclusion of control surface degrees of freedom, additional displacements must be included and the corresponding elements added to the mass matrix. (Mass and mass-inertia effects of a control surface are included in the basic surface terms of Equations 19 and 20, since, in effect, the control surface in a locked position is part of the basic surface.)

Let $\bar{\delta}_{w_c}$ be the angular deflection of the control surface about its hinge-line, relative to the basic surface as shown in Figure 3,

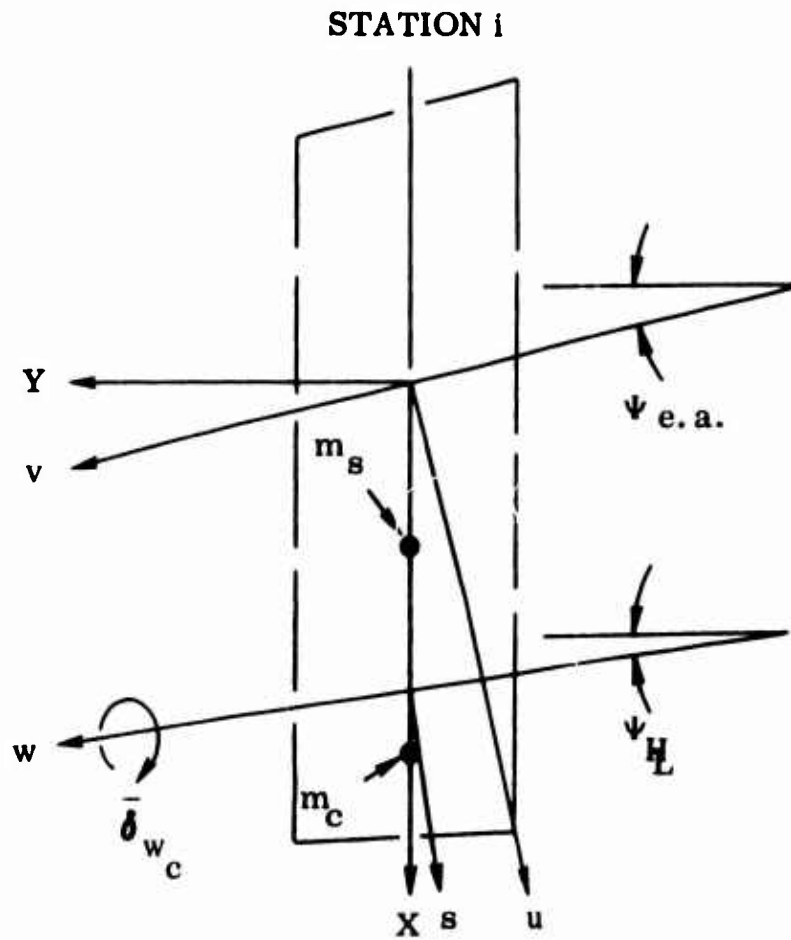


Figure 3 Control Surface Coordinate System

where the w -axis is the hinge-line of the control surface and is non-parallel to the elastic-axis as shown.

Upon including the control surface degree of freedom $\bar{\delta}_{w_c}$, Equation 19 takes the following form:

$$2T = \begin{bmatrix} \dot{\delta}_X & \dot{\delta}_Y & \dot{\delta}_Z & \dot{\delta}_u & \dot{\delta}_v & \dot{\delta}_Z & \dot{\delta}_{w_c} \end{bmatrix} \begin{bmatrix} m & 0 & 0 & 0 & 0 & 0 & 0 \\ 0 & m & 0 & 0 & 0 & S_u \sin \psi_{e.a.} + S_v \cos \psi_{e.a.} & 0 \\ 0 & 0 & m & S_u & S_v & 0 & S_{w_c} \\ 0 & 0 & S_u & I_u & P_{uv} & 0 & P_{uw_c} \\ 0 & 0 & S_v & P_{uv} & I_v & 0 & P_{vw_c} \\ S_u \sin \psi_{e.a.} & S_v \cos \psi_{e.a.} & 0 & 0 & 0 & I_Z & 0 \\ 0 & 0 & S_{w_c} & P_{uw_c} & P_{vw_c} & 0 & I_{w_c} \end{bmatrix} \begin{bmatrix} \dot{\delta}_X \\ \dot{\delta}_Y \\ \dot{\delta}_Z \\ \dot{\delta}_u \\ \dot{\delta}_v \\ \dot{\delta}_Z \\ \dot{\delta}_{w_c} \end{bmatrix}$$

or

$$2T = \underline{\dot{\delta}}^{(2)'} \underline{J}^{(2)} \underline{\dot{\delta}}^{(2)} \quad (21)$$

And Equation 20 becomes

$$2T = \begin{bmatrix} \dot{\delta}_X & \dot{\delta}_Y & \dot{\delta}_Z & \dot{\delta}_u & \dot{\delta}_v & \dot{\delta}_Z & \dot{\delta}_{w_c} \end{bmatrix} \begin{bmatrix} m & 0 & 0 & 0 & 0 & S_v \sin \psi_{e.a.} & 0 \\ 0 & m & 0 & 0 & 0 & S_v \cos \psi_{e.a.} & 0 \\ 0 & 0 & m & 0 & S_v & 0 & S_{w_c} \\ 0 & 0 & 0 & I_u & 0 & 0 & P_{uw_c} \\ 0 & 0 & S_v & 0 & I_v & 0 & P_{vw_c} \\ S_v \sin \psi_{e.a.} & S_v \cos \psi_{e.a.} & 0 & 0 & 0 & I_Z & 0 \\ 0 & 0 & S_{w_c} & P_{uw_c} & P_{vw_c} & 0 & I_{w_c} \end{bmatrix} \begin{bmatrix} \dot{\delta}_X \\ \dot{\delta}_Y \\ \dot{\delta}_Z \\ \dot{\delta}_u \\ \dot{\delta}_v \\ \dot{\delta}_Z \\ \dot{\delta}_{w_c} \end{bmatrix}$$

or

$$2T = \underline{\dot{\delta}}^{(2)'} \underline{J}^{(3)} \underline{\dot{\delta}}^{(2)} \quad (22)$$

where:

I_{w_c}

is the mass moment of inertia of the control surface portion of section i about the w axis (control surface hinge-line)

P_{uw_c} is the mass product of inertia of the control surface portion of section i about the u and w axes
 (= $I_{w_c} \sin \varphi + P_{sw_c} \cos \varphi + S_{w_c} l \sin \Psi_{e.a.}$)

P_{vw_c} is the mass product of inertia of the control surface portion of section i about the v and w axes
 (= $I_{w_c} \cos \varphi - P_{sw_c} \sin \varphi + S_{w_c} l \cos \Psi_{e.a.}$)

S_{w_c} is the static mass moment of the control surface portion of section i about the w axis (control surface hinge-line)

P_{sw_c} is the mass product of inertia of the control surface portion of section i about the s and w axes

$\varphi = \Psi_{e.a.} - \Psi_{H_L}$, where Ψ_{H_L} is the sweep back angle of the control surface hinge-line

l is the streamwise distance from the v-axis to the w-axis at station i

Having established the kinetic energy in terms of elastic axis deflections, we may now write these deflections in terms of generalized coordinates as

$$\underline{\delta}^{(2)} = \underline{\varphi} \underline{q} \quad (23)$$

where the φ 's are the chosen modal functions and the matrix φ may be termed the generalized displacement matrix.

Substituting Equation 23 into Equations 21 and 22 and summing over all the sections of the surface, the kinetic energy expression for the surface is then,

$$2T = \dot{\underline{q}}' \underline{\varphi}' \underline{J}^{(2)} \underline{\varphi} \dot{\underline{q}} = \dot{\underline{q}}' \underline{M} \dot{\underline{q}} \quad (24)$$

or

$$2T = \dot{\underline{q}}' \underline{\varphi}' \underline{J}^{(3)} \underline{\varphi} \dot{\underline{q}} = \dot{\underline{q}}' \underline{M} \dot{\underline{q}} \quad (25)$$

where the matrix \underline{M} is the generalized mass and the mass matrix \underline{J} takes the form as in Equation 21 or 22 but as diagonal matrices for each mass

parameter. The generalized displacement matrix $\underline{\varphi}$ is now of the following form,

$$\underline{\varphi} = \begin{bmatrix} \varphi_{11} & \text{-----} \varphi_{1j} & \text{-----} \varphi_{1n} \\ \varphi_{21} & & \\ \varphi_{31} & & \\ \varphi_{41} & & \\ \varphi_{51} & & \\ \varphi_{61} & & \\ \varphi_{71} & \text{-----} \varphi_{7j} & \text{-----} \varphi_{7n} \end{bmatrix}$$

where the φ_{ij} elements are column matrices relating the displacements of the elastic axis ($\delta_X, \delta_Y, \delta_Z$, etc.) to the "n" generalized coordinates.

3.1.2 Generalized Stiffness Matrix

In any linear elastic system, the forces acting may be related to the deflections by the following equation;

$$\underline{F} = \underline{K} \underline{\delta} \tag{26}$$

where the matrix \underline{K} is the stiffness influence coefficient matrix, an element of which yields the force at point i due to a unit deflection at point j.

The total internal strain energy of the system therefore may be written as

$$U = \frac{1}{2} \underline{\delta}' \underline{K} \underline{\delta} \tag{27}$$

Expressing these deflections in terms of generalized coordinates, as

$$\underline{\delta} = \underline{\varphi} \underline{q} \tag{28}$$

and substituting into Equation 27, we obtain an expression for the internal strain energy which is in terms of the generalized coordinates of the system:

$$\begin{aligned} U &= \frac{1}{2} \underline{q}' \underline{\varphi}' \underline{K} \underline{\varphi} \underline{q} \\ &= \frac{1}{2} \underline{q}' \underline{\bar{K}} \underline{q} \end{aligned} \quad (29)$$

where the matrix $\underline{\bar{K}}$ is the generalized stiffness matrix.

Equation 1, Section 3.1, states that there is one Lagrange's equation of free undamped vibration for each generalized coordinate ($j=1,2,3 \dots n$).

Therefore, for the j^{th} coordinate,

$$\frac{d}{dt} \frac{\partial T}{\partial \dot{q}_j} + \frac{\partial U}{\partial q_j} = Q_j \quad (30)$$

Applying Equation 30 to Equation 24, Paragraph 3.1.1, and Equation 29, Paragraph 3.1.2, results in the following: (For the generalized force Q_j equal to zero)

$$\begin{bmatrix} M_{j1} & M_{j2} & \dots & M_{jn} \end{bmatrix} \begin{Bmatrix} \ddot{q}_1 \\ \ddot{q}_2 \\ \vdots \\ \ddot{q}_n \end{Bmatrix} + \begin{bmatrix} K_{j1} & K_{j2} & \dots & K_{jn} \end{bmatrix} \begin{Bmatrix} q_1 \\ q_2 \\ \vdots \\ q_n \end{Bmatrix} = 0 \quad (31)$$

If we assume all coordinates except the j^{th} equal to zero, the system moves in one coordinate and has a natural frequency appropriate to that coordinate. This is usually called the uncoupled frequency of the j^{th} coordinate.

Therefore, Equation 31 reduces to

$$M_{jj} \ddot{q}_j + \bar{K}_{jj} q_j = 0 \quad (32)$$

If we assume harmonic motion in the system,

$$\ddot{q}_j = -\omega_j^2 q_j \quad (33)$$

Substituting Equation 33 into Equation 32,

$$-\omega_j^2 M_{jj} q_j + \bar{K}_{jj} q_j = 0$$

or

$$\left(\omega_j^2 M_{jj} - \bar{K}_{jj} \right) q_j = 0 \quad (34)$$

Since $q_j \neq 0$,

$$\bar{K}_{jj} = \omega_j^2 M_{jj} \quad (35)$$

And the generalized stiffness matrix $\bar{\mathbf{K}}$ reduces to the following diagonal form:

$$\bar{\mathbf{K}} = \begin{bmatrix} & & & \\ & & & \\ & & \omega_j^2 M_{jj} & \\ & & & \end{bmatrix}$$

Equation 35 shows that zero elastic coupling exists between the coordinates as is the case with uncoupled or orthogonal modes.

3.1.3 Generalized Aerodynamic Matrix

Consider the following displacements of the i^{th} strip shown in Figure 4 which represents a streamwise portion of the lifting surface as shown:

δ_X = Deflection of the elastic-axis in the X-direction

δ_Y = Deflection of the elastic-axis in the Y-direction

δ_Z = Deflection of the elastic-axis in the Z-direction

$\bar{\delta}_u$ = Angular rotation of the surface about the u-axis

$\bar{\delta}_v$ = Angular rotation of the surface about the v-axis

$\bar{\delta}_Z$ = Angular rotation of the surface about the Z-axis

$\bar{\delta}_{w_c}$ = Angular rotation of the control surface about the w-axis, relative to the basic surface

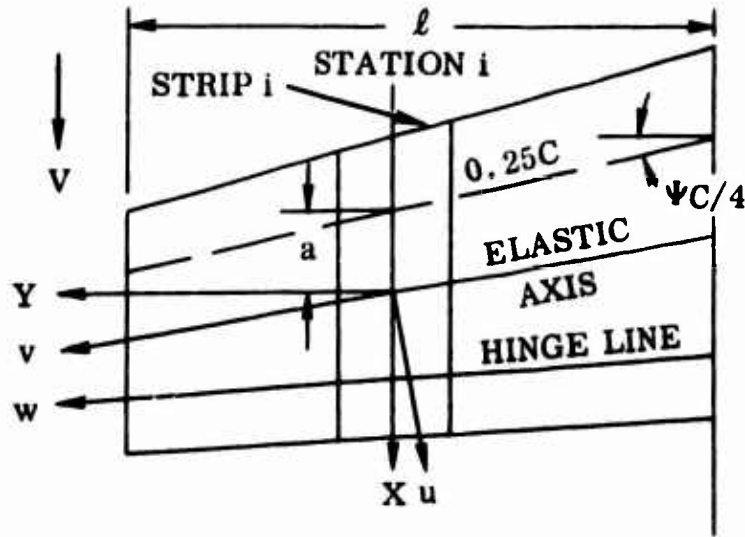


Figure 4 i^{th} Strip Aerodynamic Simulation

These displacements may be expressed in terms of the generalized coordinates as

$$\underline{\delta}^{(2)} = \underline{\varphi} \underline{q} \quad (36)$$

Now, since the above displacements represent displacements in terms of elastic-axis displacements, we may transform them so as to reflect displacements about axes perpendicular and parallel to the free stream through the i^{th} strip.

Let

δ_X = Deflection of the elastic-axis in the X direction

δ_Y = Deflection of the elastic-axis in the Y direction

δ_Z = Deflection of the elastic-axis in the Z direction

$\bar{\delta}_X$ = Angular rotation of the surface about the X-axis

$\bar{\delta}_Y$ = Angular rotation of the surface about the Y-axis

$\bar{\delta}_Z$ = Angular rotation of the surface about the Z-axis

$\bar{\delta}_{Y_c}$ = Angular rotation of the control surface about the Y-axis, relative to the basic surface

Therefore,

$$\underline{\delta}^{(1)} = \underline{T}^{(1)} \underline{\delta}^{(2)} \quad (37)$$

where the matrix \underline{T} is a transformation matrix relating displacements about the u, v axes to displacements about the X, Y axes through the same point.

Since the aerodynamic forces are written for quarter-chord displacements, a transformation of displacements from the elastic-axis to the quarter-chord is required. Accordingly, let

h = Vertical displacement of the quarter-chord point, plus positive down

α = Angular rotation of the surface about a line parallel to the Y-axis through the quarter-chord point, plus leading edge up

β = Angular rotation of the control surface about a line parallel to the Y-axis through the control surface hinge-line, relative to the basic surface, plus trailing edge down,

And the transformation is

$$\begin{pmatrix} h \\ \alpha \\ \beta \end{pmatrix} = \underline{T}^{(2)} \underline{\delta}^{(1)} \quad (38)$$

The aerodynamic forces acting per unit span are (utilizing two-dimensional aerodynamic oscillatory coefficients)

$$\begin{pmatrix} L' b \\ M' \\ T' \end{pmatrix} = \pi \rho \omega^2 b^4 \cos \Psi \frac{c}{4} \underline{\Delta} \begin{pmatrix} h/b \\ \alpha \\ \beta \end{pmatrix} \quad (39)$$

where the matrix $\underline{\Delta}$ contains the oscillatory coefficients as given in References 2 and 3, that is

$$\underline{\Delta} = \begin{bmatrix} L_{hh} & L_{h\alpha} & L_{h\beta} \\ M_{\alpha h} & M_{\alpha\alpha} & M_{\alpha\beta} \\ T_{\beta h} & T_{\beta\alpha} & T_{\beta\beta} \end{bmatrix}$$

From the principle of virtual work, the work done by these forces acting through a virtual displacement is equal to,

$$\delta W = \int_0^{\ell} \left[L' b \delta \frac{h}{b} + M' \delta \alpha + T' \delta \beta \right] dY \quad (40)$$

where ℓ is the semi-span parallel to the Y-axis.

Expressing Equation 40 in matrix form,

$$\delta W = \int_0^{\ell} \begin{bmatrix} \delta \frac{h}{b} & \delta \alpha & \delta \beta \end{bmatrix} \begin{Bmatrix} L'b \\ M' \\ T' \end{Bmatrix} dY \quad (41)$$

Substituting Equations 36, 37, 38, and 39 into Equation 41 results in a virtual work expression in terms of the generalized coordinates:

$$\delta W = \delta \underline{q}' \int_0^{\ell} \pi \rho \omega^2 b^4 \cos \psi_{c/4} \underline{\varphi}' \underline{T}^{(1)'} \underline{T}^{(2)'} \underline{\wedge} \underline{T}^{(2)} \underline{T}^{(1)} \underline{\varphi} dY \underline{q} \quad (42)$$

The generalized force Q_j required for Equation 1, Section 3.1 is simply,

$$Q_j = \frac{\delta W_j}{\delta q_j} \quad (43)$$

Applying Equation 43 to Equation 42 results in the required column of generalized aerodynamic forces:

$$\underline{Q} = \pi \rho \omega^2 \int_0^{\ell} b^4 \cos \psi_{c/4} \underline{\varphi}' \underline{T}^{(1)'} \underline{T}^{(2)'} \underline{\wedge} \underline{T}^{(2)} \underline{T}^{(1)} \underline{\varphi} dY \underline{q}$$

or

$$\underline{Q} = \omega^2 \underline{A} \underline{q} \quad (44)$$

$$\text{where } \underline{A} = \pi \rho \int_0^l b^4 \cos \Psi_{c/4} \underline{\varphi}' \underline{T}^{(1)'} \underline{T}^{(2)'} \underline{\Delta} \underline{T}^{(2)} \underline{T}^{(1)} \underline{\varphi} dY$$

and is termed the generalized aerodynamic matrix.

Aspect Ratio Corrections

Aspect ratio corrections were applied to the two-dimensional aerodynamics which forced the air-load distribution to take on an elliptical distribution.

The two-dimensional air forces used were seen to be equal to the following:

$$\begin{Bmatrix} L' b \\ M' \\ T' \end{Bmatrix} = \pi \rho \omega^2 b^4 \cos \Psi_{c/4} \underline{\Delta} \begin{Bmatrix} h/b \\ \alpha \\ \beta \end{Bmatrix} \quad (39)$$

The application of Equation 39 required the division of the lifting surface into a finite number of strips, evaluating the above expression at n stations and integrating numerically across the span to obtain the generalized aerodynamic matrix.

With the above representation of the air forces, a factor was determined which, when multiplied by Equation 39 at each station, forced the air load to assume the required elliptical distribution.

Consider the function G plotted in Figure 5, in which the function assumes the value of one at $Y = 0$ and zero at $Y = l$ and describes an ellipse between these extremes.

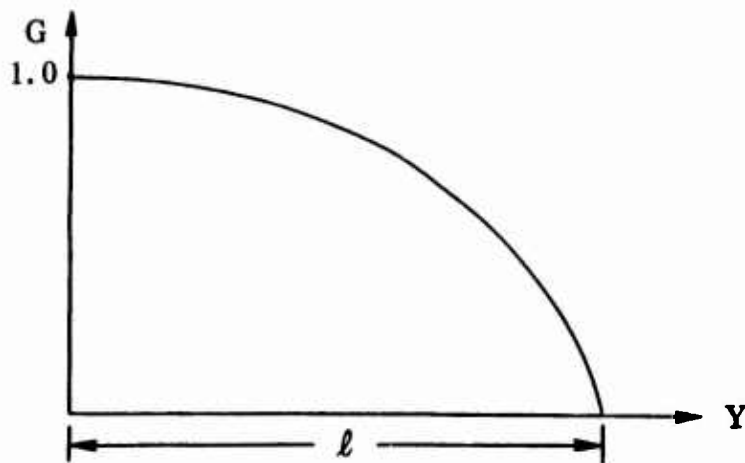


Figure 5 Plot of Function G

The equation of the function G may be written as

$$\frac{Y^2}{l^2} + \frac{G^2}{1.0} = 1.0$$

or

$$G = \sqrt{1 - \frac{Y^2}{l^2}} \quad (45)$$

Equation 45 lends itself to a factor which can be used to modify the air forces given in Equation 39.

Letting $G = F_F = \sqrt{1 - Y^2/l^2}$, Equation 39 may be written as

$$\begin{Bmatrix} L' b \\ M' \\ T' \end{Bmatrix} = \pi \rho \omega^2 b^4 \cos \Psi_{c/4} F_F \underline{\Delta} \begin{Bmatrix} h/b \\ \alpha \\ \beta \end{Bmatrix} \quad (46)$$

Following the same procedure as in Paragraph 3.1.3, the column of generalized forces is,

$$\underline{Q} = \pi \rho \omega^2 \int_0^l b^4 \cos \Psi_{c/4} F_F \underline{\varphi}' \underline{T}^{(1)'} \underline{T}^{(2)'} \underline{\Delta} \underline{T}^{(2)} \underline{T}^{(1)} \underline{\varphi} dY \underline{q}$$

or

$$\underline{Q} = \omega^2 \underline{A} \underline{q}$$

where \underline{A} , the generalized aerodynamic matrix, is now equal to

$$\pi \rho \int_0^l b^4 \cos \Psi_{c/4} F_F \underline{\varphi}' \underline{T}^{(1)'} \underline{T}^{(2)'} \underline{\Delta} \underline{T}^{(2)} \underline{T}^{(1)} \underline{\varphi} dY$$

3.2 SYMMETRIC FLUTTER ANALYSIS

Study of the flutter characteristics of the empennage, symmetric sense, was initially restricted to an investigation of the basic horizontal stabilizer with an assumed cantilevered restraint at the horizontal stabilizer pivot. Subsequent coupling of the stabilizer with the fuselage allowed an investigation into this added effect.

3.2.1 Cantilevered Analysis

The constrained empennage coordinates are the appropriate normal vibration modes of the horizontal stabilizer consistent with the assumed cantilevered restraint. Therefore, the following generalized coordinates are considered:

- q_1 - Horizontal stabilizer rigid body pitch (about pitch axis)
- q_2 - Elevator rotation
- q_3 - 1st coupled horizontal stabilizer elastic mode
- q_4 - 2nd coupled horizontal stabilizer elastic mode
- q_5 - 3rd coupled horizontal stabilizer elastic mode

3.2.1.1 Generalized Mass Matrix

Since only the horizontal tail is involved, the total generalized mass matrix is:

$$\underline{M} = \underline{M}_{H.T.}$$

For the generalized coordinates given in Paragraph 3.2.1, the generalized displacement matrix for the horizontal tail takes the following form for the displacements indicated in Equation 21, Paragraph 3.1.1:

$$\begin{bmatrix} \varphi_{11} & 0 & 0 & 0 & 0 \\ 0 & 0 & 0 & 0 & 0 \\ \varphi_{31} & 0 & \varphi_{33} & \varphi_{34} & \varphi_{35} \\ \varphi_{41} & 0 & \varphi_{43} & \varphi_{44} & \varphi_{45} \\ \varphi_{51} & 0 & \varphi_{53} & \varphi_{54} & \varphi_{55} \\ 0 & 0 & 0 & 0 & 0 \\ 0 & \varphi_{72} & 0 & 0 & 0 \end{bmatrix}$$

where the φ_{ij} are column matrices relating the appropriate column matrix $\underline{\delta}$ to the j^{th} generalized coordinate.

The mass matrix \underline{J} for the horizontal tail is that given by Equation 21, Paragraph 3.1.1.

3.2.1.2 Aerodynamic Matrix

For the generalized coordinates stated in Paragraph 3.2.1, the generalized displacement matrix $\underline{\varphi}$ is that given in Paragraph 3.2.1.1, and the generalized aerodynamic matrix is simply

$$\underline{A} = \underline{A}_{H.T.}$$

The transformation matrices \underline{T} take on the following forms:

$$\underline{T}^{(1)} = \begin{bmatrix} 1.0 & 0 & 0 & 0 & 0 & 0 & 0 \\ 0 & 1.0 & 0 & 0 & 0 & 0 & 0 \\ 0 & 0 & 1.0 & 0 & 0 & 0 & 0 \\ 0 & 0 & 0 & \cos \psi_{e.a.} & -\sin \psi_{e.a.} & 0 & 0 \\ 0 & 0 & 0 & \sin \psi_{e.a.} & \cos \psi_{e.a.} & 0 & 0 \\ 0 & 0 & 0 & 0 & 0 & 1.0 & 0 \\ 0 & 0 & 0 & 0 & 0 & 0 & \cos \psi_H \end{bmatrix}$$

$$\underline{T}^{(2)} = \begin{bmatrix} 0 & 0 & 1.0 & 0 & -a & 0 & 0 \\ 0 & 0 & 0 & 0 & 1.0 & 0 & 0 \\ 0 & 0 & 0 & 0 & 0 & 0 & 1.0 \end{bmatrix}$$

where a is the streamwise distance from the quarter chord to the elastic-axis, positive aft of the quarter chord.

3.2.2 Free-Free Analysis

The unrestrained fuselage coordinates considered for this analysis are the free-free normal vibration modes of the fuselage with wing and empennage mass effects included. The empennage coordinates are the same normal vibration modes utilized in the cantilevered analysis. Therefore, the following generalized coordinates were considered:

- q_1 - Aircraft vertical translation
- q_2 - Aircraft pitch
- q_3 - Horizontal stabilizer rigid body pitch (about pitch axis)
- q_4 - Elevator rotation
- q_5 - 1st fuselage vertical bending mode
- q_6 - 2nd fuselage vertical bending mode
- q_7 - 3rd fuselage vertical bending mode
- q_8 - 4th fuselage vertical bending mode
- q_9 - 1st coupled horizontal stabilizer elastic mode
- q_{10} - 2nd coupled horizontal stabilizer elastic mode

3.2.2.1 Generalized Mass Matrix

For the free-free analysis, the total generalized mass matrix is of the form,

$$\underline{M} = 2 \underline{M}_{H.T.} + \underline{M}_F$$

where the wing mass and mass-inertia effects are included as lumped elements in the fuselage mass distribution.

For the generalized coordinates given in Paragraph 3.2.2, the generalized displacement matrix $\underline{\varphi}$ for the horizontal tail takes the following form for the displacements indicated in Equation 21, Paragraph 3.1.1:

$$\begin{bmatrix} 0 & \varphi_{12} & \varphi_{13} & 0 & \varphi_{15} & \varphi_{16} & \varphi_{17} & \varphi_{18} & 0 & 0 \\ 0 & 0 & 0 & 0 & 0 & 0 & 0 & 0 & 0 & 0 \\ \varphi_{31} & \varphi_{32} & \varphi_{33} & 0 & \varphi_{35} & \varphi_{36} & \varphi_{37} & \varphi_{38} & \varphi_{39} & \varphi_{310} \\ 0 & \varphi_{42} & \varphi_{43} & 0 & \varphi_{45} & \varphi_{46} & \varphi_{47} & \varphi_{48} & \varphi_{49} & \varphi_{410} \\ 0 & \varphi_{52} & \varphi_{53} & 0 & \varphi_{55} & \varphi_{56} & \varphi_{57} & \varphi_{58} & \varphi_{59} & \varphi_{510} \\ 0 & 0 & 0 & 0 & 0 & 0 & 0 & 0 & 0 & 0 \\ 0 & 0 & 0 & \varphi_{74} & 0 & 0 & 0 & 0 & 0 & 0 \end{bmatrix}$$

where the φ_{ij} are column matrices relating the appropriate column matrix $\underline{\delta}$ to the j^{th} generalized coordinate.

The fuselage generalized displacement matrix $\underline{\varphi}$ may be formulated from Equation 14, Paragraph 3.1.1, by considering only two displacements, δ_Z and δ_Y . Therefore,

$$\underline{\varphi} = \begin{bmatrix} \varphi_{11} & \varphi_{12} & 0 & 0 & \varphi_{15} & \varphi_{16} & \varphi_{17} & \varphi_{18} & 0 & 0 \\ 0 & \varphi_{22} & 0 & 0 & \varphi_{25} & \varphi_{26} & \varphi_{27} & \varphi_{28} & 0 & 0 \end{bmatrix}$$

where the φ_{ij} elements are again column matrices relating the specified displacements δ_Z and δ_Y to the stated generalized coordinates.

The mass matrix \underline{J} for the horizontal tail is that given by Equation 21, Paragraph 3.1.1.

For the fuselage, since only two displacements are considered, the mass matrix \underline{J} takes the following form:

$$\begin{bmatrix} m & S_Y \\ S_Y & I_Y \end{bmatrix}$$

where the elements also reflect the vertical tail mass and mass-inertia effects.

3.2.2.2 Generalized Aerodynamic Matrix

The aerodynamic matrix suitable for this analysis is simply

$$\underline{A} = 2\underline{A} \text{ H. T.}$$

where the transformation matrices \underline{T} are as given in Paragraph 3.2.1.2 and the generalized displacement matrix $\underline{\varphi}$ is shown in Paragraph 3.2.2.1.

3.3 ANTISYMMETRIC FLUTTER ANALYSIS

Study of the flutter characteristics of the empennage, antisymmetric sense, as in the symmetric case, was initially restricted to an investigation of the basic vertical stabilizer with an assumed cantilevered restraint at the vertical stabilizer-fuselage intersection. This initial analysis also considered a flexible horizontal stabilizer with an assumed cantilevered restraint at the horizontal stabilizer pivot. Subsequent coupling of the empennage with the fuselage provided a set of new coordinates which then were utilized in the flutter analysis.

3.3.1 Cantilevered Analysis

The constrained empennage coordinates are the appropriate normal vibration modes of the horizontal and vertical stabilizers consistent with the assumed cantilevered restraint as mentioned in Paragraph 3.3. Therefore the following generalized coordinates were considered:

q_1 - Rudder rotation

q_2 - Elevator rotation

- q_3 - Horizontal stabilizer rigid body flapping
- q_4 - Horizontal stabilizer rigid body yawing
- q_5 - 1st coupled horizontal stabilizer elastic mode
- q_6 - 2nd coupled horizontal stabilizer elastic mode
- q_7 - 3rd coupled horizontal stabilizer elastic mode
- q_8 - 1st coupled vertical stabilizer elastic mode
- q_9 - 2nd coupled vertical stabilizer elastic mode
- q_{10} - 3rd coupled vertical stabilizer elastic mode

3.3.1.1 Generalized Mass Matrix

For this phase of the antisymmetric analysis, the generalized mass matrix is of the form,

$$\underline{M} = 2\underline{M}_{H.T.} + \underline{M}_{V.T.}$$

For the generalized coordinates given in Paragraph 3.3.1, the generalized displacement matrix $\underline{\varphi}$ for the horizontal tail takes the following form for the displacements indicated in Equation 21, Paragraph 3.1.1.

$$\begin{bmatrix} 0 & 0 & 0 & \varphi_{14} & 0 & 0 & 0 & \varphi_{18} & \varphi_{19} & \varphi_{110} \\ 0 & 0 & 0 & \varphi_{24} & 0 & 0 & 0 & \varphi_{28} & \varphi_{29} & \varphi_{210} \\ 0 & 0 & \varphi_{33} & 0 & \varphi_{35} & \varphi_{36} & \varphi_{37} & \varphi_{38} & \varphi_{39} & \varphi_{310} \\ 0 & 0 & \varphi_{43} & 0 & \varphi_{45} & \varphi_{46} & \varphi_{47} & \varphi_{48} & \varphi_{49} & \varphi_{410} \\ 0 & 0 & \varphi_{53} & 0 & \varphi_{55} & \varphi_{56} & \varphi_{57} & \varphi_{58} & \varphi_{59} & \varphi_{510} \\ 0 & 0 & 0 & \varphi_{64} & 0 & 0 & 0 & \varphi_{68} & \varphi_{69} & \varphi_{610} \\ 0 & \varphi_{72} & 0 & 0 & 0 & 0 & 0 & 0 & 0 & 0 \end{bmatrix}$$

The generalized displacement matrix $\underline{\varphi}$ for the vertical tail may be written in the following form for the same displacements as for the horizontal tail except for the displacement $\bar{\delta}_Z$ which is replaced by $\bar{\delta}_Y$:

$$\begin{bmatrix} 0 & 0 & 0 & 0 & 0 & 0 & 0 & 0 & 0 & 0 \\ 0 & 0 & 0 & 0 & 0 & 0 & 0 & \varphi_{28} & \varphi_{29} & \varphi_{210} \\ 0 & 0 & 0 & 0 & 0 & 0 & 0 & 0 & 0 & 0 \\ 0 & 0 & 0 & 0 & 0 & 0 & 0 & \varphi_{48} & \varphi_{49} & \varphi_{410} \\ 0 & 0 & 0 & 0 & 0 & 0 & 0 & \varphi_{58} & \varphi_{59} & \varphi_{510} \\ 0 & 0 & 0 & 0 & 0 & 0 & 0 & 0 & 0 & 0 \\ \varphi_{71} & 0 & 0 & 0 & 0 & 0 & 0 & 0 & 0 & 0 \end{bmatrix}$$

The mass matrix \underline{J} for the horizontal tail is that given by Equation 21, Paragraph 3.1.1.

The mass matrix \underline{J} for the vertical tail is given by Equation 22, Paragraph 3.1.1 with the subscript Z replaced by Y.

3.3.1.2 Generalized Aerodynamic Matrix

Since we have aerodynamics acting on both the horizontal and vertical tails, the total aerodynamic matrix is

$$\underline{A} = 2\underline{A}_{H.T.} + \underline{A}_{V.T.}$$

where the transformation matrices for both the horizontal and vertical tails are as given in Paragraph 3.2.1.2.

The generalized displacement matrices $\underline{\varphi}$ for both the horizontal and vertical tails are as given in Paragraph 3.3.1.1.

3.3.2 Free-Free Analysis

Due to the large number of coordinates required to describe adequately the motion of the aircraft in an antisymmetric sense, a set of new generalized coordinates was determined for use in the flutter analysis.

3.3.2.1 Modal Coupling

For determination of a new set of coordinates, the unrestrained fuselage coordinates considered are the free-free normal vibration modes of the fuselage with wing and empennage mass and mass-inertia effects included. The empennage coordinates are the same normal vibration modes utilized in the cantilevered analysis. The following generalized coordinates were considered for the modal coupling phase:

- q_1 - Aircraft side translation
- q_2 - Aircraft yaw
- q_3 - Aircraft roll
- q_4 - 1st fuselage lateral bending mode
- q_5 - 2nd fuselage lateral bending mode
- q_6 - 3rd fuselage lateral bending mode
- q_7 - 4th fuselage lateral bending mode
- q_8 - 1st fuselage torsion mode
- q_9 - 2nd fuselage torsion mode
- q_{10} - 3rd fuselage torsion mode
- q_{11} - 4th fuselage torsion mode
- q_{12} - 1st coupled vertical stabilizer elastic mode
- q_{13} - 2nd coupled vertical stabilizer elastic mode
- q_{14} - 3rd coupled vertical stabilizer elastic mode
- q_{15} - 1st coupled horizontal stabilizer elastic mode
- q_{16} - 2nd coupled horizontal stabilizer elastic mode
- q_{17} - 3rd coupled horizontal stabilizer elastic mode

q_{18} - Rudder rotation

q_{19} - Elevator rotation

q_{20} - Horizontal stabilizer rigid body flapping

The applicable equations of motion are those given in Equation 6, Section 3.1, with the generalized aerodynamic matrix \underline{A} equal to zero and the complex eigenvalue Ω reducing to $\Omega = 1/\omega$ for free undamped vibrations.

With the elements of the generalized stiffness matrix \bar{K} taken as in Equation 35, Paragraph 3.1.2, only inertia coupling is involved in the generation of the new set of generalized coordinates.

Generalized Mass Matrix

Since we are dealing with three components, i.e., horizontal and vertical tails plus the fuselage, the generalized mass matrix may be broken up as follows:

$$\underline{M} = 2\underline{M}_{H.T.} + \underline{M}_{V.T.} + \underline{M}_F$$

The generalized displacement matrix $\underline{\phi}$ for the horizontal tail for the coordinates given in Paragraph 3.3.2.1 may be written as

$$\begin{bmatrix} 0 & \phi_{12} & 0 & \phi_{14} & \phi_{15} & \phi_{16} & \phi_{17} & 0 & 0 & 0 & 0 & \phi_{112} & \phi_{113} & \phi_{114} & 0 & 0 & 0 & 0 & 0 & 0 \\ \phi_{21} & \phi_{22} & \phi_{23} & \phi_{24} & \phi_{25} & \phi_{26} & \phi_{27} & \phi_{28} & \phi_{29} & \phi_{210} & \phi_{211} & \phi_{212} & \phi_{213} & \phi_{214} & 0 & 0 & 0 & 0 & 0 & 0 \\ 0 & 0 & \phi_{33} & 0 & 0 & 0 & 0 & \phi_{34} & \phi_{39} & \phi_{310} & \phi_{311} & \phi_{312} & \phi_{313} & \phi_{314} & \phi_{315} & \phi_{316} & \phi_{317} & 0 & 0 & \phi_{320} \\ 0 & 0 & \phi_{43} & 0 & 0 & 0 & 0 & \phi_{48} & \phi_{49} & \phi_{410} & \phi_{411} & \phi_{412} & \phi_{413} & \phi_{414} & \phi_{415} & \phi_{416} & \phi_{417} & 0 & 0 & \phi_{420} \\ 0 & 0 & \phi_{53} & 0 & 0 & 0 & 0 & \phi_{58} & \phi_{59} & \phi_{510} & \phi_{511} & \phi_{512} & \phi_{513} & \phi_{514} & \phi_{515} & \phi_{516} & \phi_{517} & 0 & 0 & \phi_{520} \\ 0 & \phi_{62} & 0 & \phi_{64} & \phi_{65} & \phi_{66} & \phi_{67} & 0 & 0 & 0 & 0 & \phi_{612} & \phi_{613} & \phi_{614} & 0 & 0 & 0 & 0 & 0 & 0 \\ 0 & 0 & 0 & 0 & 0 & 0 & 0 & 0 & 0 & 0 & 0 & 0 & 0 & 0 & 0 & 0 & 0 & 0 & 0 & \phi_{719} & 0 \end{bmatrix}$$

for the displacements given in Paragraph 3.1.1.

For the vertical tail, the generalized displacement matrix $\underline{\varphi}$ is

$$\begin{bmatrix} 0 & 0 & 0 & 0 & 0 & 0 & 0 & 0 & 0 & 0 & 0 & 0 & 0 & 0 & 0 & 0 & 0 & 0 & 0 \\ \varphi_{21} & \varphi_{22} & \varphi_{23} & \varphi_{24} & \varphi_{25} & \varphi_{26} & \varphi_{27} & \varphi_{28} & \varphi_{29} & \varphi_{210} & \varphi_{211} & \varphi_{212} & \varphi_{213} & \varphi_{214} & 0 & 0 & 0 & 0 & 0 \\ 0 & 0 & 0 & 0 & 0 & 0 & 0 & 0 & 0 & 0 & 0 & 0 & 0 & 0 & 0 & 0 & 0 & 0 & 0 \\ 0 & \varphi_{42} & \varphi_{43} & \varphi_{44} & \varphi_{45} & \varphi_{46} & \varphi_{47} & \varphi_{48} & \varphi_{49} & \varphi_{410} & \varphi_{411} & \varphi_{412} & \varphi_{413} & \varphi_{414} & 0 & 0 & 0 & 0 & 0 \\ 0 & \varphi_{52} & \varphi_{53} & \varphi_{54} & \varphi_{55} & \varphi_{56} & \varphi_{57} & \varphi_{58} & \varphi_{59} & \varphi_{510} & \varphi_{511} & \varphi_{512} & \varphi_{513} & \varphi_{514} & 0 & 0 & 0 & 0 & 0 \\ 0 & 0 & 0 & 0 & 0 & 0 & 0 & 0 & 0 & 0 & 0 & 0 & 0 & 0 & 0 & 0 & 0 & 0 & 0 \\ 0 & 0 & 0 & 0 & 0 & 0 & 0 & 0 & 0 & 0 & 0 & 0 & 0 & 0 & 0 & 0 & 0 & \varphi_{718} & 0 \end{bmatrix}$$

for the same displacements as for the horizontal tail except for the displacement δ_Z , which is replaced by δ_Y .

The generalized matrix $\underline{\varphi}$ for the fuselage is

$$\begin{bmatrix} \varphi_{11} & \varphi_{12} & \varphi_{13} & \varphi_{14} & \varphi_{15} & \varphi_{16} & \varphi_{17} & 0 & 0 & 0 & 0 & 0 & 0 & 0 & 0 & 0 & 0 & 0 & 0 \\ 0 & 0 & \varphi_{23} & 0 & 0 & 0 & 0 & \varphi_{28} & \varphi_{29} & \varphi_{210} & \varphi_{211} & 0 & 0 & 0 & 0 & 0 & 0 & 0 & 0 \\ 0 & \varphi_{32} & 0 & \varphi_{34} & \varphi_{35} & \varphi_{36} & \varphi_{37} & 0 & 0 & 0 & 0 & 0 & 0 & 0 & 0 & 0 & 0 & 0 & 0 \end{bmatrix}$$

for only three considered displacements, δ_Y , δ_X and δ_Z .

The mass matrix \underline{J} for the horizontal tail is that given by Equation 21, Paragraph 3.1.1.

The mass matrix \underline{J} for the vertical tail is given by Equation 22, Paragraph 3.1.1 with the subscript Z replaced by Y.

For the three displacements considered for the fuselage, the mass matrix \underline{J} takes the following form:

$$\begin{bmatrix} m & -S_X & 0 \\ -S_X & I_X & 0 \\ 0 & 0 & I_Z \end{bmatrix}$$

where the elements also reflect the wing mass and mass-inertia effects.

3.3.2.2 Flutter Analysis

The new set of generalized coordinates determined from a solution of the equations of motion described in Paragraph 3.3.2.1, is as follows:

- q_1 - Aircraft side translation
- q_2 - Aircraft yaw
- q_3 - Aircraft roll
- q_4 - Horizontal stabilizer rigid body yawing
- q_5 - 1st coupled fuselage - empennage elastic mode
- q_6 - 2nd coupled fuselage - empennage elastic mode
- q_7 - 3rd coupled fuselage - empennage elastic mode
- q_8 - 4th coupled fuselage - empennage elastic mode
- q_9 - 5th coupled fuselage - empennage elastic mode
- q_{10} - 6th coupled fuselage - empennage elastic mode

Generalized Mass Matrix

As in the modal coupling phase, the generalized mass matrix may be split up into parts:

$$\underline{M} = 2\underline{M}_{H.T.} + \underline{M}_{V.T.} + \underline{M}_F$$

where the generalized displacement matrix $\underline{\varphi}$ for the horizontal tail, vertical tail and fuselage are, respectively,

$$\begin{bmatrix} 0 & \varphi_{12} & 0 & \varphi_{14} & \varphi_{15} & \varphi_{16} & \varphi_{17} & \varphi_{18} & \varphi_{19} & \varphi_{110} \\ \varphi_{21} & \varphi_{22} & \varphi_{23} & \varphi_{24} & \varphi_{25} & \varphi_{26} & \varphi_{27} & \varphi_{28} & \varphi_{29} & \varphi_{210} \\ 0 & 0 & \varphi_{33} & 0 & \varphi_{35} & \varphi_{36} & \varphi_{37} & \varphi_{38} & \varphi_{39} & \varphi_{310} \\ 0 & 0 & \varphi_{43} & 0 & \varphi_{45} & \varphi_{46} & \varphi_{47} & \varphi_{48} & \varphi_{49} & \varphi_{410} \\ 0 & 0 & \varphi_{53} & 0 & \varphi_{55} & \varphi_{56} & \varphi_{57} & \varphi_{58} & \varphi_{59} & \varphi_{510} \\ 0 & \varphi_{62} & 0 & \varphi_{64} & \varphi_{65} & \varphi_{66} & \varphi_{67} & \varphi_{68} & \varphi_{69} & \varphi_{610} \\ 0 & 0 & 0 & 0 & \varphi_{75} & \varphi_{76} & \varphi_{77} & \varphi_{78} & \varphi_{79} & \varphi_{710} \end{bmatrix}$$

$$\begin{bmatrix} 0 & 0 & 0 & 0 & 0 & 0 & 0 & 0 & 0 & 0 \\ \varphi_{21} & \varphi_{22} & \varphi_{23} & 0 & \varphi_{25} & \varphi_{26} & \varphi_{27} & \varphi_{28} & \varphi_{29} & \varphi_{210} \\ 0 & 0 & 0 & 0 & 0 & 0 & 0 & 0 & 0 & 0 \\ 0 & \varphi_{42} & \varphi_{43} & 0 & \varphi_{45} & \varphi_{46} & \varphi_{47} & \varphi_{48} & \varphi_{49} & \varphi_{410} \\ 0 & \varphi_{52} & \varphi_{53} & 0 & \varphi_{55} & \varphi_{56} & \varphi_{57} & \varphi_{58} & \varphi_{59} & \varphi_{510} \\ 0 & 0 & 0 & 0 & 0 & 0 & 0 & 0 & 0 & 0 \\ 0 & 0 & 0 & 0 & \varphi_{75} & \varphi_{76} & \varphi_{77} & \varphi_{78} & \varphi_{79} & \varphi_{710} \end{bmatrix}$$

$$\begin{bmatrix} \varphi_{11} & \varphi_{12} & \varphi_{13} & 0 & \varphi_{15} & \varphi_{16} & \varphi_{17} & \varphi_{18} & \varphi_{19} & \varphi_{110} \\ 0 & 0 & \varphi_{23} & 0 & \varphi_{25} & \varphi_{26} & \varphi_{27} & \varphi_{28} & \varphi_{29} & \varphi_{210} \\ 0 & \varphi_{32} & 0 & 0 & \varphi_{35} & \varphi_{36} & \varphi_{37} & \varphi_{38} & \varphi_{39} & \varphi_{310} \end{bmatrix}$$

The mass matrices \underline{J} for the three components are as given in Paragraph 3.3.2.1.

Generalized Aerodynamic Matrix

As in the antisymmetric cantilevered analysis, the aerodynamic matrix may be written as

$$\underline{A} = 2\underline{A}_{H.T.} + \underline{A}_{V.T.}$$

where the transformation matrices for both the horizontal and vertical tail are as given in Paragraph 3.2.1.2.

The generalized displacement matrix $\underline{\varphi}$ for both the horizontal and vertical tail are given under Generalized Mass Matrix.

4.0 DISCUSSION AND RESULTS

The presentation and discussion of the results of the empennage flutter analysis, in general, follows the sequence of Sections 3.2 and 3.3. Also, this section presents the idealization of the empennage used for the analysis, the structural properties of such structure, and other data required for the flutter analysis of the empennage.

4.1 IDEALIZATION OF AIRCRAFT

As previously mentioned, structural idealization of the empennage and fuselage was restricted to equivalent beams possessing both flexure and torsional stiffness distributions, with the aerodynamic loading represented by two-dimensional or strip-theory aerodynamic forces. Figure 6 of Reference 1 presents the actual structure of the XV-5A empennage and fuselage to be idealized.

4.1.1 Structural Representation

As the aircraft structure shown in Figure 6 of Reference 1 shows, this may be thought of as a number of components assembled to form the complete structure, i. e., fuselage and horizontal and vertical stabilizers plus control surfaces. From this standpoint, the following paragraphs deal with these components as they were treated during the analysis.

4.1.1.1 Horizontal Stabilizer-Elevator

Figure 6 shows the planform of the horizontal stabilizer and elevator. The elastic-axis shown represents the equivalent beam which replaces the actual structure shown in Figure 6 of Reference 1. The elevator was taken as a rigid body having distributed mass and mass-inertia properties. The elevator system is manual; therefore, its rotational restraint was idealized into an equivalent spring. This, in conjunction with the pitching inertia of the elevator, resulted in an elevator rotational frequency, which was varied to cover expected ranges. Figure 8 presents a plot of the spanwise distribution of the bending and torsional stiffnesses for the horizontal stabilizer. These stiffness values reflect a maneuver flight condition, i. e., they reflect a minimum stiffness due to skin ineffectiveness.

4.1.1.2 Vertical Stabilizer-Rudder

Figure 7 shows the planform of the vertical stabilizer and rudder, with the elastic-axis shown representing the orientation of the equivalent beam which replaces the actual structure shown in Figure 6 of Reference 1. The rudder system, being equivalent to the elevator system, was idealized in the same fashion. Figure 9 presents a plot of the spanwise distributions of the bending and torsional stiffnesses for the vertical stabilizer. As for the horizontal stabilizer, these plots reflect a minimum stiffness, also.

4.1.1.3 Fuselage

The fuselage structure shown in Figure 6 of Reference 1 was idealized into an equivalent beam having vertical, lateral and torsional stiffness. These distributions are shown in Figure 10. The elastic axis of the fuselage was assumed to be at the intersection of the vertical plane at B. L. 0 with the horizontal plane at W. L. 113.00. With this representation, the vertical stabilizer elastic-axis intersects the fuselage at F. S. 459.37, as shown in Figure 7.

4.1.2 Aerodynamic Representation

Since aerodynamic forces acting on the wing normally are small, compared to forces on the empennage when predominant empennage motion is involved, the wing contribution to the formulation of the aerodynamic matrix was neglected. Flutter analyses were performed for several different altitudes to observe effects of air density. The aerodynamic coefficients used reflected both incompressible and compressible flow. The former coefficients were based largely on the work of References 2 and 3, whereas the compressible coefficients were derived from those covered by References 4 and 5.

4.1.2.1 Empennage

Application of Equation 44, Paragraph 3.1.3, required the division of the horizontal and vertical tails into a number of spanwise strips oriented parallel to the free stream. Evaluation of Equation 44 at each of the air-force stations was then required, and the total aerodynamic matrix for the surface was formed by numerical integration. Figures 6 and 7 also depict the planforms which were used for generation of the aerodynamic matrix for the horizontal and vertical tails, respectively.

4.1.3 Mass Representation

Only one gross weight condition, that of the design gross weight of approximately 9200 lbs, was studied during the analysis. This weight condition was applied only to the free-free analysis, both symmetric and antisymmetric. From a given mass distribution, the distribution was reworked to reflect a lumped-parameter system which was governed by an axis system dictated by Equation 21 or 22 of Paragraph 3.1.1. Inconsistencies between distributions shown for the symmetric and antisymmetric analyses are attributed to the relative time between completion of each analysis with the consequent up-dating of a distribution.

4.1.3.1 Symmetric Analysis

The mass distribution of the two components, the horizontal tail and fuselage, required for both the initial cantilever analysis and the free-free analysis, are presented in Tables 1 and 2 for the horizontal tail and fuselage, respectively. The properties shown reflect the nomenclature as described by Equation 21 of Paragraph 3.1.1. Elevator and elevator mass-balance are also shown separately to indicate the mass-balance distribution utilized in the analysis. Table 2 presents, in addition to the basic fuselage distribution, the wing and empennage mass properties which made up the inertial force and moment contributions of these components to the fuselage symmetric normal modes.

4.1.3.2 Antisymmetric Analysis

The mass distribution of the three components, namely the horizontal tail, vertical tail and fuselage, required for both the initial cantilevered analysis and the free-free analysis, are presented in Tables 3 through 5 for the horizontal tail, vertical tail and fuselage, respectively. The properties shown again reflect the nomenclature as described by Equation 21 of Paragraph 3.1.1. To show elevator and rudder mass-balance, separate tables of the balanced control surface and of the balance weights are also shown in Tables 3 and 4. Also shown in Table 4 are the horizontal tail mass properties which made up the inertial force and moment contribution of this component to the vertical stabilizer normal modes. Table 5 presents, in addition to the basic fuselage distribution, the wing and empennage mass properties which made up the inertial force and moment contributions of these components to the fuselage antisymmetric normal modes.

4.2 MODAL FUNCTIONS

As mentioned in Section 3.0, the equations of motion were formulated in terms of modal functions. These were principally the normal modes of vibration of the component consistent with an assumed constraint.

4.2.1 Symmetric Analysis

As mentioned in Section 3.2, the components involved in the symmetric analysis were the horizontal stabilizer, fuselage and elevator. The horizontal stabilizer normal modes are the coupled modes (inertial) of bending and torsion of the equivalent beam considered cantilevered at the horizontal stabilizer pivot. The normal modes of the fuselage are the uncoupled free-free modes of the fuselage equivalent beam with wing and empennage mass and mass-inertia effects included. Vertical shear effects (AG) are also considered in the determination of these latter modes.

4.2.1.1 Cantilevered

Figures 11, 12 and 13 depict the first three cantilevered mode shapes of the horizontal stabilizer, while Table 6 gives a tabulation of the modal data. The vertical bending is denoted by φ whereas the torsion of the surface about the elastic-axis is denoted by θ .

4.2.1.2 Free-Free

In addition to the horizontal stabilizer normal modes, the fuselage degrees of freedom were included, and these shapes are plotted in Figures 14 and 15, with the modal data tabulated in Table 7.

4.2.2 Antisymmetric Analysis

Also, as mentioned in Section 3.3, the components involved in the anti-symmetric analysis were the horizontal stabilizer, vertical stabilizer, and fuselage, plus elevator and rudder. The horizontal stabilizer normal modes are the coupled modes (inertial) of bending and torsion of the equivalent beam considered cantilevered at the horizontal stabilizer pivot. The vertical stabilizer normal modes are also the inertially coupled modes of bending and torsion of the equivalent beam considered cantilevered at the intersection of the elastic-axis with the assumed fuselage elastic-axis (F.S. 459.37). Mass and mass-inertia effects of the horizontal tail were considered in these latter modes. The

normal modes of the fuselage are the uncoupled free-free modes of the fuselage equivalent beam, with wing and empennage mass and mass-inertia effects included.

4.2.2.1 Cantilevered

Figures 16, 17 and 18 present the first three cantilevered mode shapes of the horizontal stabilizer, while Table 8 tabulates the modal data. The equivalent information for the vertical stabilizer is presented in Figures 19, 20, and 21 and Table 9.

4.2.2.2 Free-Free

For the free-free analysis, as mentioned in Paragraph 3.3.2, coupled modes for the aircraft were calculated, and a new set of generalized coordinates was chosen for the flutter analysis. The horizontal and vertical stabilizer normal modes utilized in the coupling are the same constrained modes of vibration utilized in the cantilevered analysis. The fuselage mode shapes are presented in Figures 22 and 23 for the uncoupled lateral bending and in Figures 24 and 25 for uncoupled torsion, the modal data being shown in Table 10.

4.3 FLUTTER ANALYSIS

As explained previously, the analysis of the empennage has been divided into a symmetric and an antisymmetric investigation. Each of these analyses was then divided further into basic cantilevered analyses and then extended to allow for fuselage flexibility and aircraft rigid body degrees of freedom.

In general, most of the results of the flutter analyses are plotted in the conventional sense, i. e., overall damping (g) versus forward velocity (V). In addition, the flutter frequency (f) is also plotted versus velocity. Equation 6 of Section 3.1 implies that these will be $n-r$ roots, where n is the number of generalized coordinates considered for the problem, and r is the number of generalized coordinates defining rigid body degrees of freedom of zero frequency. Since generation of the air-force matrix Δ requires the selection of a reduced frequency parameter (k_0), the curves of damping-frequency versus flutter speed were generated by considering a range of reduced frequency parameters. The flutter parameters were noted by recording the lowest velocity at which a $V-g$ plot crossed the $g = 0$ axis and then noting the flutter frequency at this velocity from the $V-f$ plot for the appropriate root.

4.3.1 Symmetric

The initial phase of the symmetric analysis, as explained previously, was restricted to the basic horizontal tail, which was assumed cantilevered at the pivot. The next phase included fuselage effects and also aircraft rigid body degrees of freedom.

4.3.1.1 Cantilevered Analysis

The large number of parameters involved in the flutter analysis, such as elevator rotational frequency, horizontal tail pitch frequency, density, aerodynamic parameters (aspect-ratio corrections and effect of aerodynamic balance) precluded an extensive variation of these parameters. Therefore, only those parameters which were felt to be significant were varied over a larger range. Both incompressible and compressible aerodynamic coefficients were used in this analysis, as the incompressible analysis indicated that a flutter problem existed on the basic horizontal tail.

Incompressible

Figures 26 through 30 present the results of the basic cantilevered analysis for a variable horizontal tail pitch frequency of 25 to 80 cycles per second, for a constant elevator rotational frequency of 10 cycles per second and at an altitude of sea-level. Aerodynamic parameters were such that aspect-ratio corrections and effects of aerodynamic balance were neglected.

Figures 31 through 33 present results equivalent to those in Figures 26 through 30, but for an elevator rotational frequency of 30 cps and for horizontal tail pitch frequencies of 40, 60 and 80 cps.

Figures 34 through 36 show the results of removing the elevator degree of freedom (assuming elevator to be rigidly clamped) from the analysis. Other parameters are as in Figures 31 through 33.

Figures 37 through 39 present effects of aspect-ratio corrections (tip-round-off) for variable horizontal tail pitch frequencies of 40, 60 and 80 cps, for an elevator rotational frequency of 10 cps, and at sea-level altitude.

Figure 40 shows the effect of including aerodynamic balance in the air-force matrix for a horizontal tail pitch frequency of 60 cps and an elevator rotational frequency of 10 cps, all at sea-level altitude.

Aerodynamic balance effects were accounted for by means of the method described in References 2 and 3. These references treat any balance as external, (nose overhang exposed directly to the free stream), whereas the actual aerodynamic balance in the elevator is of an internal nature. It was felt that treatment of the balance effects by means of the techniques of References 2 and 3 would indicate trends, which would be sufficient for the analysis.

Figures 41 through 43 present altitude effects for a pitch frequency of 60 cps and an elevator rotational frequency of 10 cps. An altitude of 9300' represents the minimum altitude at which the maximum-limit dive Mach number is reached.

A cross-plot of horizontal tail pitch frequency versus flutter speed is presented in Figure 44 for the different parameteric studies shown in the V-g plots of Figures 26 through 43.

Compressible

Compressible flutter analyses, using aerodynamic coefficients for a Mach number of 0.60, 0.70 and 0.80, were conducted for a fixed horizontal tail pitch frequency of 60 cps and an elevator rotational frequency of 10 cps. Aerodynamic parameters (aspect-ratio corrections and effects of aerodynamic balance) were neglected for this phase of the analysis, with altitude variations taken for the four altitudes used in the incompressible analysis.

Figures 46 through 48 present the results for the sea-level condition, while the results for the 9300', 20,000' and 30,000' analyses are presented in Figures 49 through 57. Only the roots of concern have been plotted on both the V-g and V-f plots.

The flutter speed deduced from the above figures represents an apparent speed and not a true flutter speed. This is because the speed corresponding to the particular Mach number, in general, is not equal to the apparent flutter speed. For this reason, an auxiliary plot is given in Figure 58, wherein the apparent flutter speeds deduced from Figures 46 through 57 have been converted to equivalent air speeds. Crossing of a particular altitude line with the plot generated from the apparent flutter speeds then yields a true flutter speed. Also included in Figure 58 are the incompressible results obtained from Figures 29 and 41 through 43.

4.3.1.2 Free-Free Analysis

The free-free analysis was conducted for two values of the elevator rotational frequency and for three values of the horizontal tail pitch frequency. The analysis was conducted for a sea-level condition with the aerodynamic parameter (aspect-ratio corrections and effects of aerodynamic balance) neglected. Figures 59 through 61 present the results of the analysis for an elevator rotational frequency of 10 cps, while the same equivalent results for an elevator rotational frequency of infinity (locked elevator) are presented in Figures 62 through 64, with a cross plot of the overall effects shown in Figure 65.

4.3.2 Antisymmetric

The initial phase of the antisymmetric analysis was restricted to the basic vertical tail, assumed cantilevered at the fuselage-vertical stabilizer intersection. This analysis included the effects of a flexible horizontal stabilizer. The second phase included fuselage effects and also aircraft rigid body degrees of freedom.

4.3.2.1 Cantilevered Analysis

As in the symmetric analysis, the large number of parameters included in the flutter analysis of the empennage, such as elevator and rudder rotational frequency, horizontal tail yawing and rolling, density, and aerodynamic parameters (aspect-ratio corrections and effect of aerodynamic balance) precluded an extensive variation of these parameters. Therefore, only the parameters considered significant were varied. Only incompressible aerodynamic coefficients were used in this analysis, with aspect ratio effects and aerodynamic balancing effects ignored. The end-plating of the vertical tail by the tip-mounted, horizontal tail fully justified the use of the two-dimensional strip theory, while the neglect of the aerodynamic balance was felt to be of small concern in the overall analysis.

Figures 66 and 67 present the results of the cantilevered analysis of the empennage for a rigid body yawing frequency of 10 and 20 cps. As explained in Paragraph 4.3.2, the effects of a flexible horizontal stabilizer were included, in addition to the rigid body modes of flapping (rocking) and yawing. Antisymmetric motion of the elevators was included, with the frequency taken as 15 cps. Variations of the frequency of the latter mode, as shown in initial analyses not presented in this report, indicated no change in flutter mode or speed. Similar

earlier studies of rudder frequency variations showed the same results; therefore, the rudder rotational frequency was held to 10 cps for the analysis. Horizontal tail flapping was held to 10 cps, which was felt to be reasonable for the large rolling moment of inertia involved. Studies of variations of this parameter in initial analyses also indicated no change in flutter speed or mode.

4.3.2.2 Free-Free Analysis

As explained in Paragraph 3.3.2, because of the large number of coordinates required to define adequately the antisymmetric motion of the empennage, which would include effects of fuselage stiffness and also aircraft rigid body modes, it is a practical impossibility to vary all unknown parameters. Therefore, certain values of these parameters were fixed, based on initial analyses of the empennage assumed cantilevered from the fuselage. With this in mind, several analyses were performed for two values of the horizontal tail yawing frequency. All other structural parameters, such as rudder and elevator rotational frequency and horizontal tail flapping, were held to certain values in the modal coupling for the purpose of determining the set of new generalized coordinates required for the flutter analysis. As in the cantilevered analysis, only incompressible aerodynamic coefficients were used, with aspect ratio effects and aerodynamic balancing effects ignored.

Figures 68 and 69 present the results of the free-free antisymmetric analysis of the empennage for a horizontal tail yawing frequency of 10 and 20 cps, respectively. The parameters held fixed were rudder rotation of 10 cps, elevator rotation (assumed antisymmetric motion) of 15 cps, and a horizontal tail flapping frequency of 10 cps. The latter parameters were included in the modal coupling and were consequently reflected in the six antisymmetric fuselage-empennage modes used as generalized coordinates for the flutter analysis.

BLANK PAGE

5.0 CONCLUSIONS

Because of the manner in which the preliminary flutter analysis of the empennage was conducted, i. e., a breaking down into initial component analysis, conclusions may best be drawn based on the results presented in Section 4.0.

5.1 SYMMETRIC ANALYSIS - CANTILEVERED CONDITION

Figures 26 through 58 present the V-g plots of these analyses, in addition to cross-plots for over all evaluation. These initial analyses, preliminary in nature and done at a time when only parametric studies can be made, indicate (Figure 44) that the controlling parameter on the flutter speed of the horizontal tail is that of the horizontal tail rigid body pitch frequency.

Figure 58 presents the proposed flight boundary of the XV-5A aircraft; a 15% flutter margin on the limit dive speed at sea-level is 575 knots. The 15% requirement on V_L therefore necessitates a horizontal tail pitch frequency of approximately 55 cps, based on incompressible theory. The trend of the plots shown in Figure 44 shows that, as the pitch frequency is increased from a low value to the upper value, the flutter speed approaches the basic bending torsion flutter speed of the surface. The mode of flutter involved is that of horizontal tail pitch coupled with the first coupled elastic mode of the horizontal tail. The mode shapes of this mode are presented in Figure 11. It should be noted that this mode exhibits both a bending and torsion component, the shapes of which are characteristic of the first uncoupled bending and torsion modes of a cantilever beam. At 60 cps pitch frequency, the flutter frequency is 40 cps. Referring to Figure 29, the V-g plot for this condition shows that the 3rd root is the flutter mode. Tracing this plot back to zero airspeed, we find that the coupled mode of vibration is approximately 63 cps. Solution of the equations of motion for zero aerodynamics yields approximately the same results (65 cps). This result indicates a coupling between the pitch mode and the torsion component of the first coupled horizontal tail elastic mode. This effect is shown in Figure 45. Note that the frequencies of both the coupled and uncoupled elastic modes of the horizontal stabilizer are plotted against the results of coupling the elastic modes with a variable horizontal tail pitch frequency, for a constant elevator rotational frequency of 10 cps. From this plot, it can be seen that the mode of flutter of the horizontal tail would be dependent on the available horizontal tail

pitch frequency. For a low value of pitch frequency the bending mode would predominate, whereas, for a higher value of pitch frequency, the torsion mode would be predominant. This effect is evident also in Figures 26 through 39.

Variations of the elevator rotational frequency of 10 cps, 30 cps, and finally locking out of the elevator (infinite restraint) showed no appreciable change in the flutter trends of the surface.

Changes in the aerodynamic parameters shown in Figure 44 also showed no appreciable change in the basic flutter trend.

Altitude trends are shown mainly to present the data. These indicate increasing flutter speeds, as is normal.

Compressible analyses were conducted, since the design flight envelope (see Figure 58) encompasses the high subsonic region and the initial incompressible analyses indicated that a relatively high-pitch frequency was required. Figure 58 presents the results of these analyses for an assumed horizontal tail pitch frequency of 60 cps. The $M = 0$ results from Figure 29 and Figures 41 through 43 are also plotted. The trend of the plots indicates the usual drop in flutter speed as the transonic region is approached. Crossing of a flutter plot for a particular altitude with the altitude line radiating from the origin yields only one or two true flutter speeds (extrapolated for the sea-level and 9300' altitude). The boundary defined by these points lies within the 15% margin on equivalent airspeed, which indicates that a possible flutter situation might exist on the XV-5A aircraft if the design flight envelope is to be met.

5.2 SYMMETRIC ANALYSIS - FREE-FREE CONDITION

Figures 59 through 65 present the V-g plots of these analyses, along with a cross-plot for various elevator rotational frequencies, for three values of the horizontal tail pitch frequency. The lower boundary of Figure 65 (for an elevator frequency of 10 cps) is relatively insensitive to horizontal tail pitch frequency, whereas the upper boundary exhibits the same trend as for the cantilevered analysis (Figure 44). The flutter mode for the lower boundary is fuselage bending coupled with elevator rotation. However, raising the damping level by 0.03 (from $g = 0$), eliminates this boundary, and the flutter mode is now in effect, essentially the same as shown for the cantilevered case. That is, the flutter mode is horizontal tail pitch coupled with predominant horizontal tail torsion for the higher pitch frequencies.

5.3 ANTISYMMETRIC ANALYSIS - CANTILEVERED CONDITION

Figures 66 and 67 present the V-g plots of the initial analysis of the empennage. Results indicate a stable system throughout the proposed flight envelope for anticipated yaw frequencies of 10 and 20 cps. Early preliminary analyses of the vertical tail with and without the effects of an elastic horizontal tail showed a low flutter speed which necessitated increasing the torsional stiffness of the vertical stabilizer. Figure 9 shows the increased tip stiffness resulting from this earlier study. The results shown in Figures 66 and 67 reflect this latter stiffness distribution.

5.4 ANTISYMMETRIC ANALYSIS - FREE-FREE CONDITION

Effects of fuselage elasticity and aircraft rigid body modes on the antisymmetric flutter characteristics of the empennage, as shown in Figures 68 and 69, indicate also a stable system throughout the design flight envelope of the XV-5A aircraft.

5.5 OVERALL EVALUATION

Basic trends shown by the preliminary empennage flutter analysis indicate possible existence of a flutter situation which is dependent upon establishment of the actual pitch frequency of the horizontal tail. The required pitch frequency is approximately 55 cps, based on the results of the symmetric cantilevered analysis. Compressible analyses indicate a required pitch frequency of somewhat greater than 55 cps; however, if one were to determine the required pitch frequency at a structural damping level of 0.03 (see Figures 59 through 61), the required frequency would be of the order of 55 cps. In all, the analyses presented in this report should be taken as a preliminary evaluation of the empennage. Subsequent analytical and experimental investigations should be directed toward finalization of the actual flutter characteristics of the XV-5A aircraft with due regard toward the findings presented in this report.

BLANK PAGE

6.0 APPENDIX

6.1 LIST OF REFERENCES

1. Report 163, "Preliminary Flutter Analysis, Volume I-Wing, November, 1965.
2. Smilg, B. and Wasserman, L.S.: "Application of Three-Dimensional Flutter Theory to Aircraft Structures." Air Force Technical Report 4798, 1942.
3. Wasserman, L.S., Mykytow, W. J. and Spielberg, I.N.: "Tab Flutter Theory and Applications." Air Force Technical Report 5153, 1944.
4. No Author: "Tables of Aerodynamics Coefficients for an Oscillating Wing-Flap System in a Subsonic Compressible Flow." National Aeronautical Research Institute (N. L. L.) Report F. 151, May, 1954.
5. Timman, R., Van de Vooren, A. I.: "Theory of the Oscillating Wing With Aerodynamically Balanced Control Surface in a Two-Dimensional, Subsonic, Compressible Flow." National Aeronautical Research Institute (N. L. L.) Report F. 54, June, 1949.

6.2 **TABLES**

TABLE 1

**MASS AND INERTIA DISTRIBUTION, HORIZONTAL TAIL,
SYMMETRIC ANALYSIS**

Horizontal Stabilizer and Elevator (Balanced) - Distribution 3A

Node	Weight Lbs.	I_u Lb.-In. ²	I_v Lb.-In. ²	R_{uv} Lb.-In. ²	S_u Lb.-In.	S_v Lb.-In.
0	12.37	372.6	3541.3	546.3	17.51	102.65
1	6.64	81.9	1848.9	306.4	10.03	58.72
2	6.00	70.9	1365.1	228.8	6.52	38.24
3	5.25	57.9	1070.6	179.7	5.20	30.46
4	5.40	51.0	1008.5	170.0	6.31	36.96
5	5.07	42.6	865.8	145.8	6.49	37.99
6	3.90	30.1	560.1	93.6	4.16	24.34
7	3.93	28.3	584.8	80.0	3.71	21.72
8	3.36	23.6	358.7	58.4	2.96	17.36
9	4.85	50.5	479.3	68.6	3.78	22.16
10	0.00	0.0	0.0	0.0	0.00	0.00
Σ	* 56.77	808.4	11583.1	1877.6	66.67	390.60

Elevator - Distribution 3A

Item	Elevator and Balance Weights			Balance Weights Only		
Node	Weight Lbs.	I_w Lb.-In. ²	S_w Lb.-In.	Weight Lbs.	I_w Lb.-In. ²	S_w Lb.-In.
0	2.36	24.35	0.0	0.42	4.83	- 1.43
1	2.68	60.73	0.0	0.97	10.99	- 3.27
2	1.97	48.58	0.0	0.79	7.95	- 2.51
3	1.79	43.69	0.0	0.76	6.97	- 2.31
4	1.98	35.88	0.0	0.68	5.50	- 1.94
5	2.04	32.97	0.0	0.64	4.77	- 1.75
6	1.57	27.97	0.0	0.58	3.76	- 1.48
7	1.61	26.55	0.0	0.55	4.90	- 1.82
8	1.59	21.11	0.0	0.51	2.44	- 1.12
9	0.64	4.76	0.0	0.16	0.69	- 0.33
10	0.00	0.00	0.0	0.00	0.00	0.00
Σ	18.23	326.59	0.0	6.06	52.80	-17.46

*Reflects an elevator weight of 18.25 lbs. including balance weights

TABLE 2
 MASS AND INERTIA DISTRIBUTION, FUSELAGE, SYMMETRIC ANALYSIS

Item Node	Fuselage		Wing		Horizontal Stabilizer		Vertical Stabilizer		Total Fuselage		
	Weight Lbs.	I _y Lb.-In. ²	Weight Lbs.	I _y Lb.-In. ²	Weight Lbs.	I _y Lb.-In. ²	Weight Lbs.	I _y Lb.-In. ²	Weight Lbs.	I _y Lb.-In. ²	S _y Lb.-In.
0	14.30								14.30		
1	80.25								80.25		
2	188.75								188.75		
3	287.47								287.47		
4	877.18								877.18		
5	888.41								888.41		
6	1025.23								1025.23		
7	733.38								733.38		
8		2712570							2676.27	2712570	
9	709.95								709.95		
10	860.91								860.91		
11	287.40								287.40		
12	121.80								121.80		
13	93.48								93.48		
14	44.97								44.97		
15			115.85	1274471	5486		118.79	437249	234.64	1711720	8125
16	26.36								26.36		
17	7.67								7.67		
Σ	6247.51	2712570	115.85	1274471	5486		118.79	437249	9158.42	4424290	8125

TABLE 3

**MASS AND INERTIA DISTRIBUTION, HORIZONTAL TAIL,
ANTISYMMETRIC ANALYSIS**

Horizontal Stabilizer and Elevator (Balanced) - Distribution 2

Node	Weight Lbs.	I_u Lb.-In. ²	I_v Lb.-In. ²	I_z Lb.-In. ²	P_{uv} Lb.-In. ²	S_u Lb.-In.	S_v Lb.-In.
0	12.35	299.0	2907.8	3006.4	337.0	14.52	85.04
1	6.97	109.4	2274.8	2320.7	243.7	12.77	74.81
2	6.16	76.9	1669.8	1700.6	218.1	8.40	49.21
3	5.42	61.1	1160.1	1184.6	163.7	5.73	33.54
4	5.47	45.1	963.1	983.9	121.8	5.68	33.29
5	5.23	39.3	991.3	1014.4	104.3	7.79	45.64
6	4.07	30.0	618.9	635.5	70.7	4.83	28.32
7	4.12	25.7	491.7	505.4	55.6	4.02	23.59
8	3.54	25.1	446.3	459.9	49.9	3.96	23.20
9	4.62	44.9	444.8	469.4	39.2	3.96	23.21
10	0	2.2	22.0	23.2	1.9	0.20	1.15
Σ	*57.95	758.7	11990.6	12304.0	1405.9	71.86	421.00

Elevator - Distribution 2

Item Node	Elevator and Balance Weights			Balance Weights Only		
	Weight Lbs.	I_w Lb.-In. ²	S_w Lb.-In.	Weight Lbs.	I_w Lb.-In. ²	S_w Lb.-In.
0	2.42	30.79	-0.37	.544	6.248	-1.843
1	3.33	62.50	-1.96	1.545	17.552	-5.204
2	2.14	52.03	-0.57	.957	9.593	-3.029
3	1.98	43.84	-0.55	.947	8.602	-2.852
4	2.10	36.81	-0.35	.802	6.495	-2.282
5	2.25	35.66	-0.59	.847	6.302	-2.310
6	1.81	28.47	-0.57	.807	5.261	-2.059
7	1.87	26.46	-0.59	.807	4.595	-1.924
8	1.85	21.83	-0.43	.771	3.706	-1.689
9	.62	5.40	0.06	.135	0.591	-0.283
10	0	0	0	0	0	0
Σ	20.37	343.79	-5.92	8.162	68.945	-23.475

*Reflects an elevator weight of 20.37 lbs. including balance weights

TABLE 4

**MASS AND INERTIA DISTRIBUTION,
VERTICAL TAIL, ANTISYMMETRIC ANALYSIS**

Vertical Stabilizer and Rudder (Balanced) - Distribution 1

Node	Weight Lb.	I_u Lb.-In. ²	I_v Lb.-In. ²	P_{uv} Lb.-In. ²	S_u Lb.-In.	S_v Lb.-In.
0	0	0	0	0	0	0
1	0	0	0	0	0	0
2	21.76	981.0	14796.1	2661.7	12.4	77.39
3	16.89	622.9	9013.6	1435.8	2.1	13.59
4	14.02	437.1	6164.9	962.0	4.1	25.49
5	14.81	405.3	5394.1	827.6	2.3	14.29
6	10.47	265.3	3283.8	489.0	0.3	2.20
7	12.17	264.0	3442.0	522.9	0.3	1.93
8	14.78	297.2	3913.3	614.3	-7.7	-48.39
9	11.54	281.0	2783.6	454.5	-5.0	-31.70
10	0	0	0	0	0	0
Σ	116.44*	3553.8	48791.4	7967.8	8.8	54.80
10	102.3 ‡	137926.0 ‡	154726.0 ‡	9621.0 ‡	92.53 ‡	206.26 ‡

Rudder - Distribution 1

Item	Rudder and Balance Weights			Balance Weights Only		
Node	Weight Lbs.	I_w Lb.-In. ²	S_w Lb.-In.	Weights Lbs.	I_w Lb.-In. ²	S_w Lb.-In.
0	0	0	0	0	0	0
1	0(.0045)	0.3	-.0015	0	0	0
2	6.66	258.9	.4284	1.86	54.47	-10.34
3	3.78	184.2	-.8654	2.39	67.89	-12.80
4	3.49	171.3	-.8383	1.83	46.18	-9.29
5	3.32	111.4	-.9953	1.37	30.10	-6.41
6	2.06	69.2	-.6184	.95	18.20	-4.16
7	2.46	66.7	-.6704	1.13	18.21	-4.54
8	1.45	33.9	-.3380	.59	8.46	-2.23
9	0	0	0	0	0	0
10	0	0	0	0	0	0
Σ	23.22	895.9	-3.8989	10.12	246.51	-49.77

*Reflects a rudder weight of 20.85 lbs. including balance weights

‡Reflects horizontal tail lumped mass used for vertical stabilizer modal analysis

TABLE 5

MASS AND INERTIA DISTRIBUTION, FUSELAGE, ANTISYMMETRIC ANALYSIS

Item Node	Fuselage		Wing				Horizontal Stabilizer			Vertical Stabilizer		
	Weight Lbs.	I _X Lb.-In. ²	Weight Lbs.	I _X Lb.-In. ²	I _Z Lb.-In. ²	S _X Lb.-In.	Weight Lbs.	I _X Lb.-In. ²	I _Z Lb.-In. ²	Weight Lb.	I _X Lb.-In. ²	I _Z Lb.-In. ²
0	14.30	484										
1	80.25	34018										
2	188.75	84267										
3	287.47	126017										
4	877.18	387156										
5	888.41	269249										
6	1025.23	434862										
7	733.38	438267										
8	709.95	345643										
9	860.91	251607										
10	287.40	128358										
11	121.80	58261										
12	93.48	31011										
13	44.97	11955										
14	26.36	3442										
15	7.67	253										
*			1238.27	6479172	7184964	-14188						
*			1438.00	7528472	8348565	-16486						
*							102.32	1018489	337020	116.42	323775	108794
Σ	6247.51	2604850	2676.27	14007644	15533529	-30674	102.32	1018489	337020	116.42	323775	108794

*Treated as off-station loads in fuselage modal analysis

TABLE 5 (Continued)
MASS AND INERTIA DISTRIBUTION, FUSELAGE,
ANTISYMMETRIC ANALYSIS

Item	Total Fuselage			
Node	Weight Lbs.	I_X Lb.-in. ²	I_Z Lb.-in. ²	S_X Lb.-in.
0	14.30	484		
1	80.25	34018		
2	188.75	84267		
3	287.47	126017		
4	877.18	387156		
5	888.41	269249		
6	1025.23	434862		
7	733.38	438267		
8	709.95	345643		
9	860.91	251607		
10	287.40	128358		
11	121.80	58261		
12	93.48	31011		
13	44.97	11955		
14	26.36	3442		
15	7.67	253		
*	1238.27	6479172	7184964	-14188
*	1438.00	7528472	8348565	-16486
*	218.74	1342264	445814	
Σ	9142.52	17954758	15979343	-30674

*Treated as off-station loads in fuselage modal analysis

TABLE 6

MODAL DATA, HORIZONTAL STABILIZER, SYMMETRIC ANALYSIS

B. L.	Node	1st Mode f = 29.5 cps		2nd Mode f = 91.4 cps		3rd Mode f = 110.9 cps	
		φ	$\Theta \times 10^2$	φ	Θ	φ	Θ
3.03	0	0	0	0	0	0	0
10.637	1	.009	.0336	-.0005	-.0072	-.0524	-.00445
18.244	2	.036	.0733	.0015	-.0154	-.1965	-.00892
25.851	3	.083	.1204	.0108	-.0245	-.4013	-.01264
33.458	4	.152	.1773	.0379	-.0345	-.6223	-.01448
41.065	5	.244	.2441	.0953	-.0449	-.7930	-.01179
48.672	6	.360	.3185	.1952	-.0552	-.8305	-.00131
56.279	7	.500	.4249	.3463	-.0685	-.6581	.02319
63.886	8	.658	.5486	.5447	-.0824	-.2460	.06244
71.493	9	.828	.6533	.7701	-.0936	.3506	.10275
79.100	10	1.000	.6533	1.0000	-.0936	1.0000	.10275

TABLE 7
MODAL DATA, FUSELAGE,
SYMMETRIC ANALYSIS

F. S.	Node	1st Mode	2nd Mode	3rd Mode	4th Mode
		f = 8.2 cps	f = 15.2 cps	f = 23.2 cps	f = 33.0 cps
		φ	φ	φ	φ
0	0	1.0000	1.0000	1.0000	1.0000
34.33	1	.7260	.5474	.3354	.0745
68.66	2	.4955	.2433	.0202	-.1329
102.99	3	.2890	.0120	-.1548	-.1440
137.33	4	.1211	-.1146	-.1637	-.0191
171.66	5	.0035	-.1222	-.0420	.0764
205.99	6	-.0794	-.0767	.0735	.0745
240.33	7	-.1164	-.0053	.0987	-.0028
258.34	8	-.1167	.0288	.0725	-.0336
274.66	9	-.1043	.0535	.0247	-.0409
308.99	10	-.0498	.0860	-.0851	-.0186
343.33	11	.0289	.0992	-.1943	.0389
377.66	12	.1262	.0913	-.2695	.1000
411.99	13	.2543	.0464	-.2690	.1414
446.33	14	.4083	-.0329	-.1829	.1426
459.37	15	.4739	-.0735	-.1204	.1249
480.66	16	.5789	-.1396	-.0062	.0780
514.99	17	.7539	-.2535	.1927	.0002

TABLE 8
MODAL DATA, HORIZONTAL STABILIZER,
ANTISYMMETRIC ANALYSIS

B. L.	Node	1st Mode f = 29.4 cps		2nd Mode f = 90.2 cps		3rd Mode f = 111.0 cps	
		φ	$\Theta \times 10^2$	φ	Θ	φ	Θ
3.03	0	0	0	0	0	0	0
10.637	1	.0089	.0368	-.0021	-.0068	-.0694	-.0045
18.244	2	.0365	.0805	-.0049	-.0144	-.2613	-.0088
25.851	3	.0838	.1322	-.0016	-.0226	-.5361	-.0117
33.458	4	.1526	.1947	.0180	-.0314	-.8357	-.0118
41.065	5	.2450	.2692	.0679	-.0407	-1.0747	-.0063
48.672	6	.3616	.3526	.1625	-.0493	-1.1495	.0100
56.279	7	.5012	.4721	.3121	-.0597	-.9632	.0463
63.886	8	.6594	.6141	.5153	-.0700	-.4771	.1041
71.493	9	.8285	.7255	.7536	-.0768	.2318	.1585
79.100	10	1.0000	.7320	1.0000	-.0771	1.0000	.1617

TABLE 9
 MODAL DATA, VERTICAL STABILIZER,
 ANTISYMMETRIC ANALYSIS

W. L.	Node	1st Mode f = 10.7 cps		2nd Mode f = 21.6 cps		3rd Mode f = 27.9 cps	
		φ	$\Theta \times 10^3$	φ	Θ	φ	$\Theta \times 10^2$
113.0	0	0	0	0	0	0	0
122.3	1	.0107	.0149	-.0030	-.0376	.0404	-.0058
131.6	2	.0427	.0322	-.0088	-.0811	.1543	-.0126
140.9	3	.0960	.0515	-.0122	-.1328	.3275	-.0232
150.2	4	.1682	.0745	-.0072	-.1958	.5394	-.0378
159.5	5	.2579	.1019	.0134	-.2727	.7703	-.0576
168.8	6	.3649	.1343	.0587	-.3687	.9991	-.0854
178.1	7	.4901	.1744	.1424	-.4917	1.1983	-.1233
187.4	8	.6356	.2128	.2888	-.6092	1.3235	-.1588
196.7	9	.8044	.2666	.5443	-.7610	1.3000	-.1973
206.0	10	1.0000	.3993	1.0000	-1.1071	1.0000	-.2674

TABLE 10
MODAL DATA, FUSELAGE, ANTISYMMETRIC ANALYSIS

F.S.	Node	1st Mode f = 5.6 cps		2nd Mode f = 13.6 cps		3rd Mode f = 20.6 cps		4th Mode f = 26.2 cps		1st Mode f = 13.9 cps		2nd Mode f = 19.0 cps		3rd Mode f = 29.0 cps		4th Mode f = 51.9 cps	
		ϕ	θ	ϕ	θ	ϕ	θ	ϕ	θ	ϕ	θ	ϕ	θ	ϕ	θ	ϕ	θ
0	0	1.0000		1.0000		1.0000		1.0000		1.0000		1.0000		1.0000		1.0000	
34.33	1	.5136		1.2562		-.2991		-.3002		.9940		.9887		.9735		.9152	
68.67	2	.0902		.0494		-.4657		-.3394		.9399		.8876		.7417		.2171	
103.00	3	-.0242		-.3981		-.0172		.1595		.8961		.8087		.5794		-.0527	
137.33	4	-.0244		-.2592		.0267		.1022		.8492		.7265		.4260		-.1784	
171.67	5	-.0232		-.1160		.0548		.0346		.7519		.5645		.1698		-.1150	
206.00	6	-.0196		.0226		.0489		-.0371		.6327		.3739		-.0918		.0102	
240.33	7	-.0134		.1192		.0168		-.0652		.1157		-.1654		-.0175		.0037	
274.67	8	-.0051		.1441		-.0207		-.0211		-.1325		-.4137		.0197		-.0006	
309.00	9	.0045		.1047		-.0462		.0425		-.2397		-.3653		.0193		-.0007	
343.33	10	.0149		.0160		-.0485		.0783		-.4514		-.2546		.0169		-.0007	
377.67	11	.0259		-.1172		-.0272		.0812		-.8242		-.0470		.0112		-.0006	
412.00	12	.0376		-.2926		.0187		.0450		-1.2946		.2204		.0035		-.0003	
446.33	13	.0499		-.5215		.1005		-.0561		-1.9423		.5912		-.0075		.0001	
480.67	14	.0625		-.7870		.2093		-.2106		-1.9454		.5930		-.0075		.0001	
515.00	15	.0755		-1.0771		.3353		-.3979		-1.9489		.5950		-.0076		.0001	

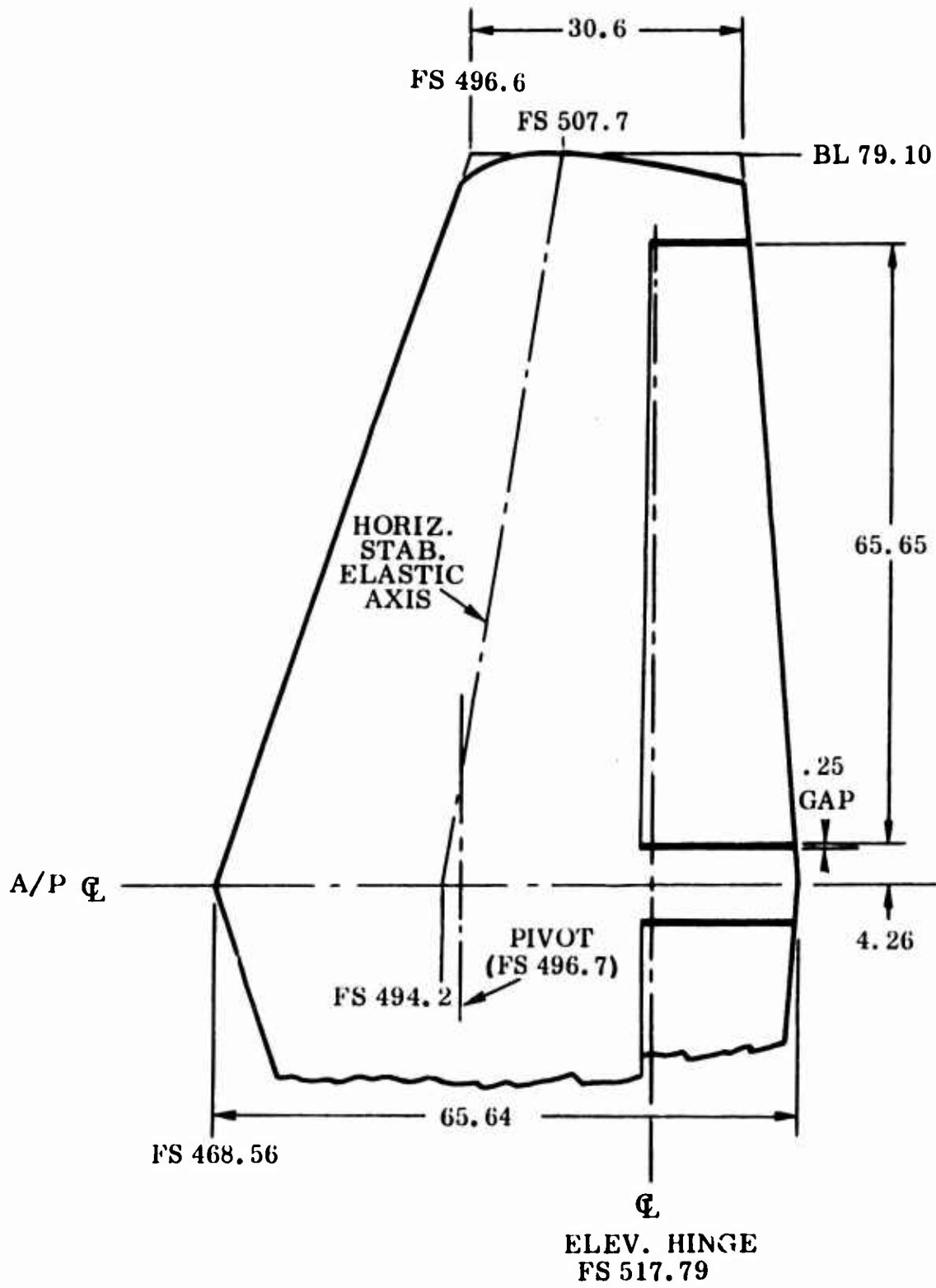


Figure 6 Planform Horizontal Tail

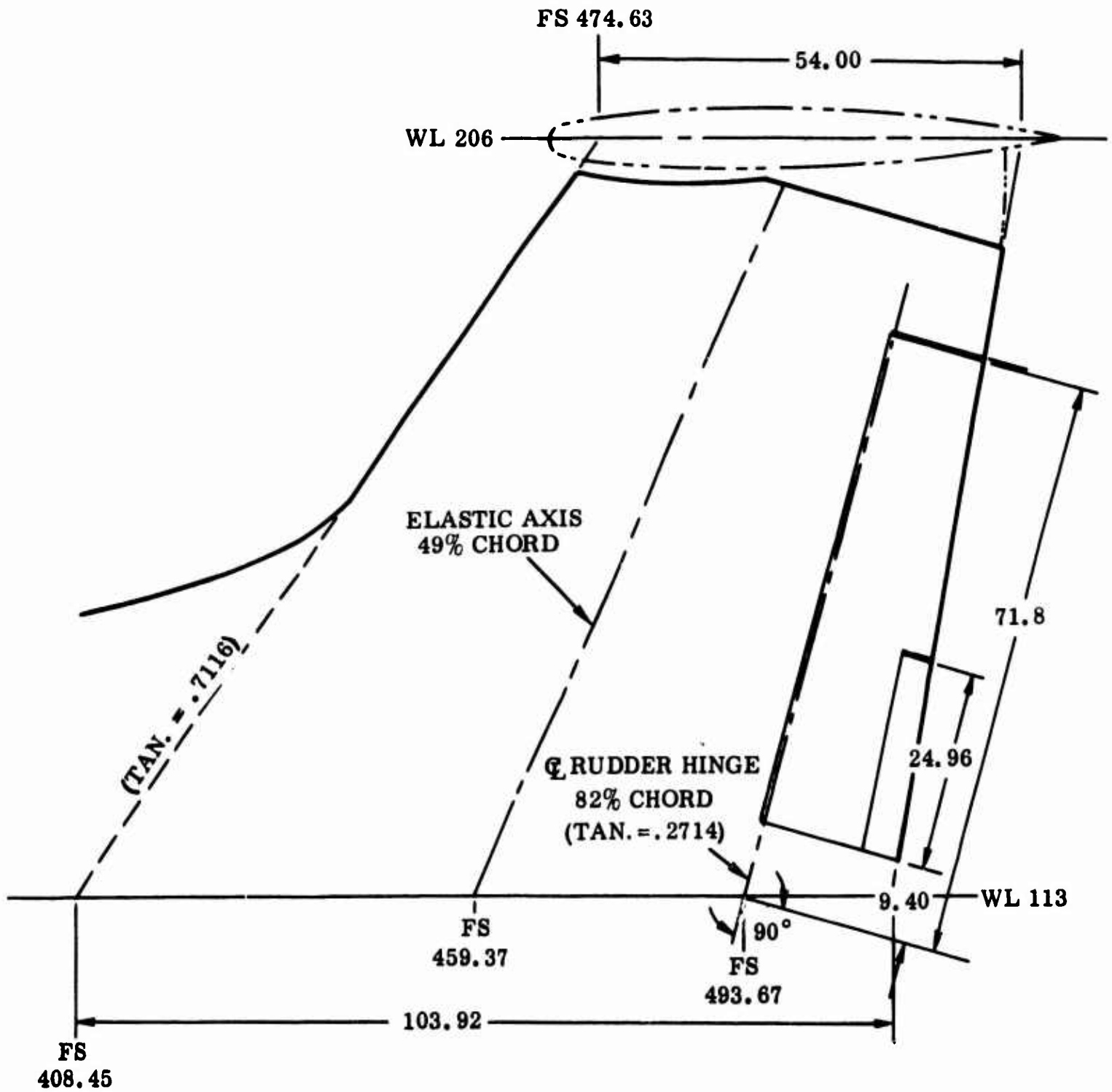


Figure 7 Planform Vertical Tail

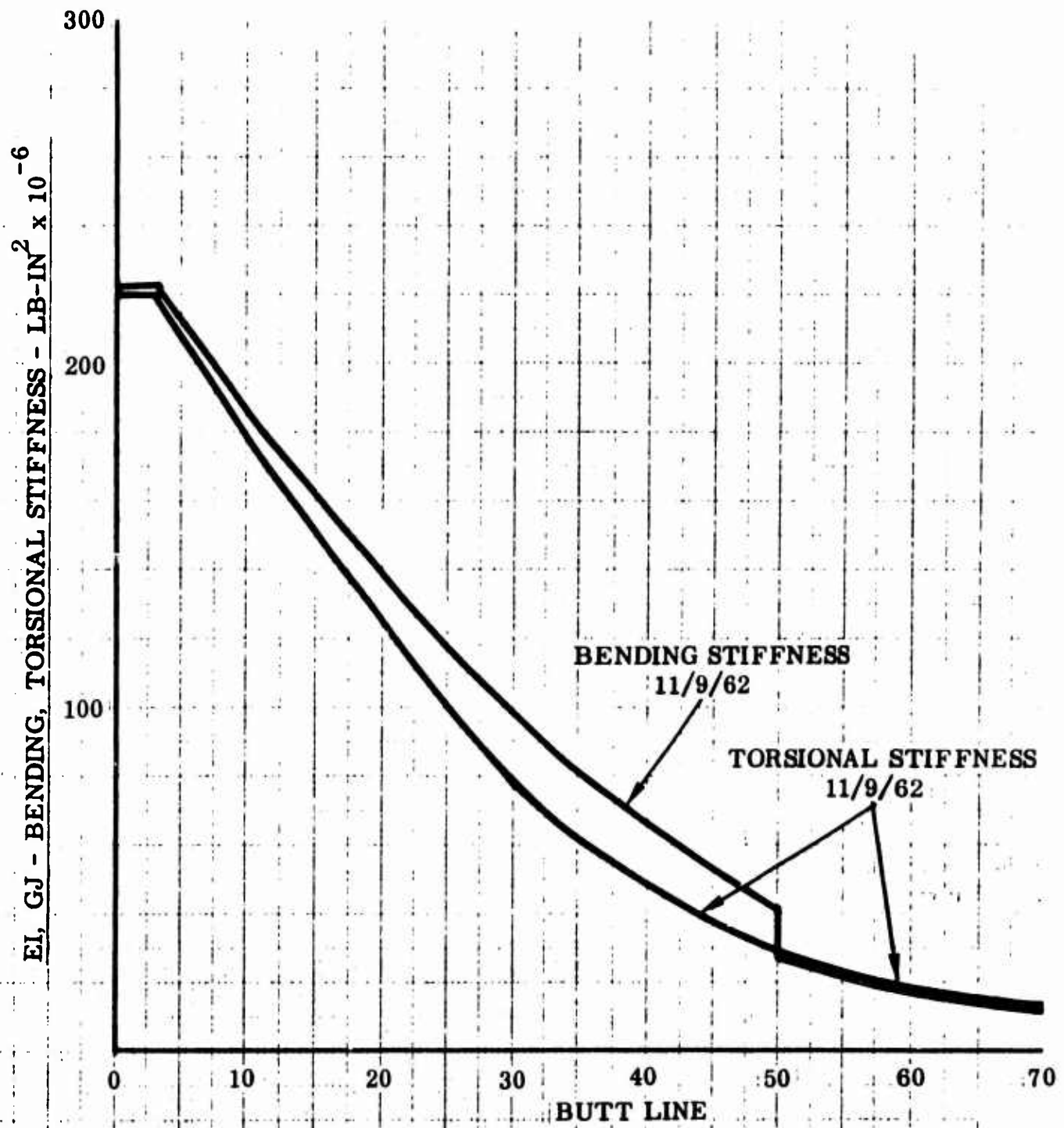


Figure 8 Stiffness Distribution - Horizontal Stabilizer

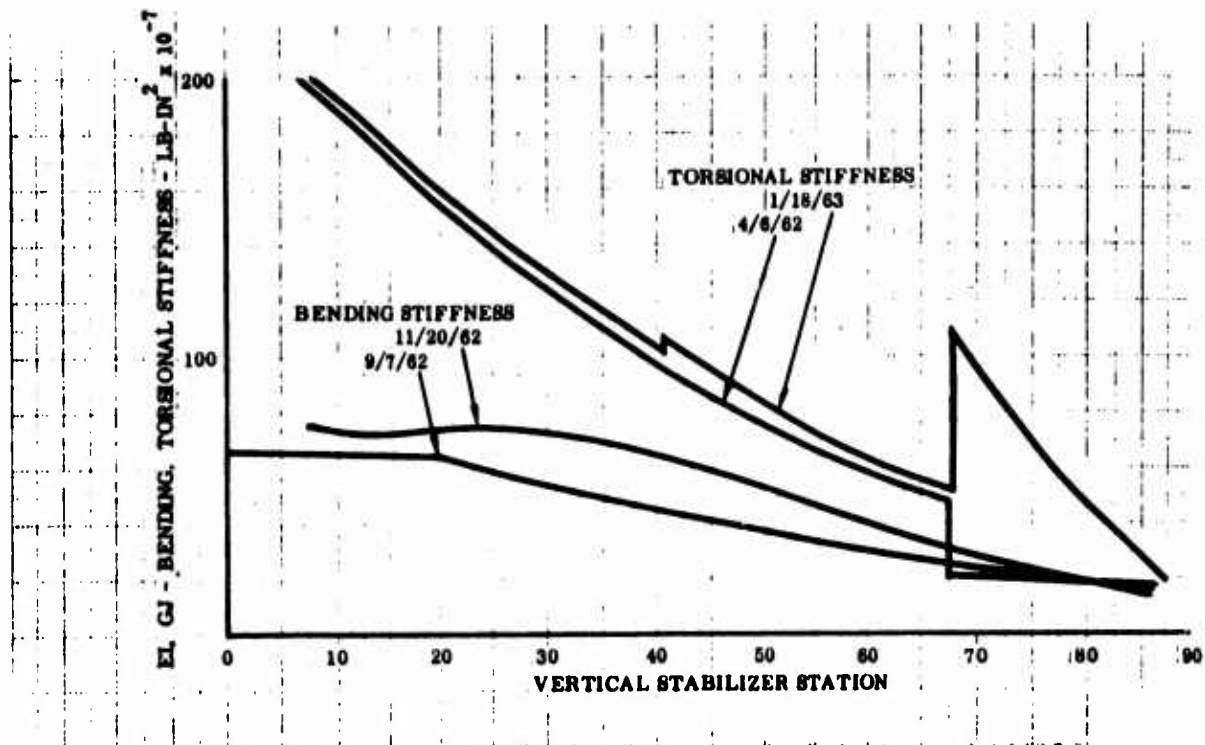


Figure 9 Stiffness Distribution - Vertical Stabilizer

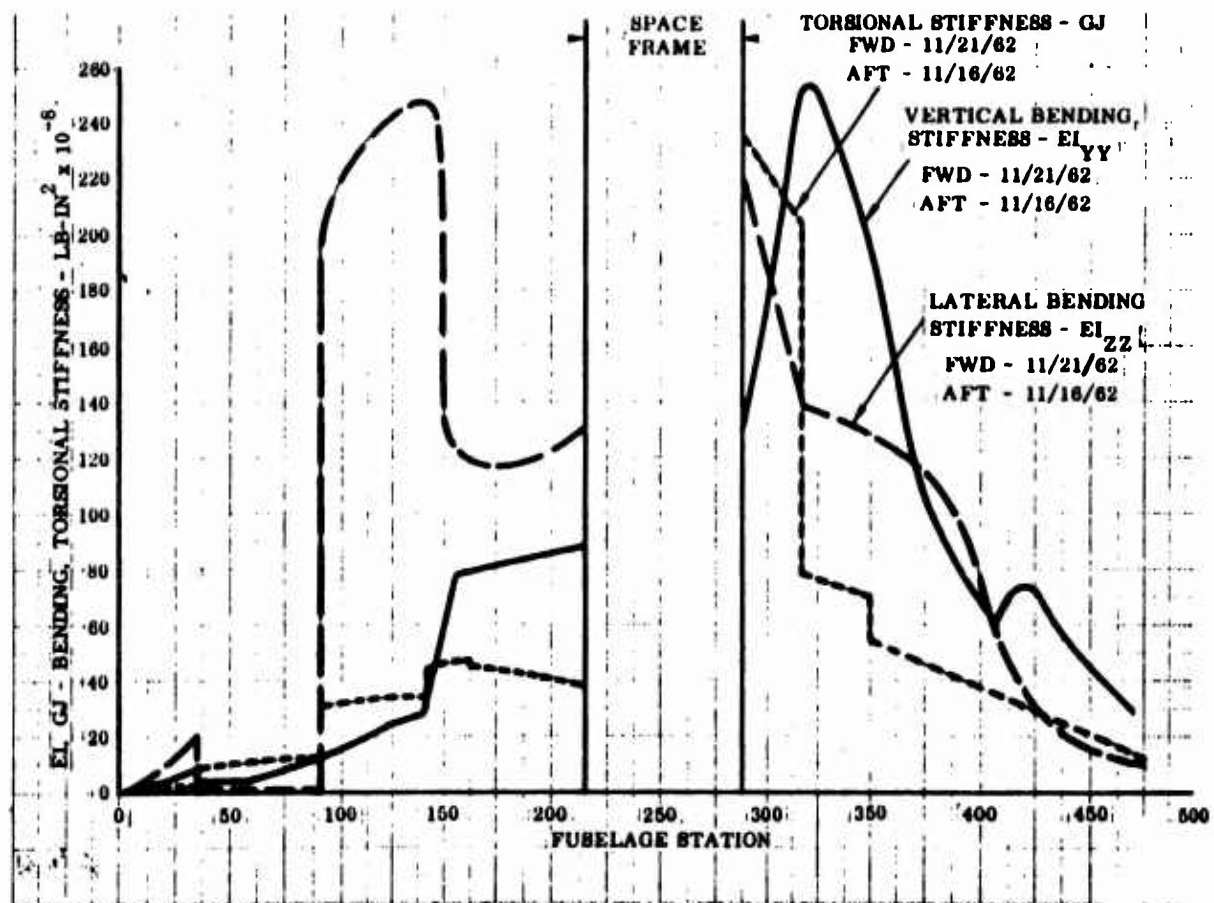


Figure 10 Stiffness Distribution - Fuselage

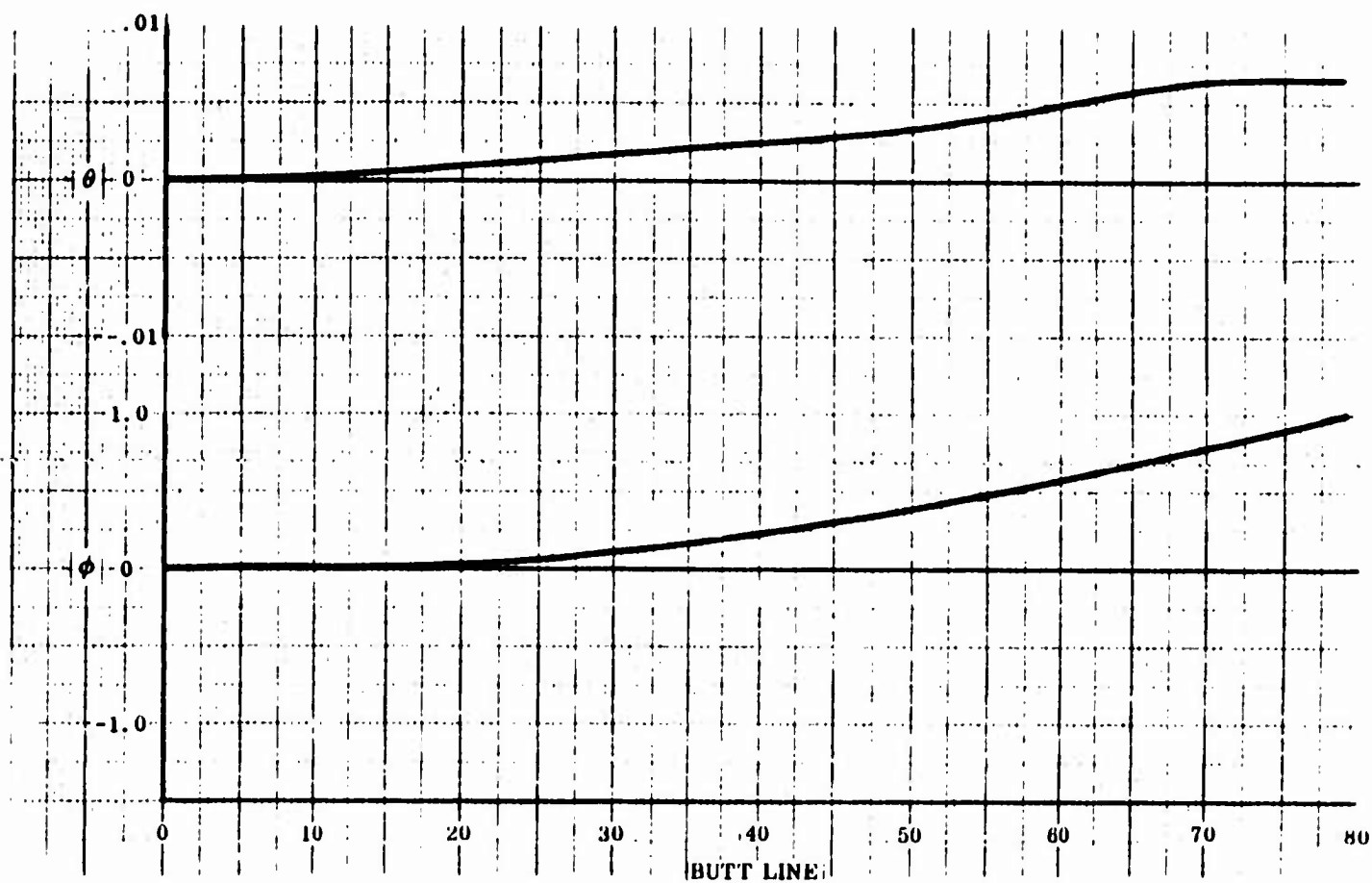


Figure 11 Mode Shapes - Horizontal Stabilizer - Symmetric Analysis
(Mode 1-f = 29.5 cps)

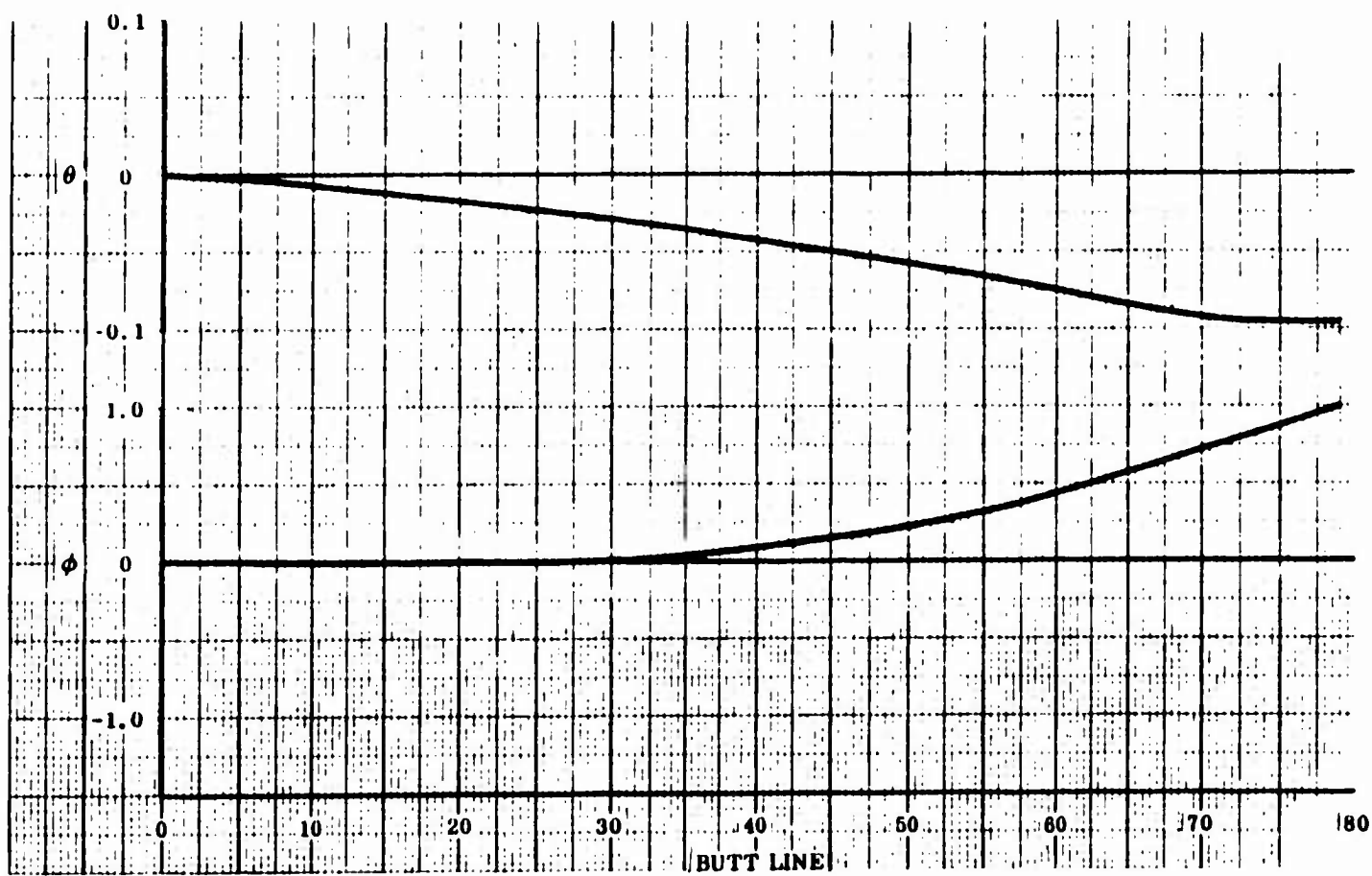


Figure 12 Mode Shapes - Horizontal Stabilizer - Symmetric Analysis
(Mode 2 - f = 91.4 cps)

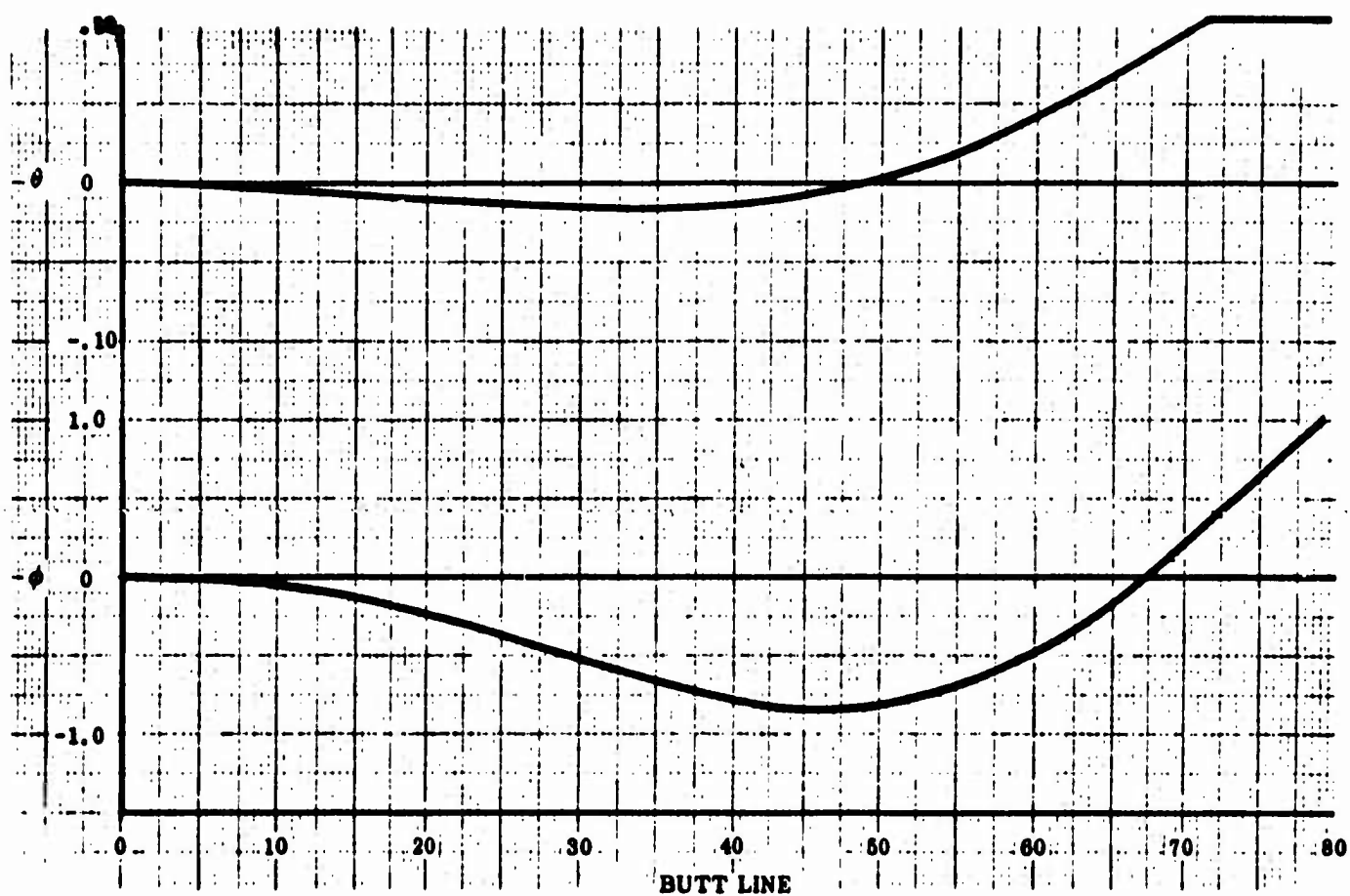


Figure 13 Mode Shapes - Horizontal Stabilizer - Symmetric Analysis
(Mode 3 - $f = 110.9$ cps)

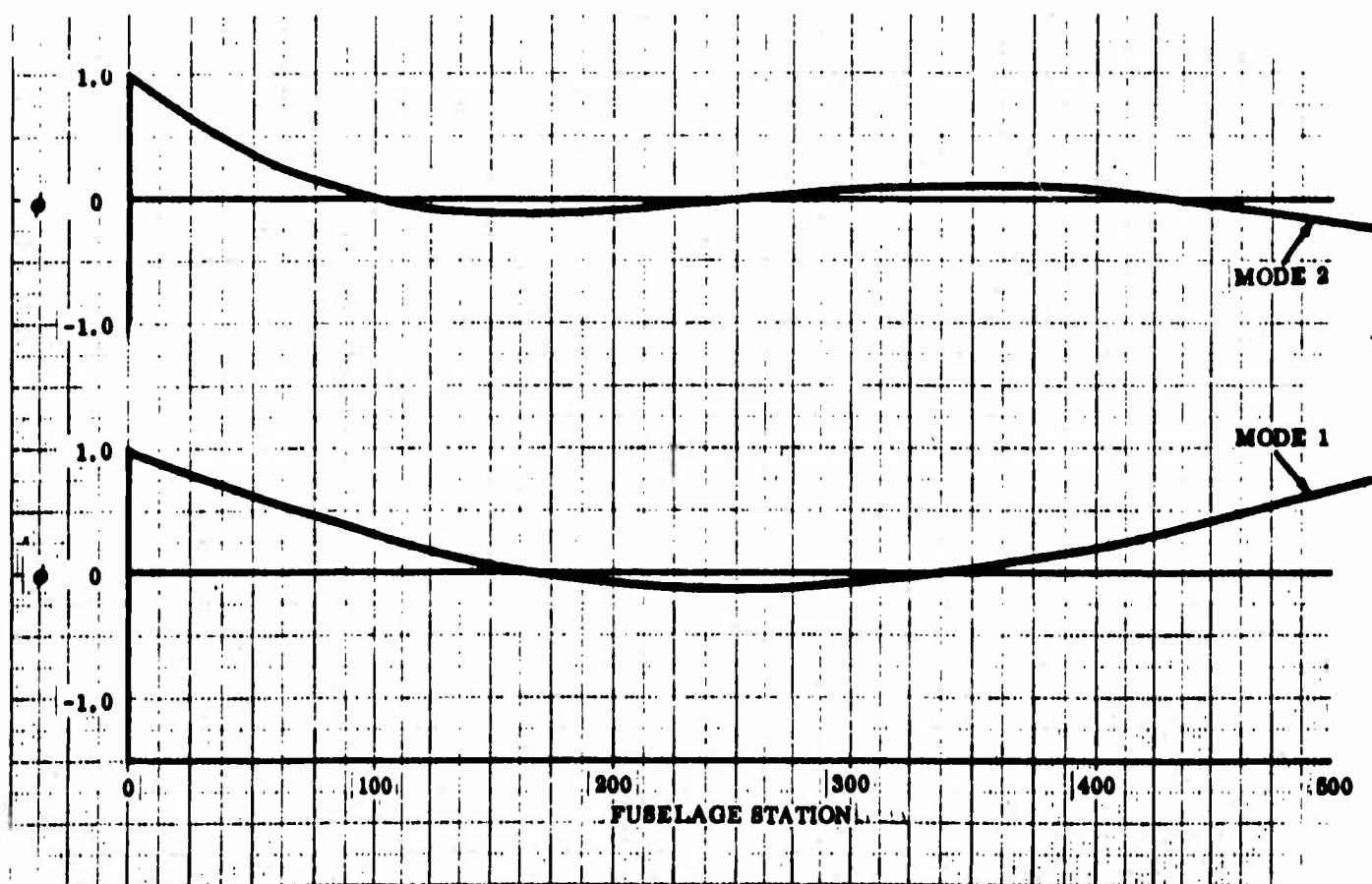


Figure 14 Mode Shapes - Fuselage - Symmetric Analysis
(Mode 1, $f = 8.2$ cps - Mode 2, $f = 15.2$ cps)

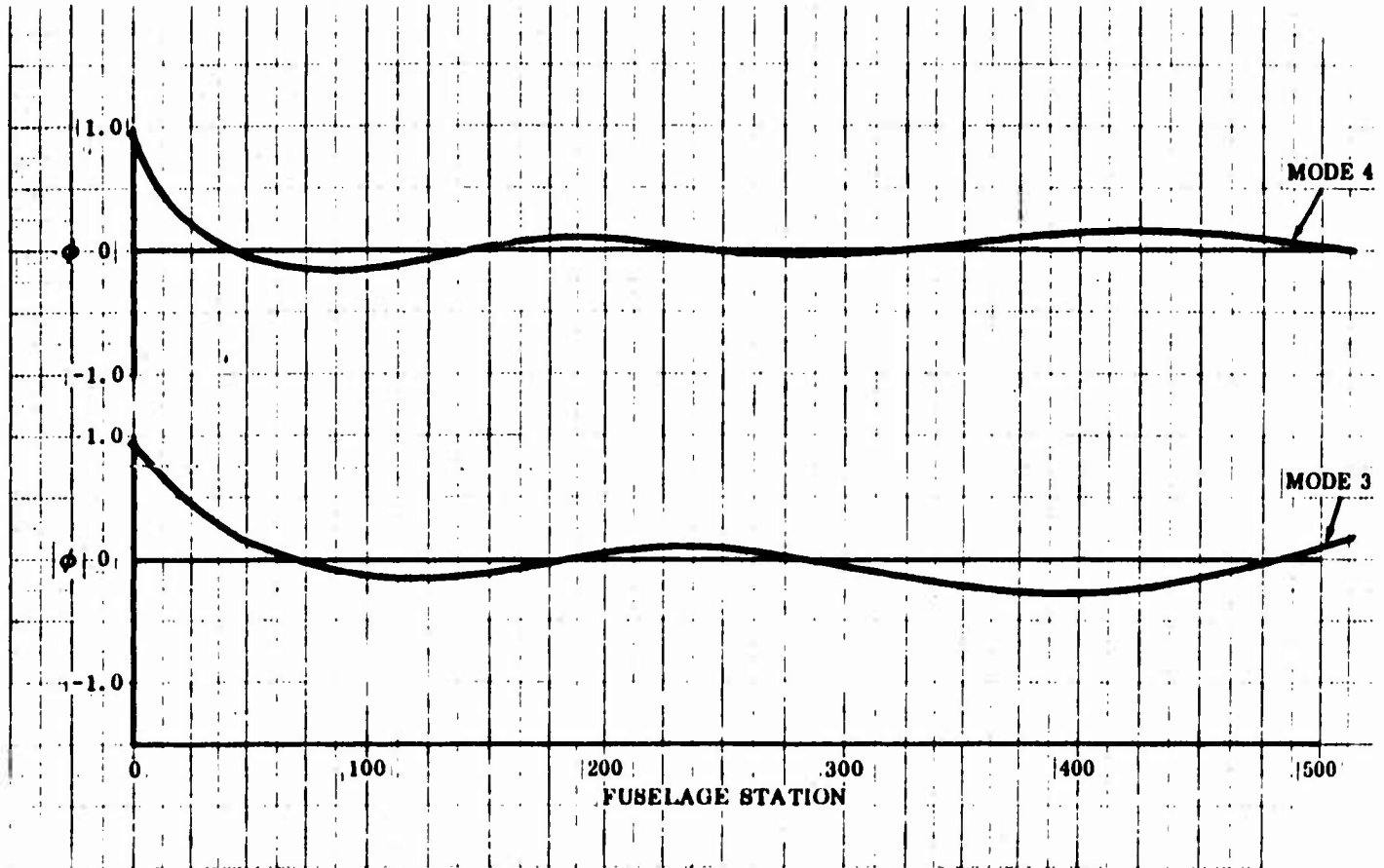


Figure 15 Mode Shapes - Fuselage - Symmetric Analysis
(Mode 3, $f = 23.2$ cps - Mode 4, $f = 33.0$ cps)

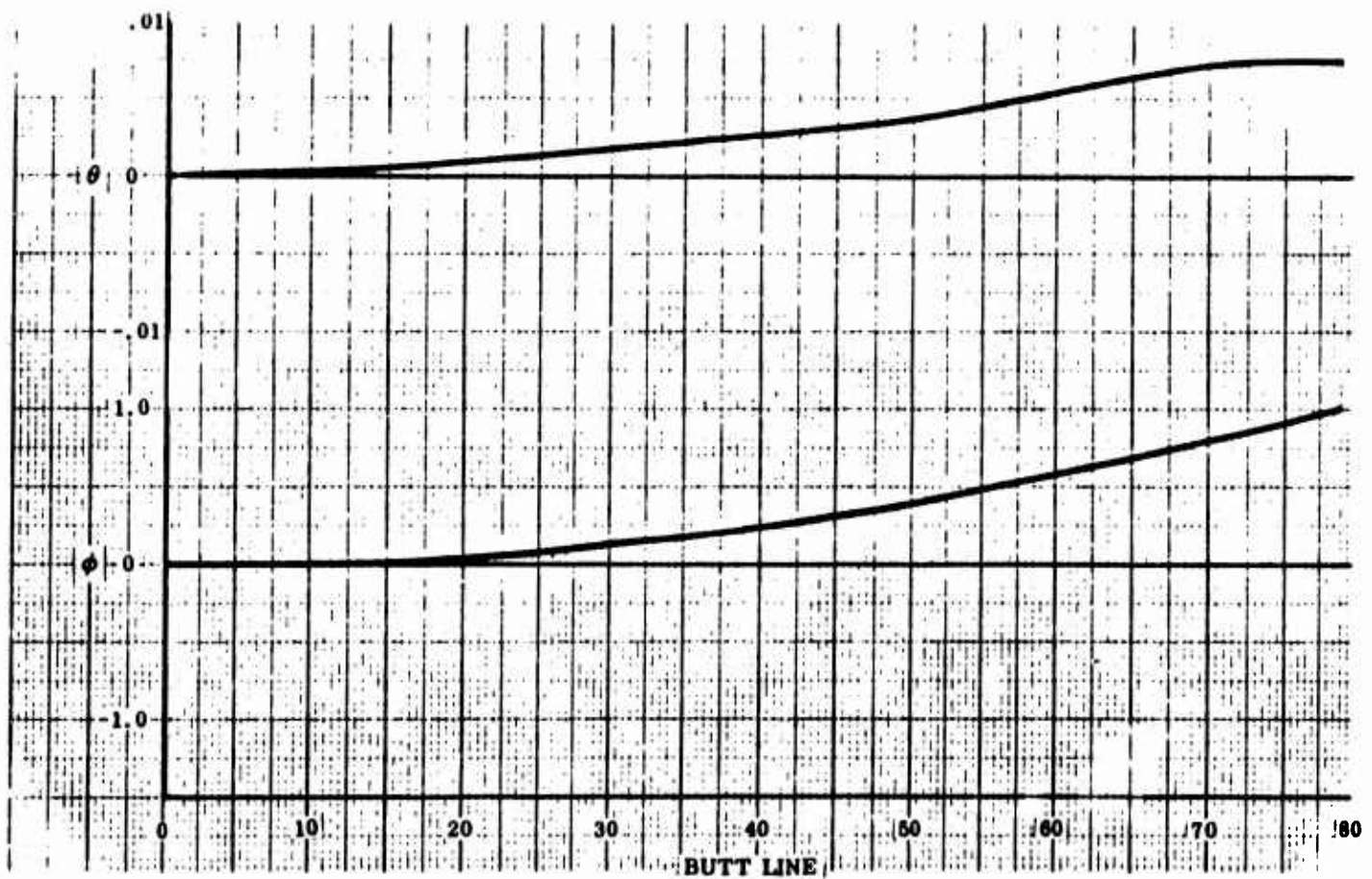


Figure 16 Mode Shapes - Horizontal Stabilizer - Antisymmetric Analysis
(Mode 1 - $f = 29.4$ cps)

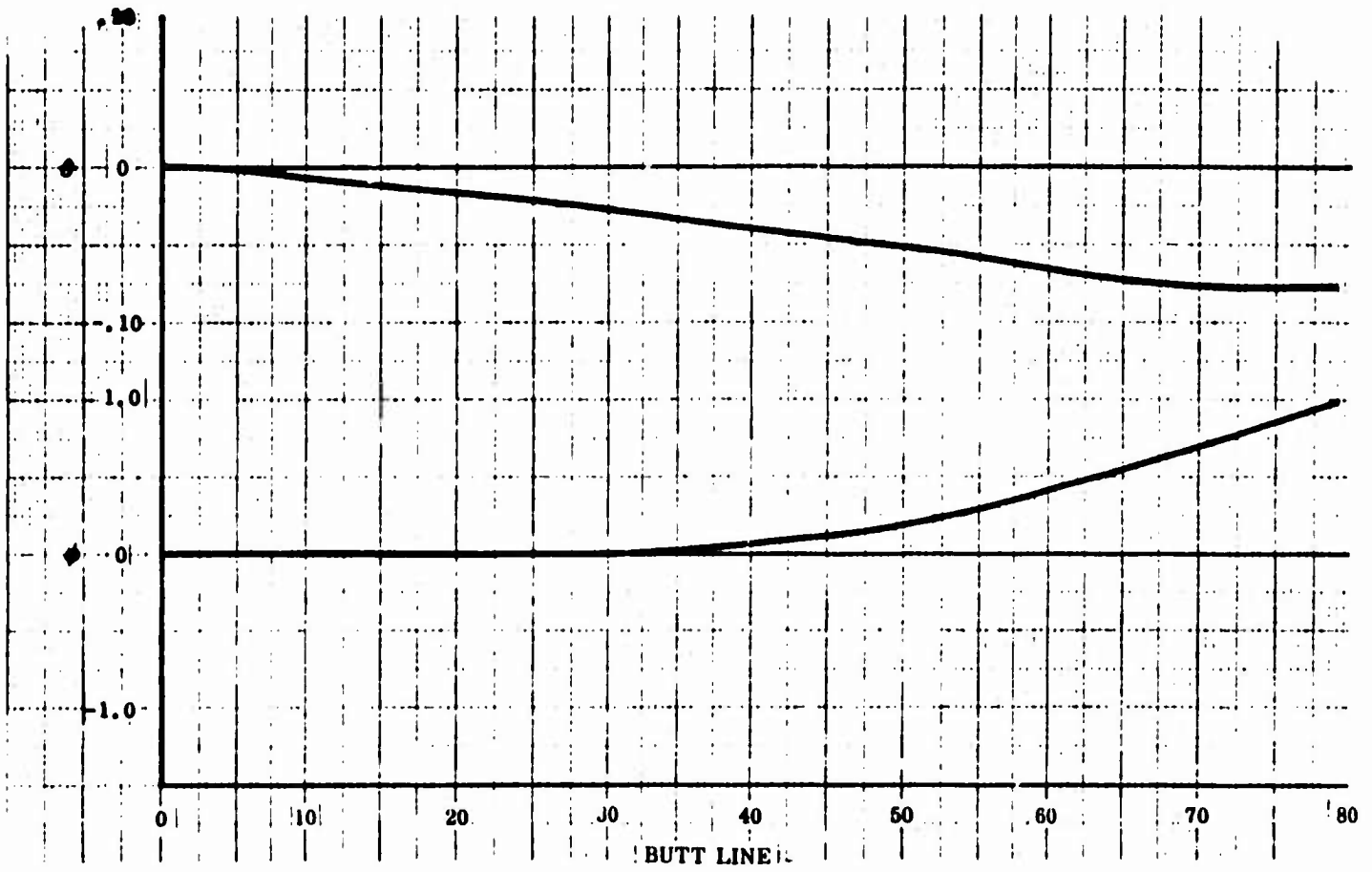


Figure 17 Mode Shapes - Horizontal Stabilizer - Antisymmetric Analysis
(Mode 2 - $f = 90.2$ cps)

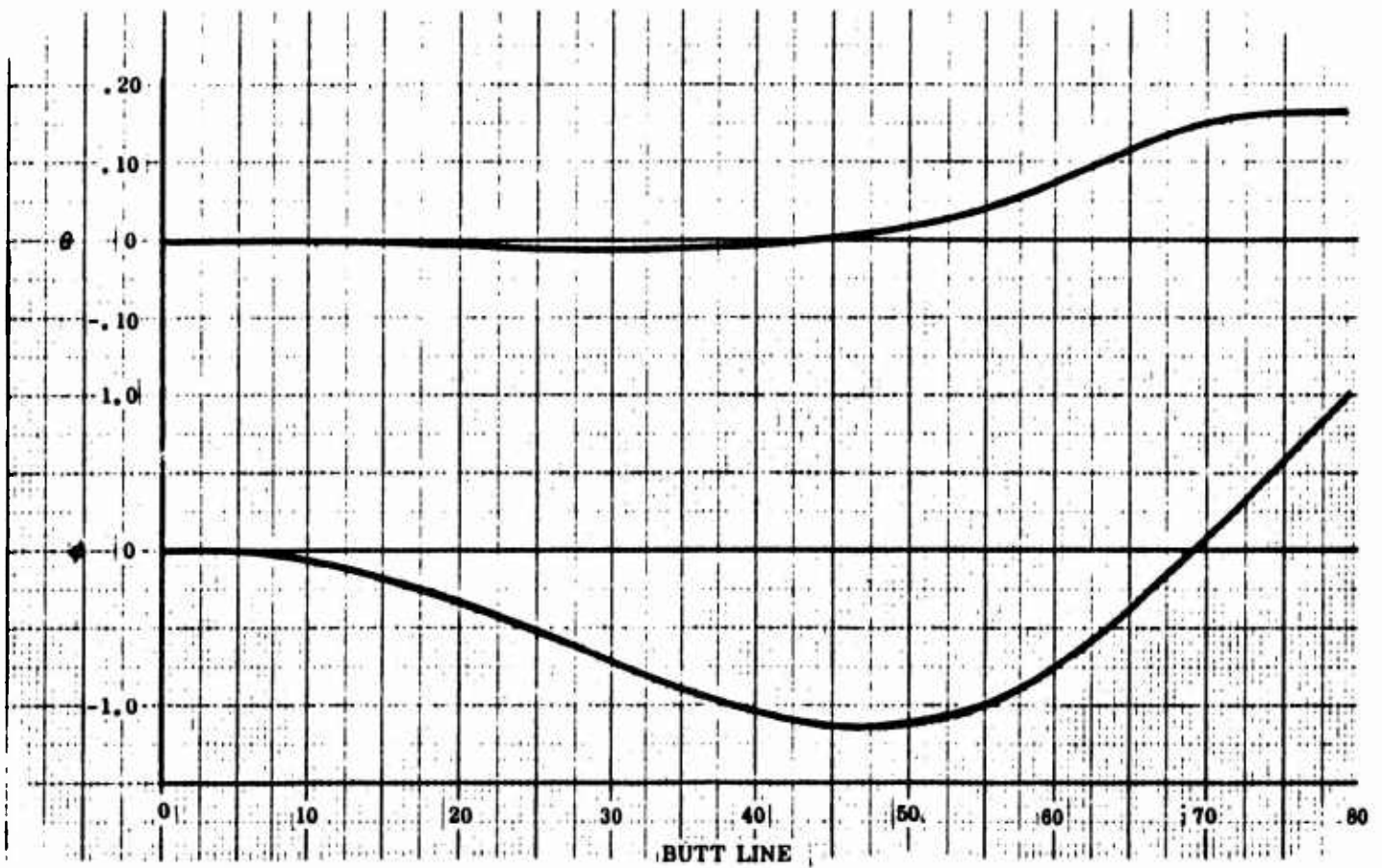


Figure 18 Mode Shapes - Horizontal Stabilizer - Antisymmetric Analysis
(Mode 3 - $f = 111.0$ cps)

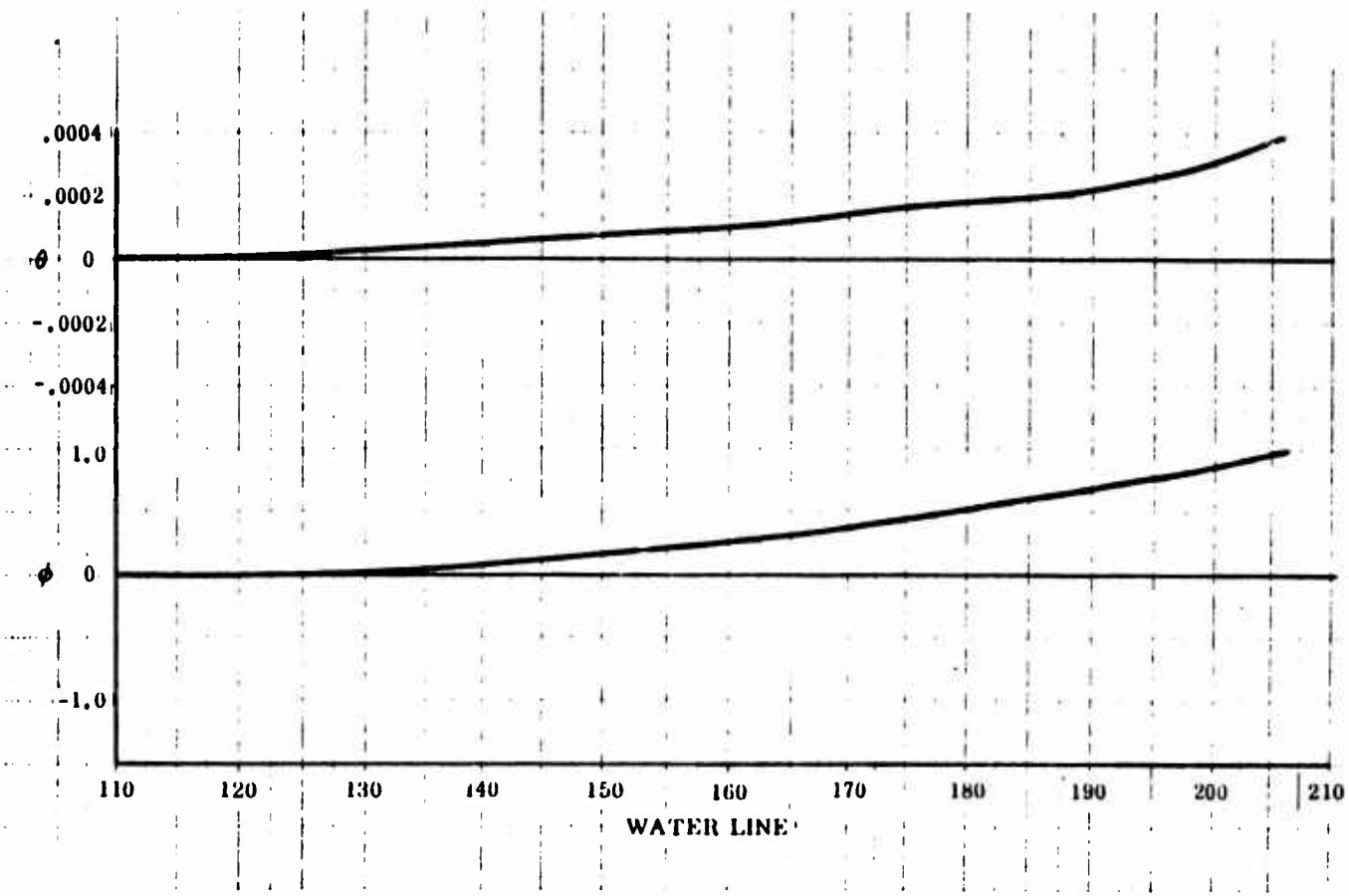


Figure 19 Mode Shapes - Vertical Stabilizer - Antisymmetric Analysis
(Mode 1 - $f = 10.7$ cps)

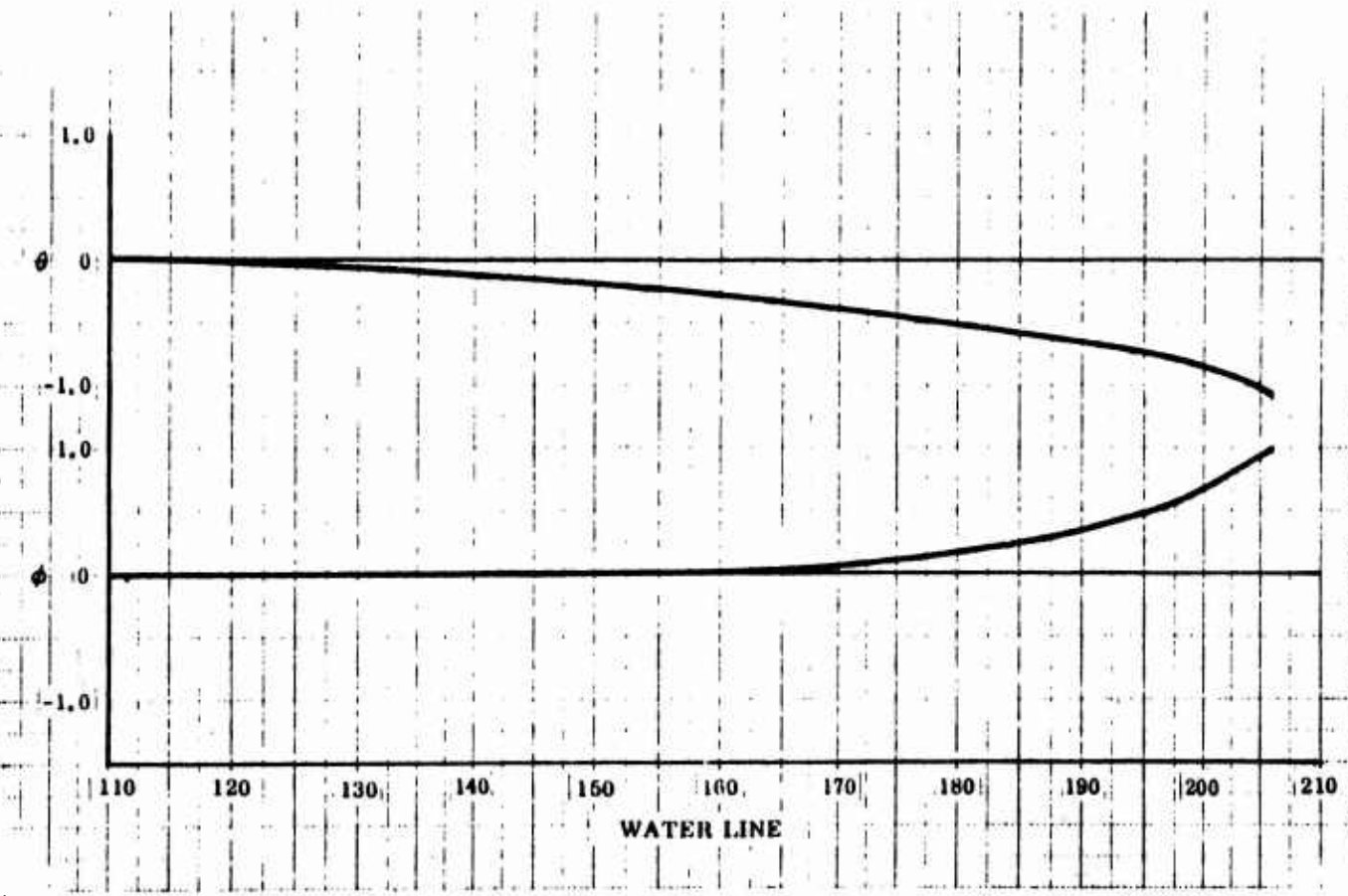


Figure 20 Mode Shapes - Vertical Stabilizer - Antisymmetric Analysis
(Mode 2 - $f = 21.6$ cps)

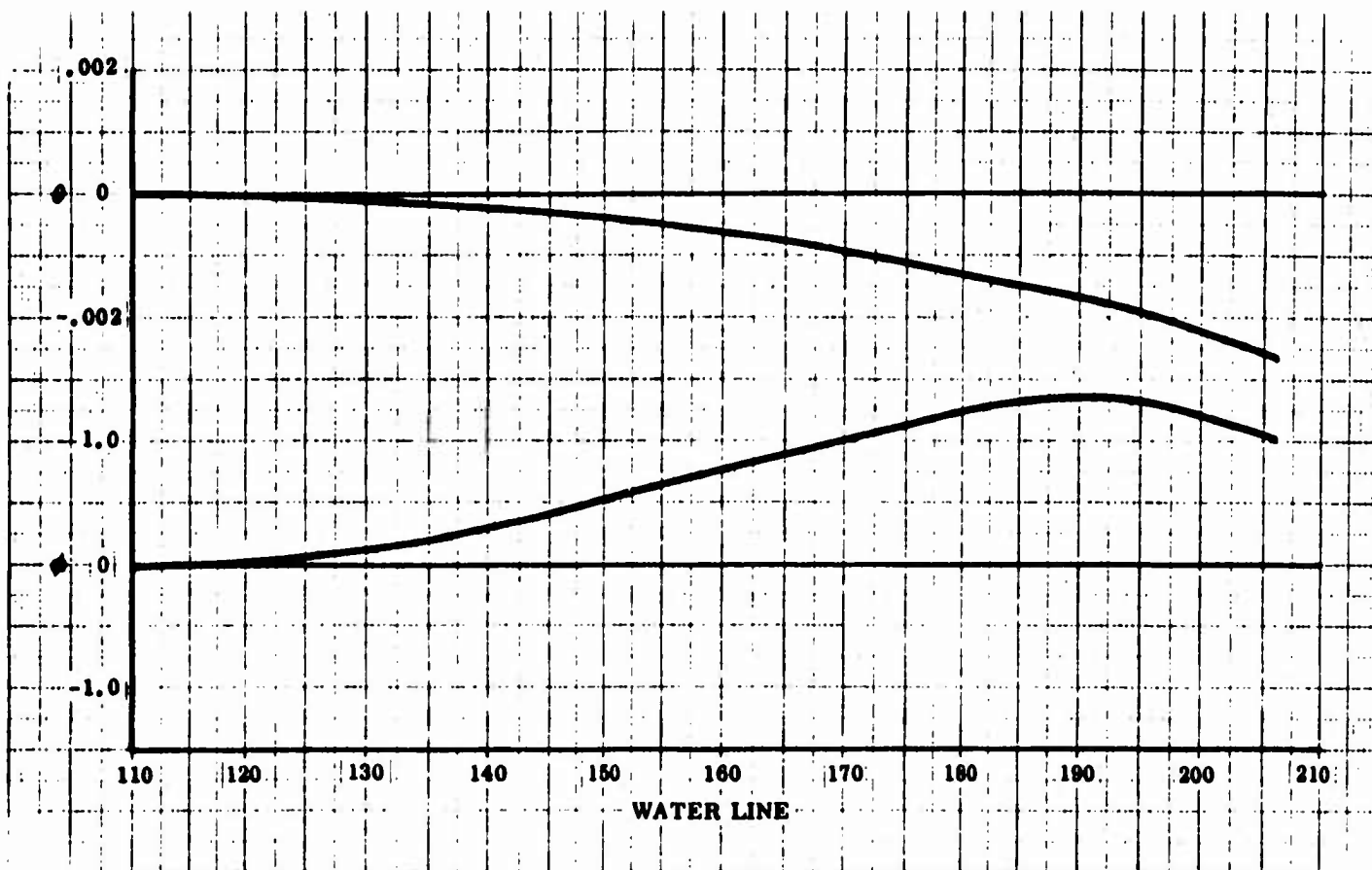


Figure 21 Mode Shapes - Vertical Stabilizer - Antisymmetric Analysis
(Mode 3 - $f = 27.9$ cps)

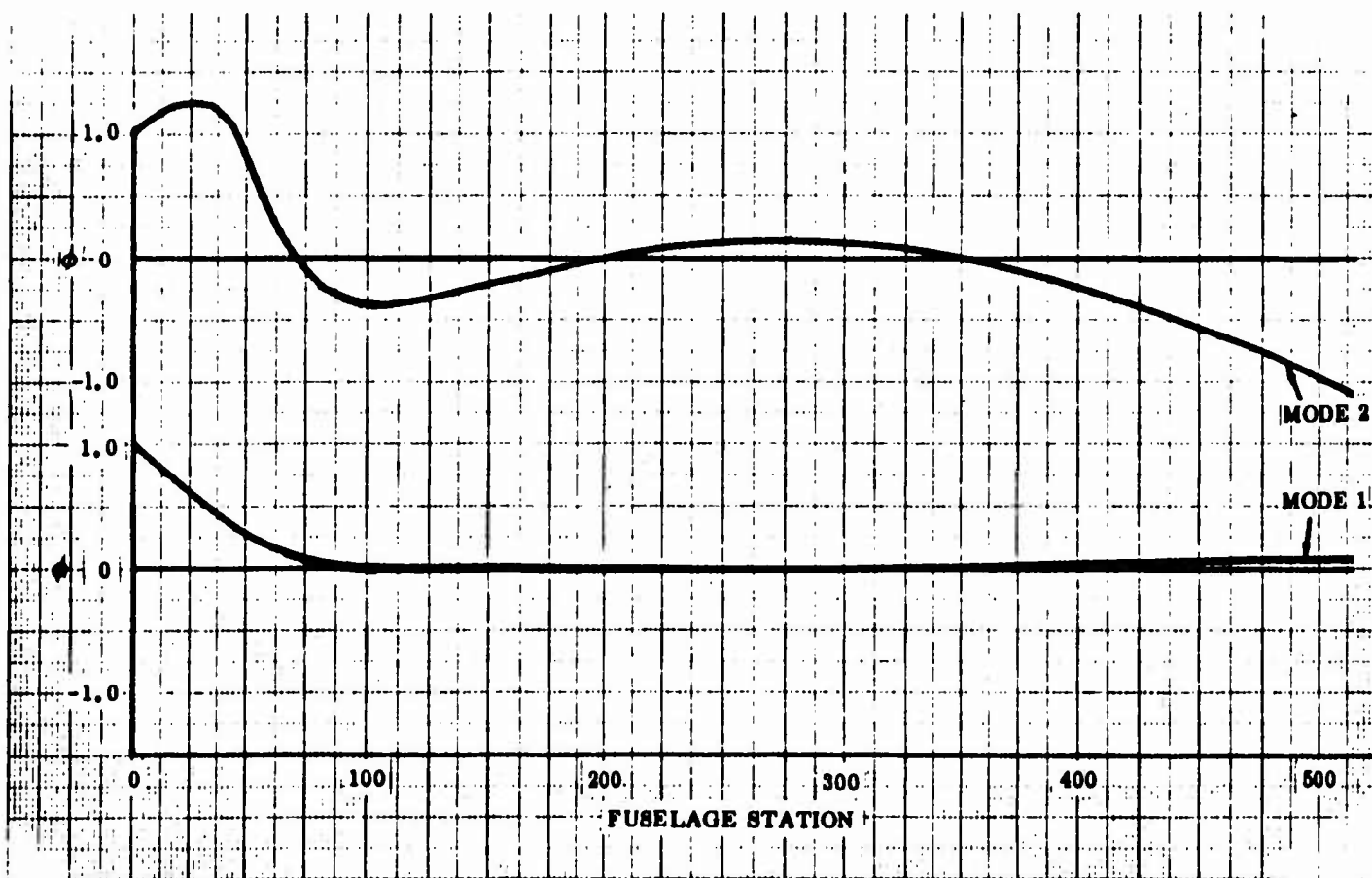


Figure 22 Mode Shapes - Fuselage - Antisymmetric Analysis
(Mode 1, $f = 5.6$ cps - Mode 2, $f = 13.6$ cps)

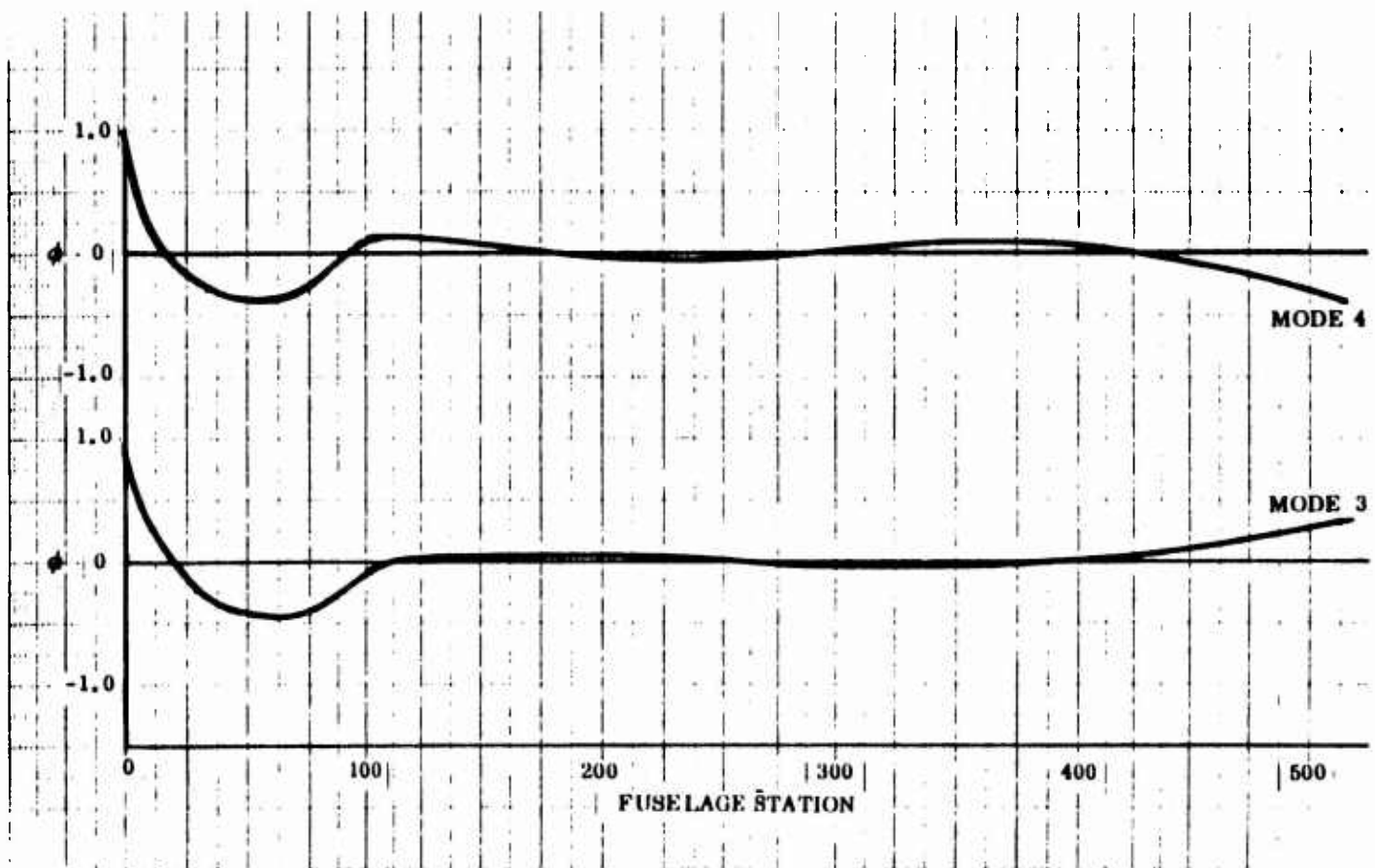


Figure 23 Mode Shapes - Fuselage - Antisymmetric Analysis
(Mode 3, $f = 20.6$ cps - Mode 4, $f = 26.2$ cps)

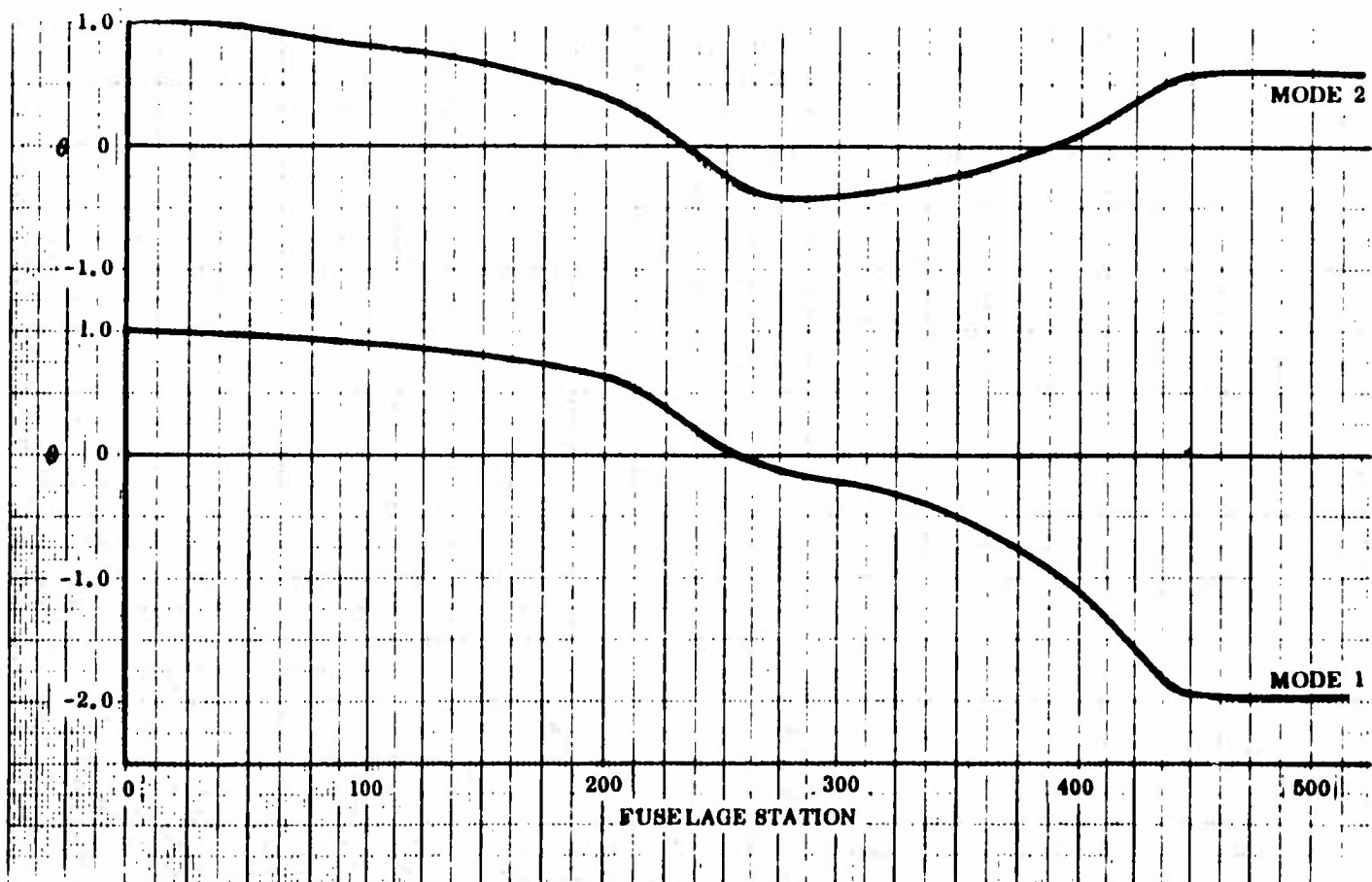
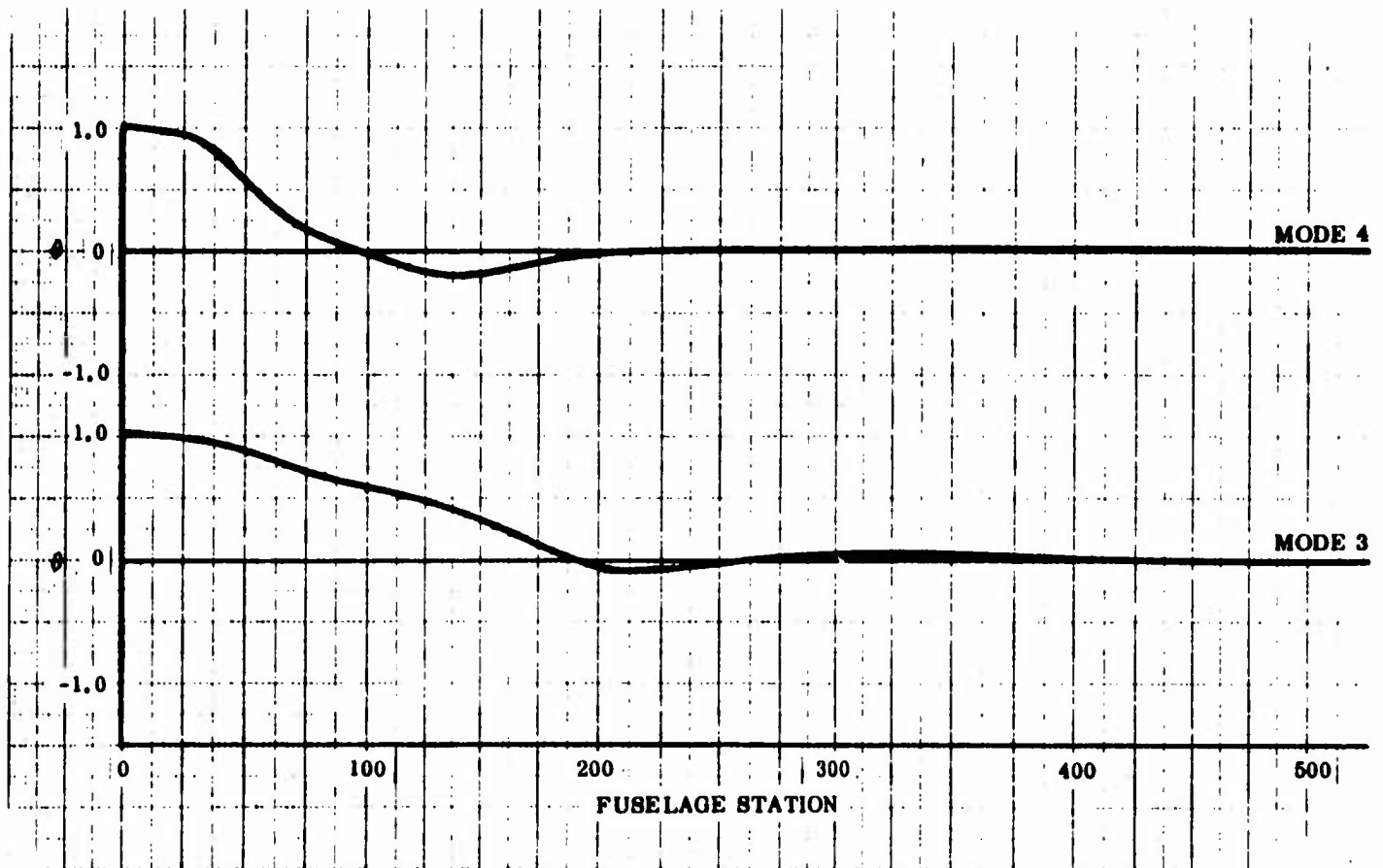


Figure 24 Mode Shapes - Fuselage - Antisymmetric Analysis
(Mode 1, $f = 13.9$ cps - Mode 2, $f = 19.0$ cps)



**Figure 25 Mode Shapes - Fuselage - Antisymmetric Analysis
(Mode 3, $f = 29.0$ cps - Mode 4, $f = 51.9$ cps)**

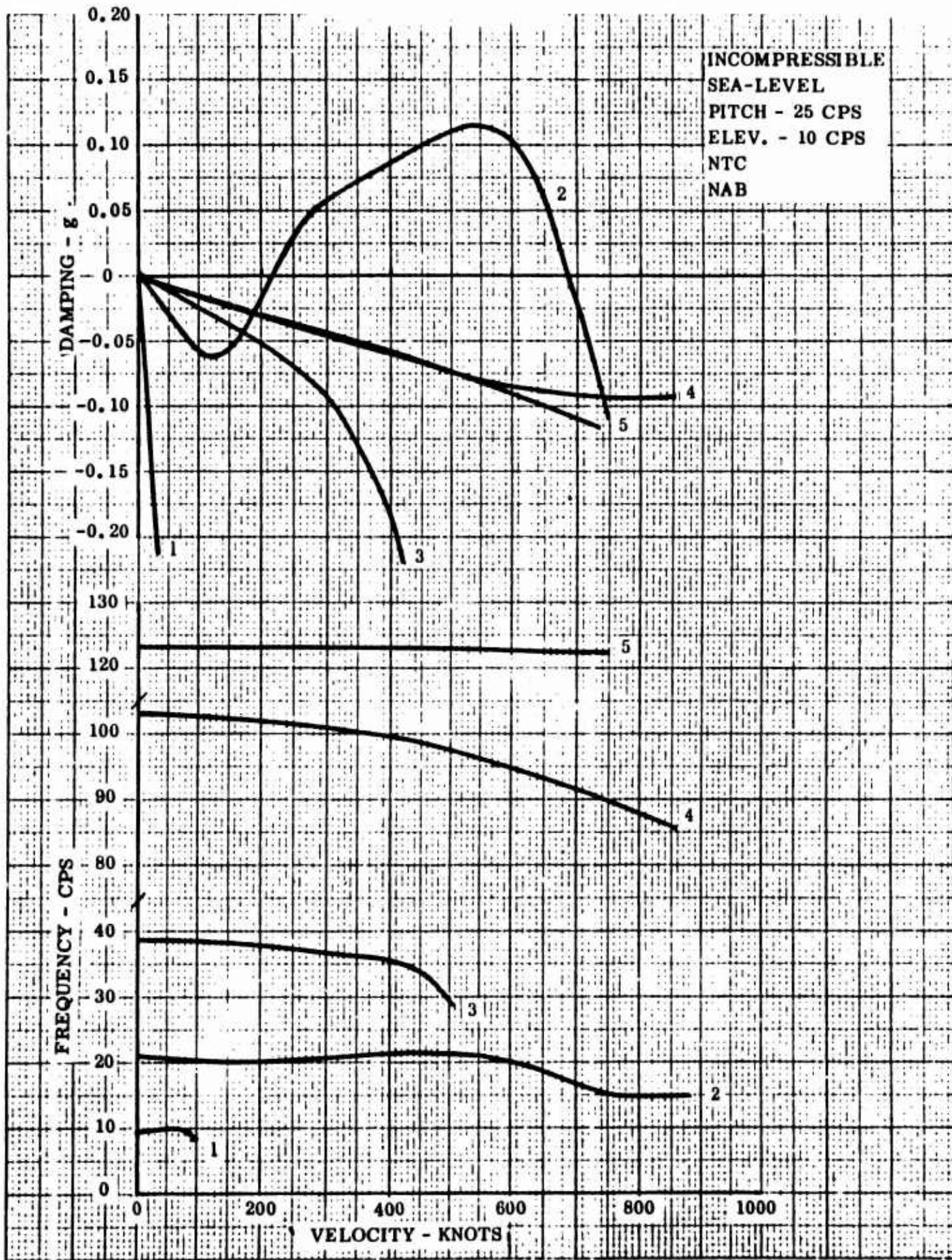


Figure 26 Symmetric Analysis - Cantilevered Condition

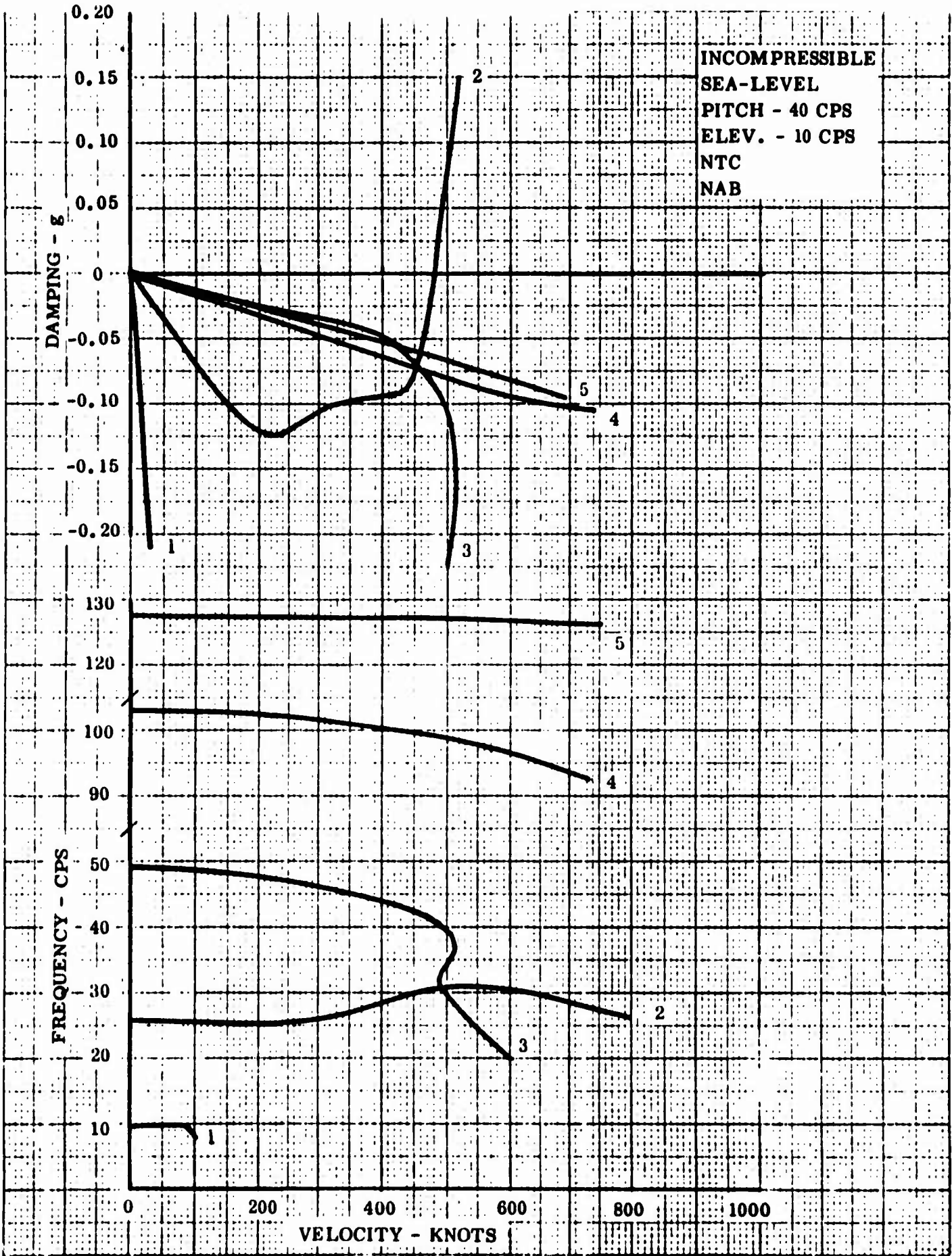


Figure 27 Symmetric Analysis - Cantilevered Condition

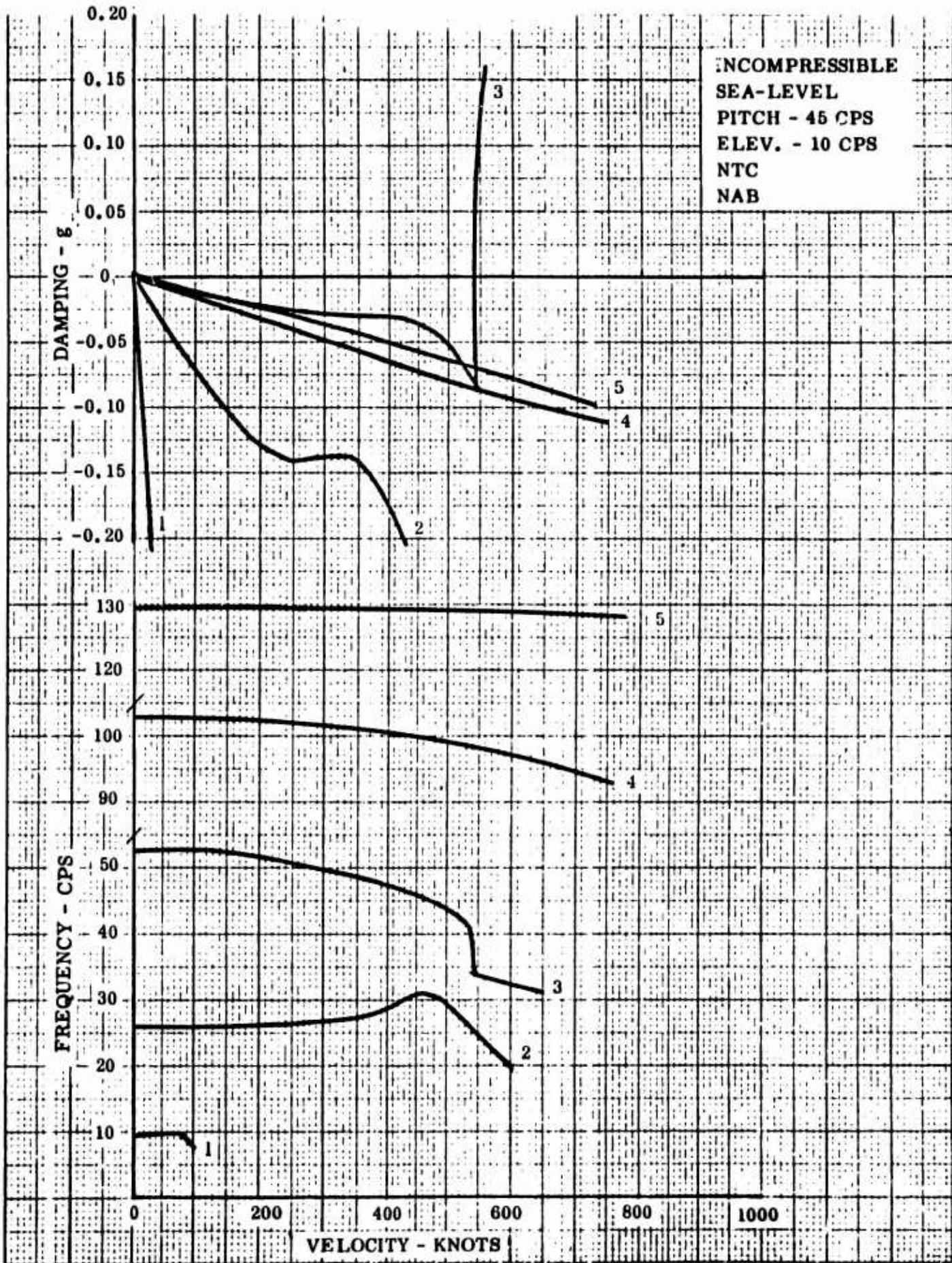


Figure 28 Symmetric Analysis - Cantilevered Condition

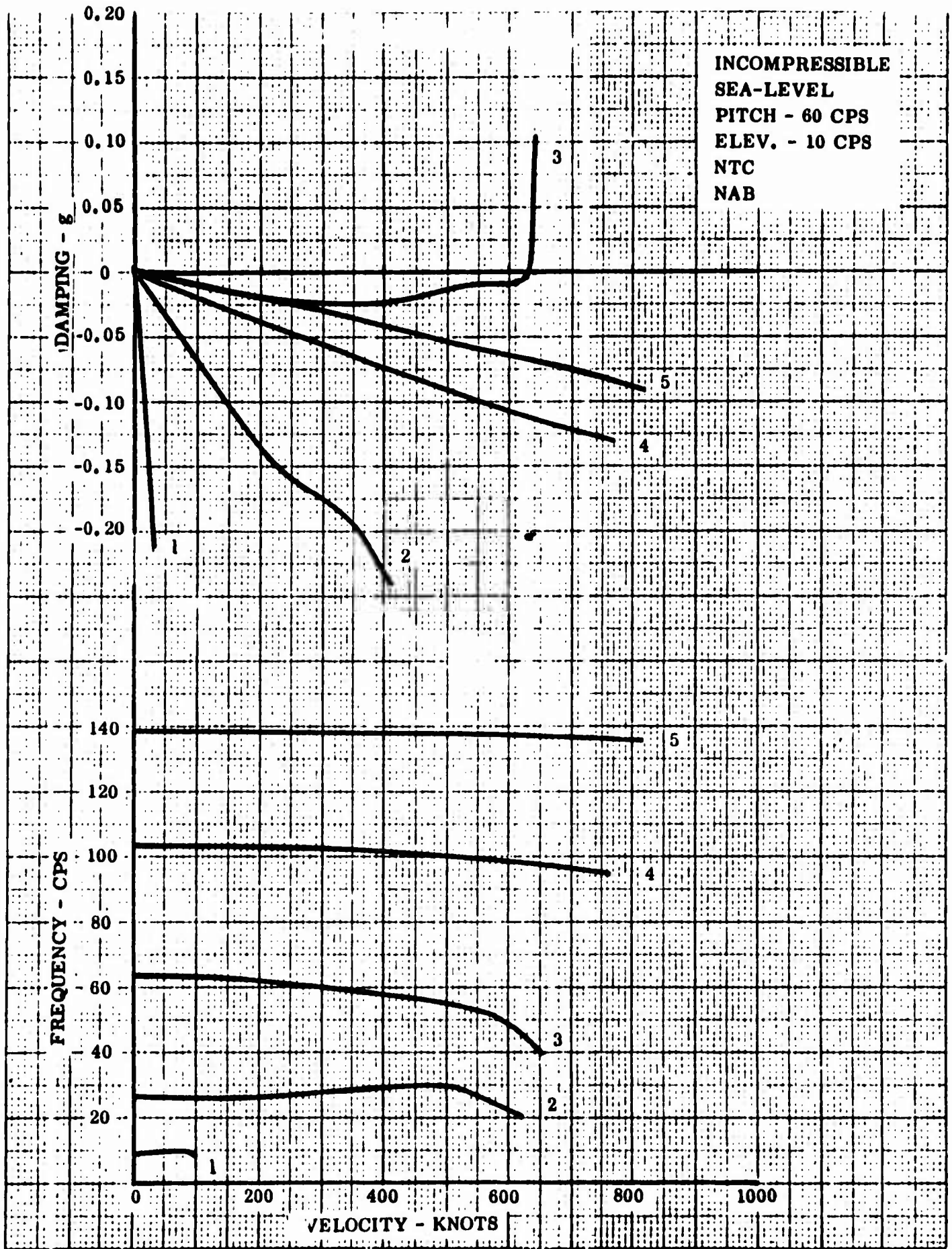


Figure 29 Symmetric Analysis - Cantilevered Condition

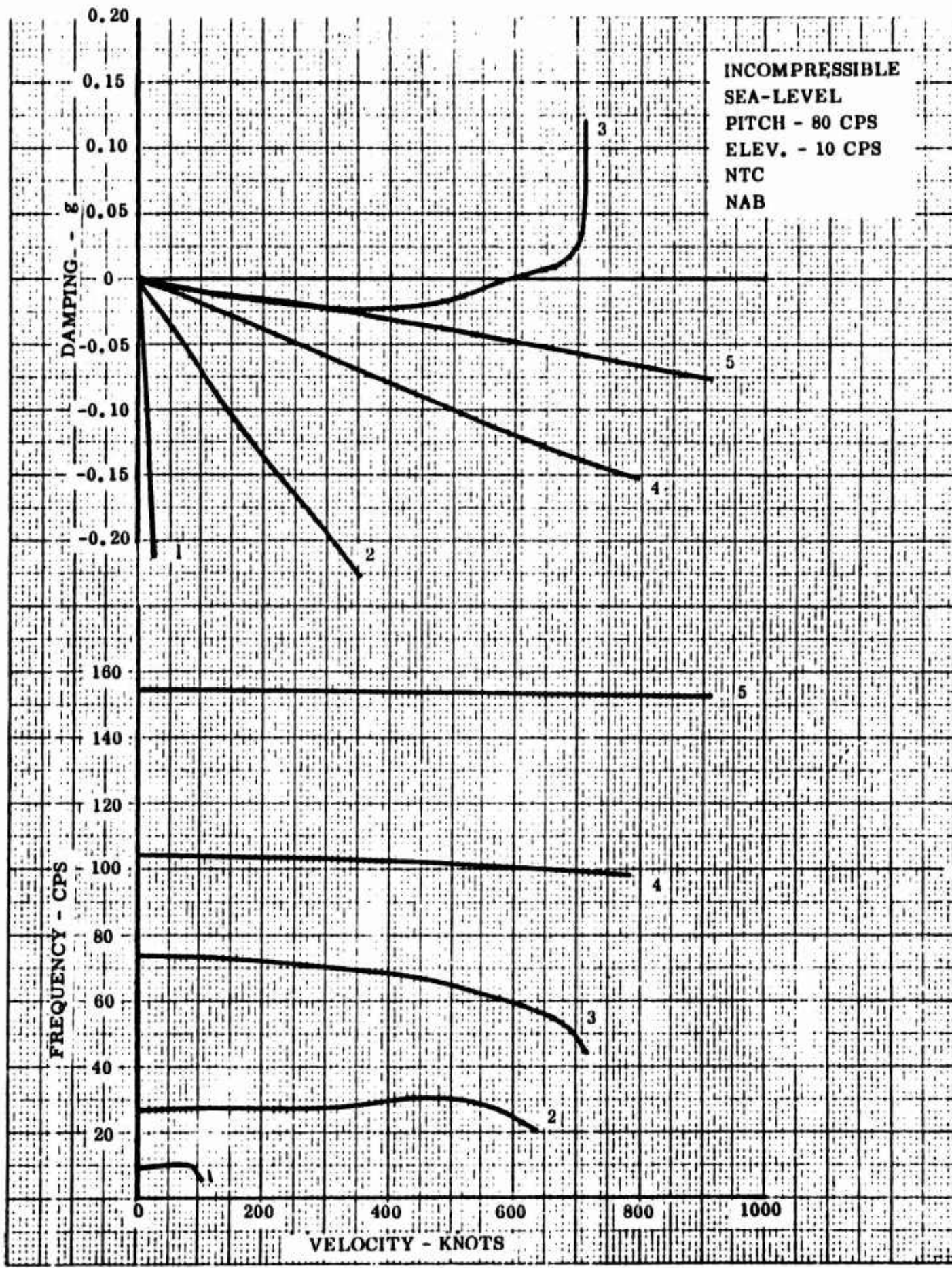


Figure 30 Symmetric Analysis - Cantilevered Condition

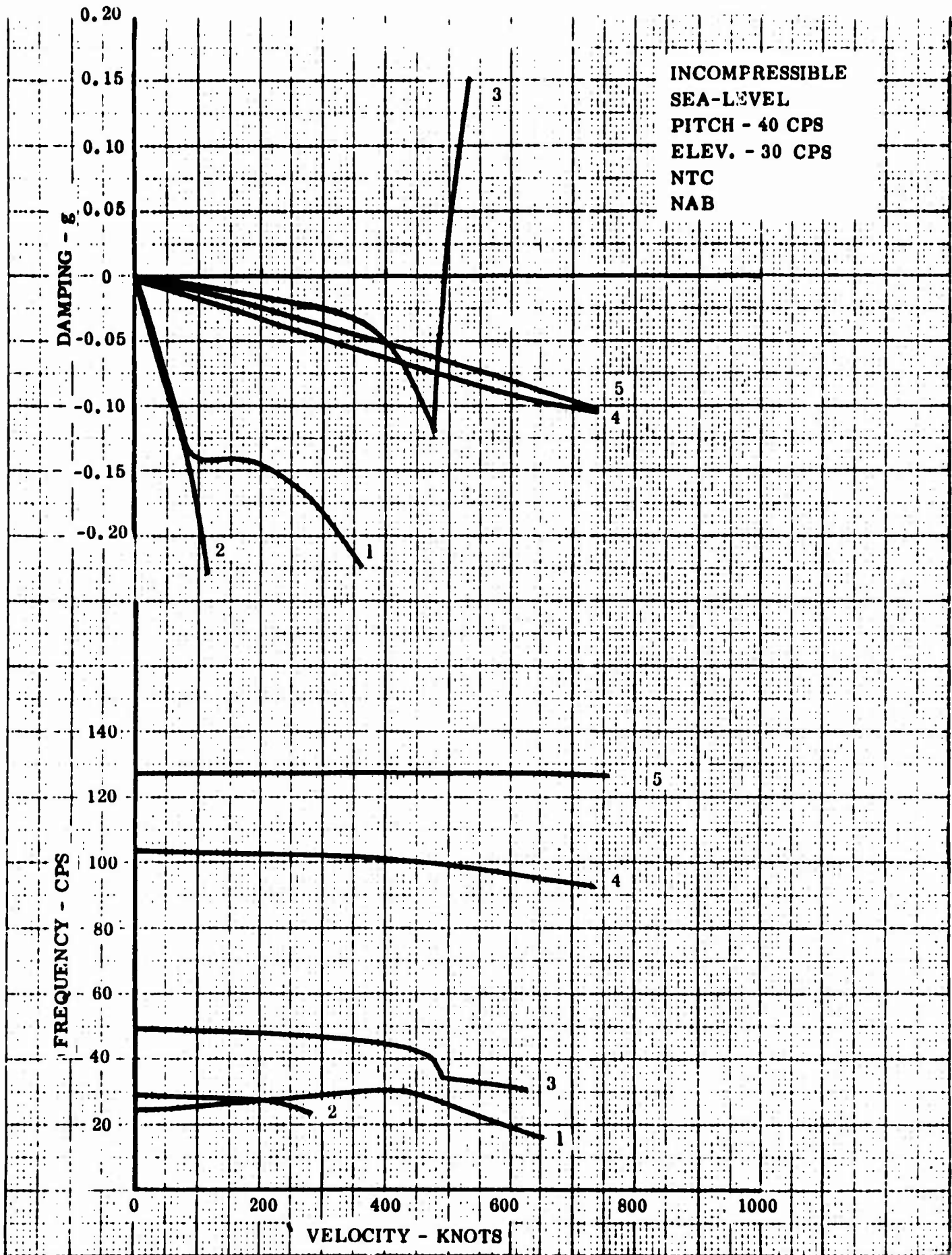


Figure 31 Symmetric Analysis - Cantilevered Condition

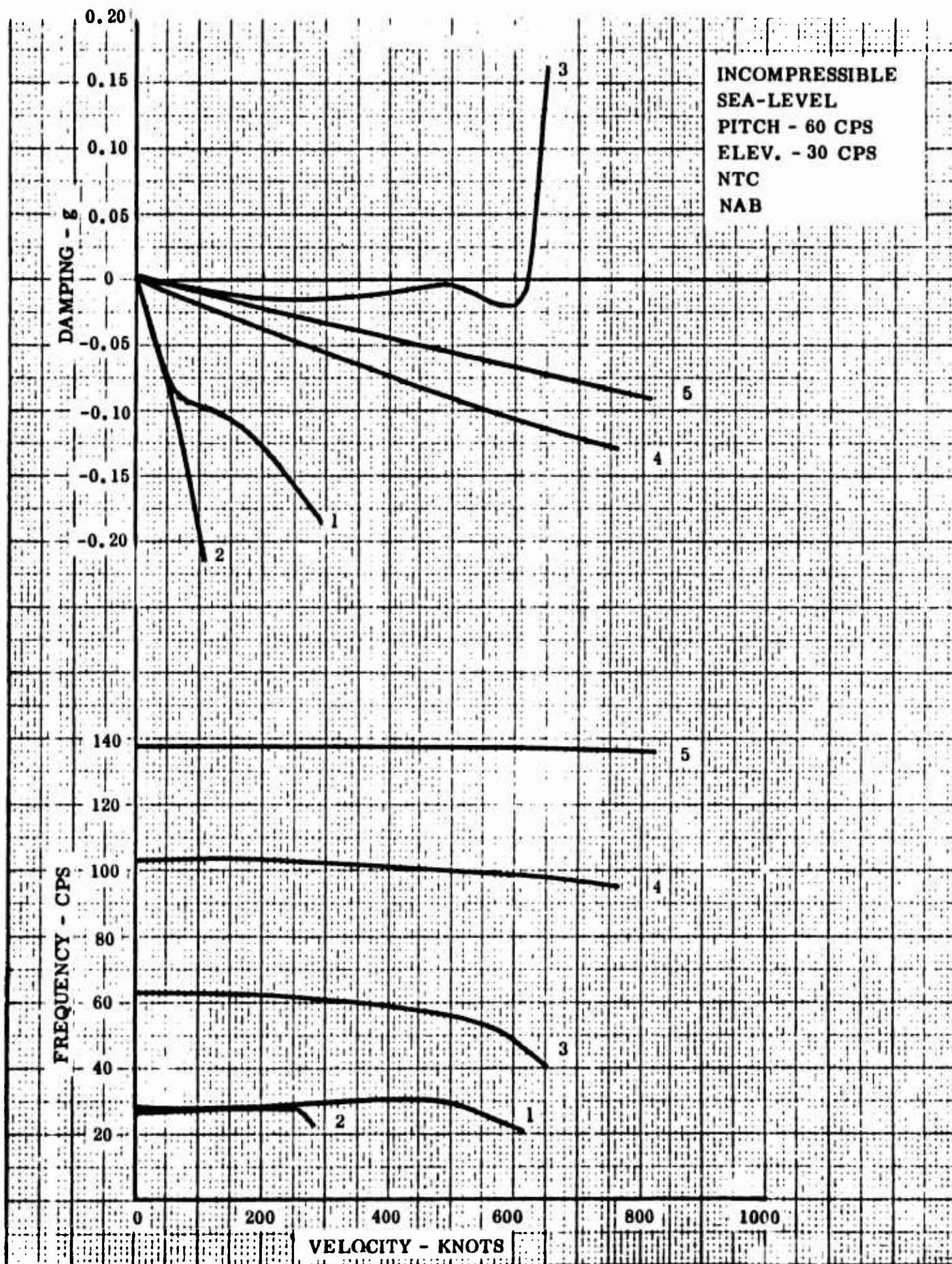


Figure 32 Symmetric Analysis - Cantilevered Condition

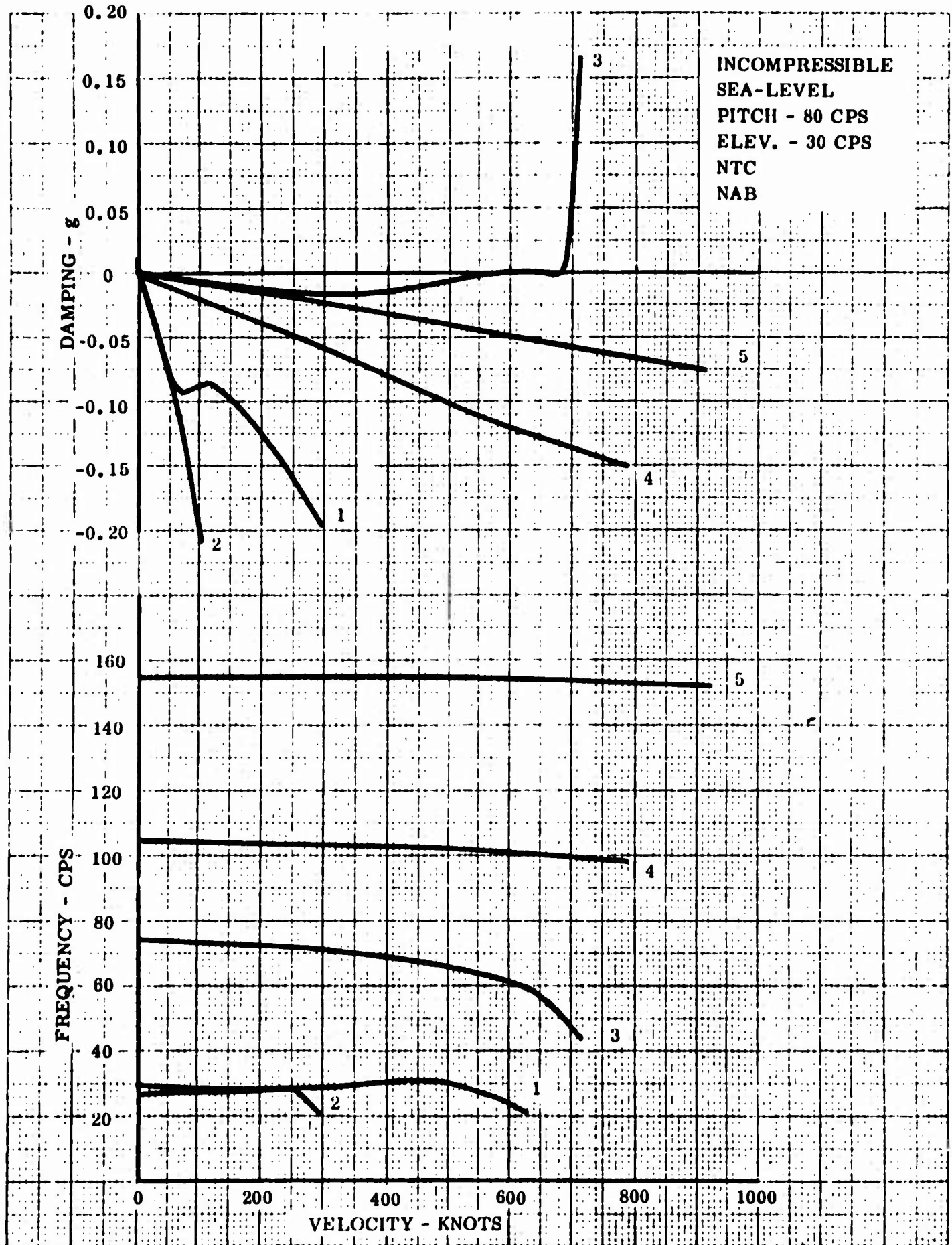


Figure 33 Symmetric Analysis - Cantilevered Condition

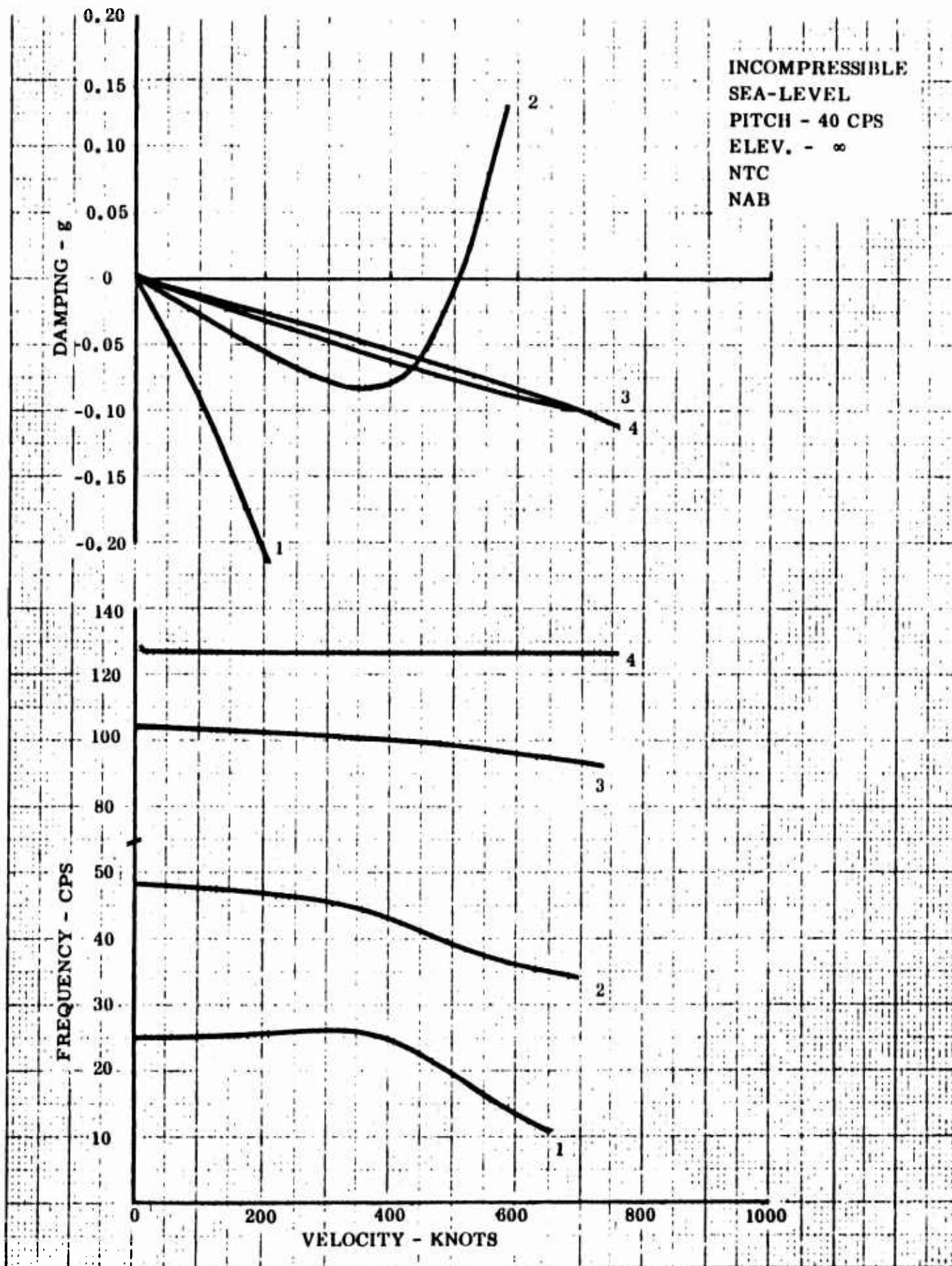


Figure 34 Symmetric Analysis - Cantilevered Condition

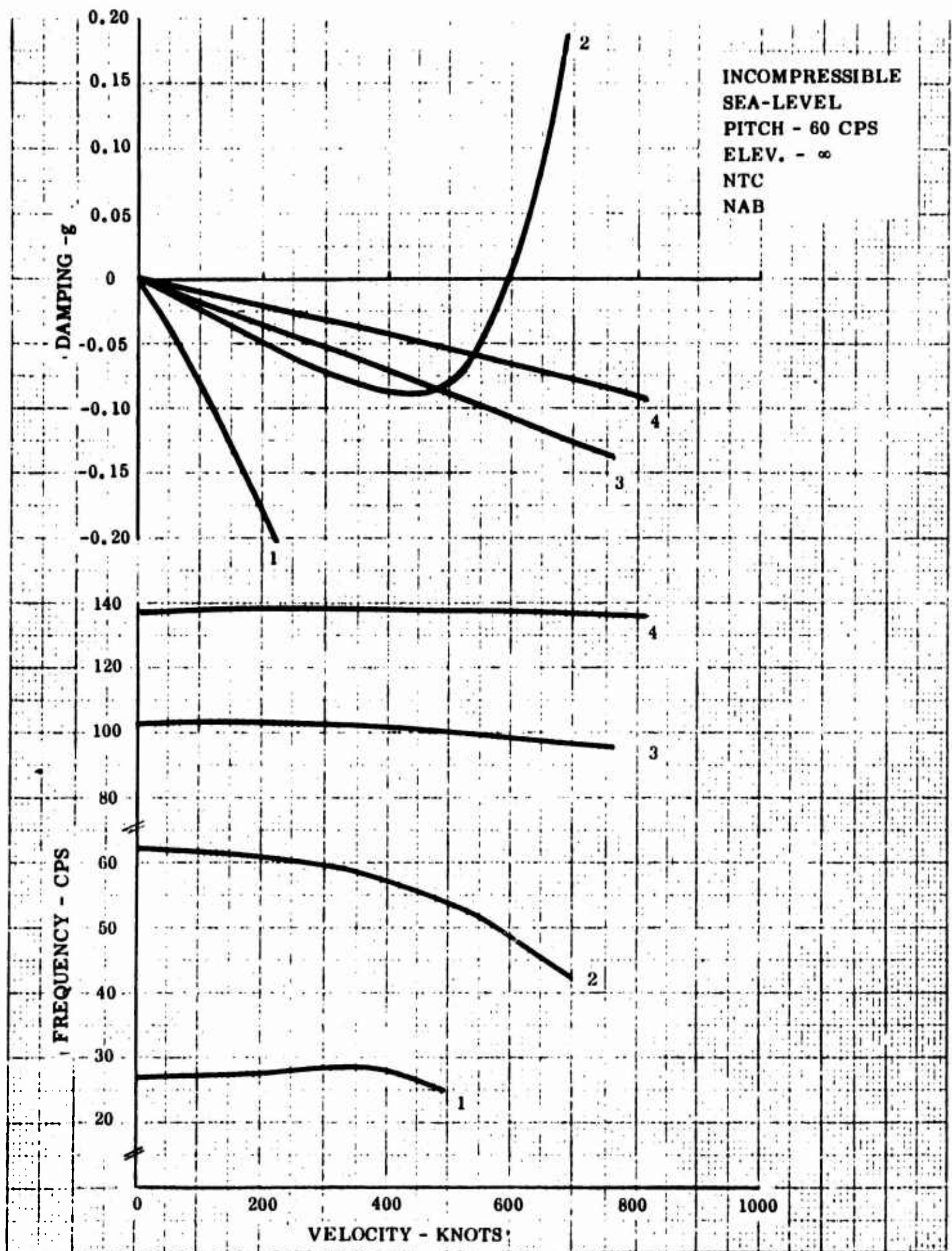


Figure 35 Symmetric Analysis - Cantilevered Condition

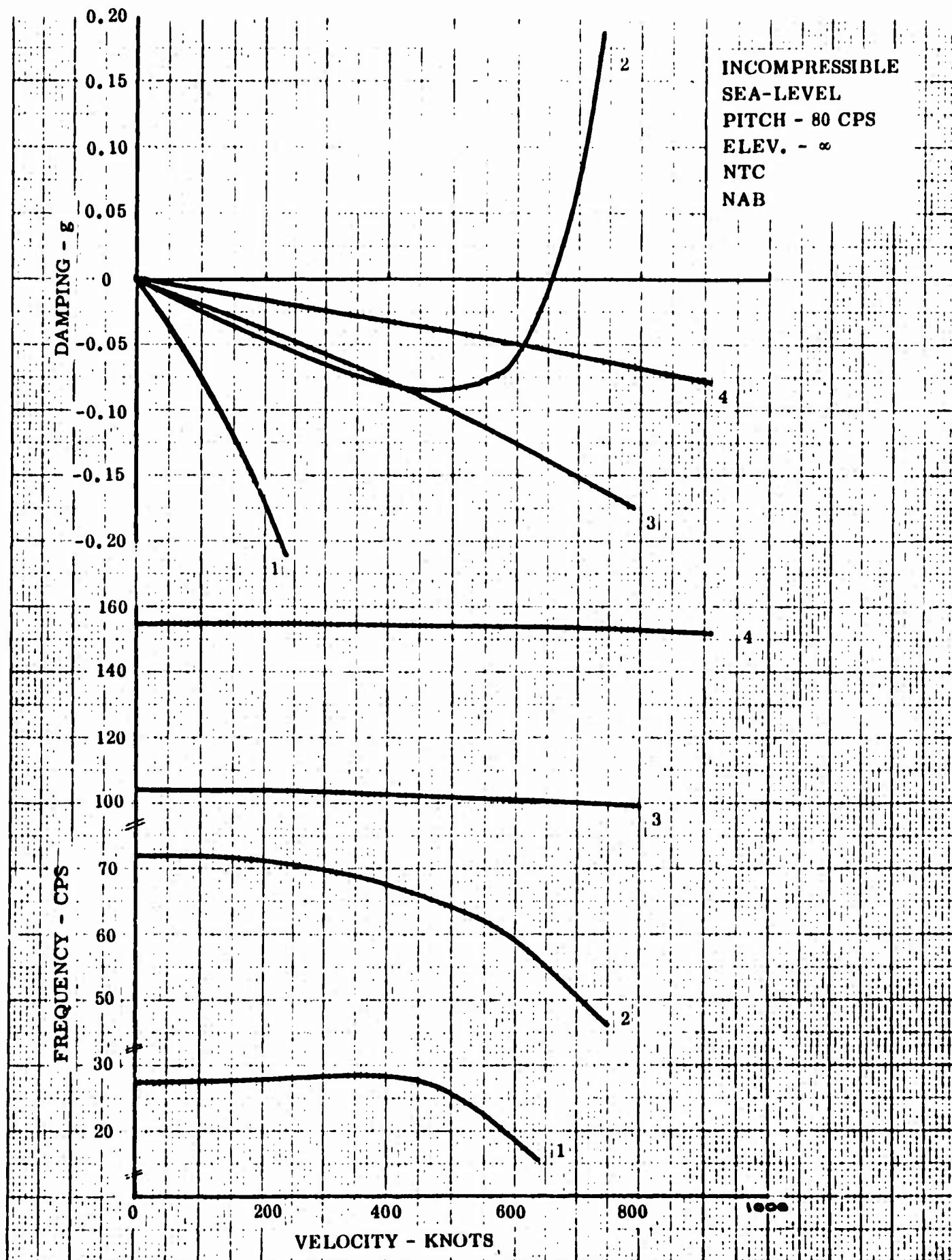


Figure 36 Symmetric Analysis - Cantilevered Condition

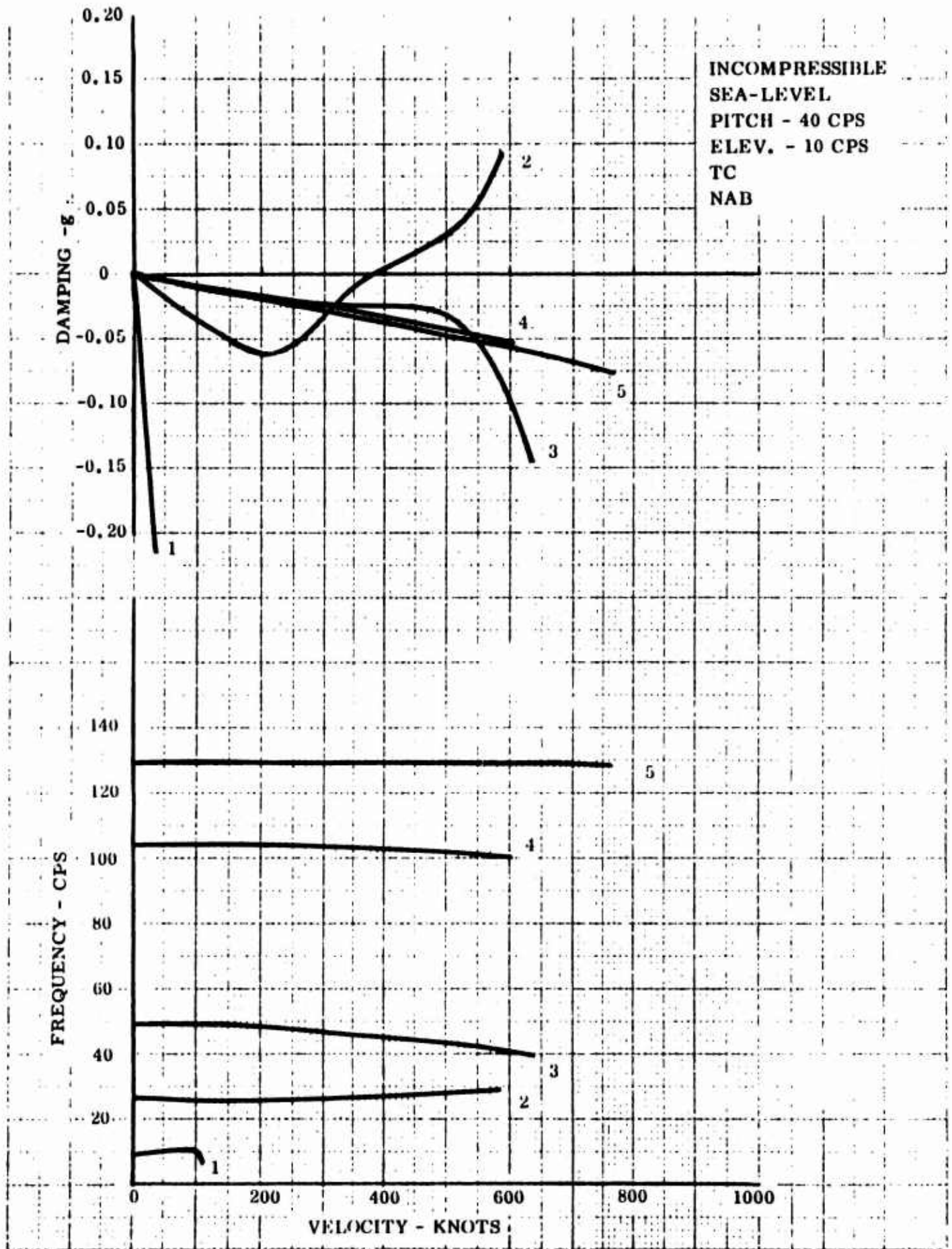


Figure 37 Symmetric Analysis - Cantilevered Condition

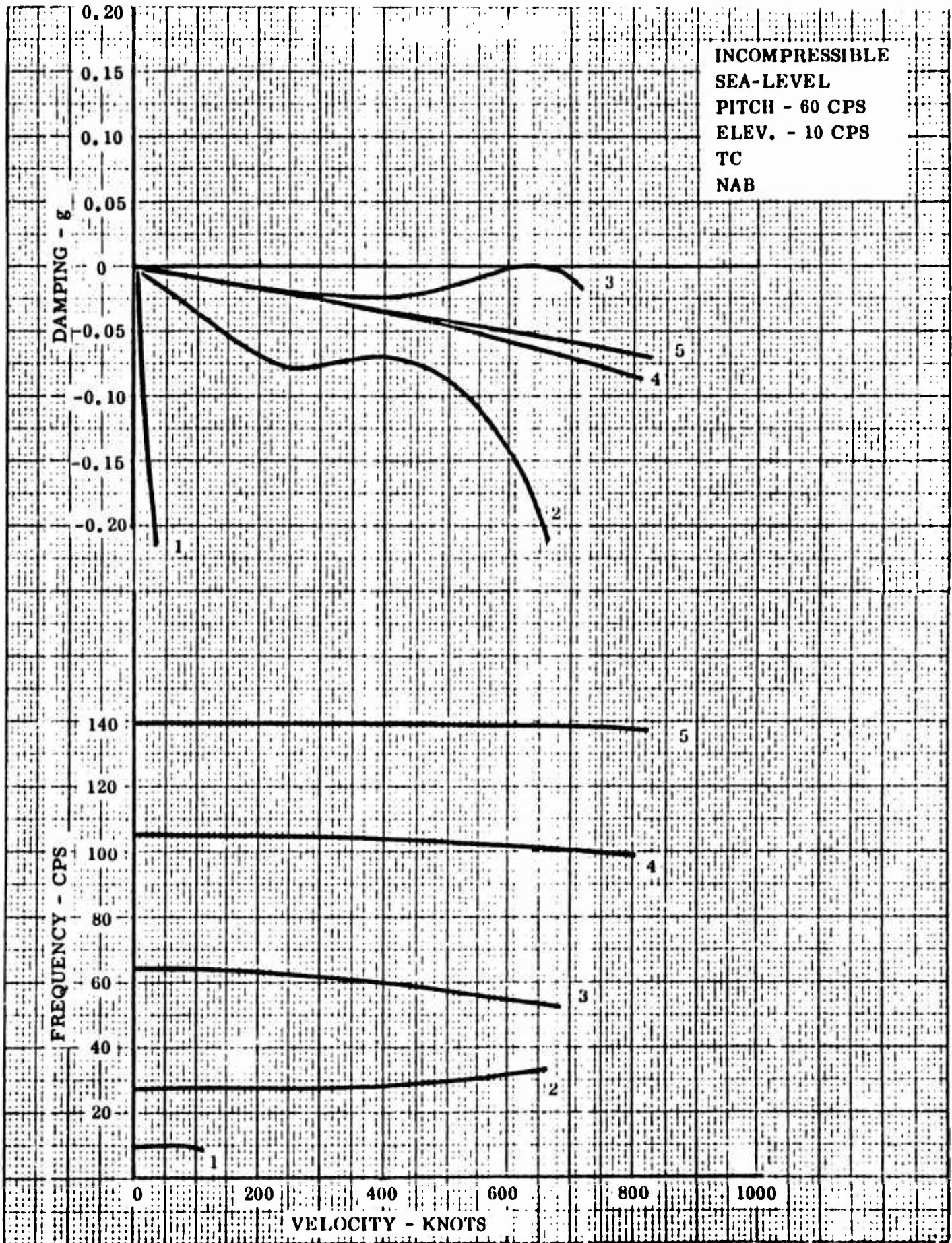


Figure 38 Symmetric Analysis - Cantilevered Condition

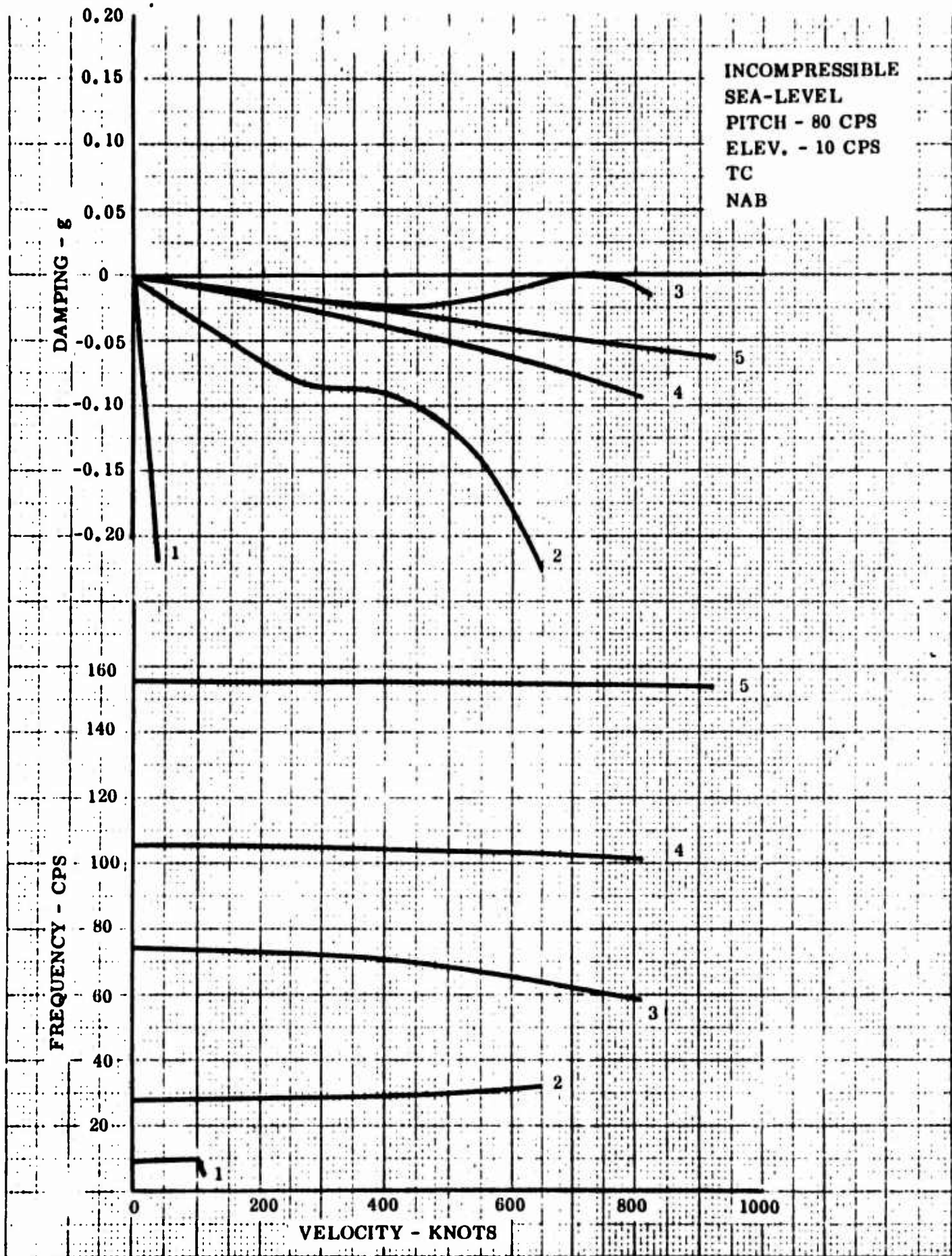


Figure 39 Symmetric Analysis - Cantilevered Condition

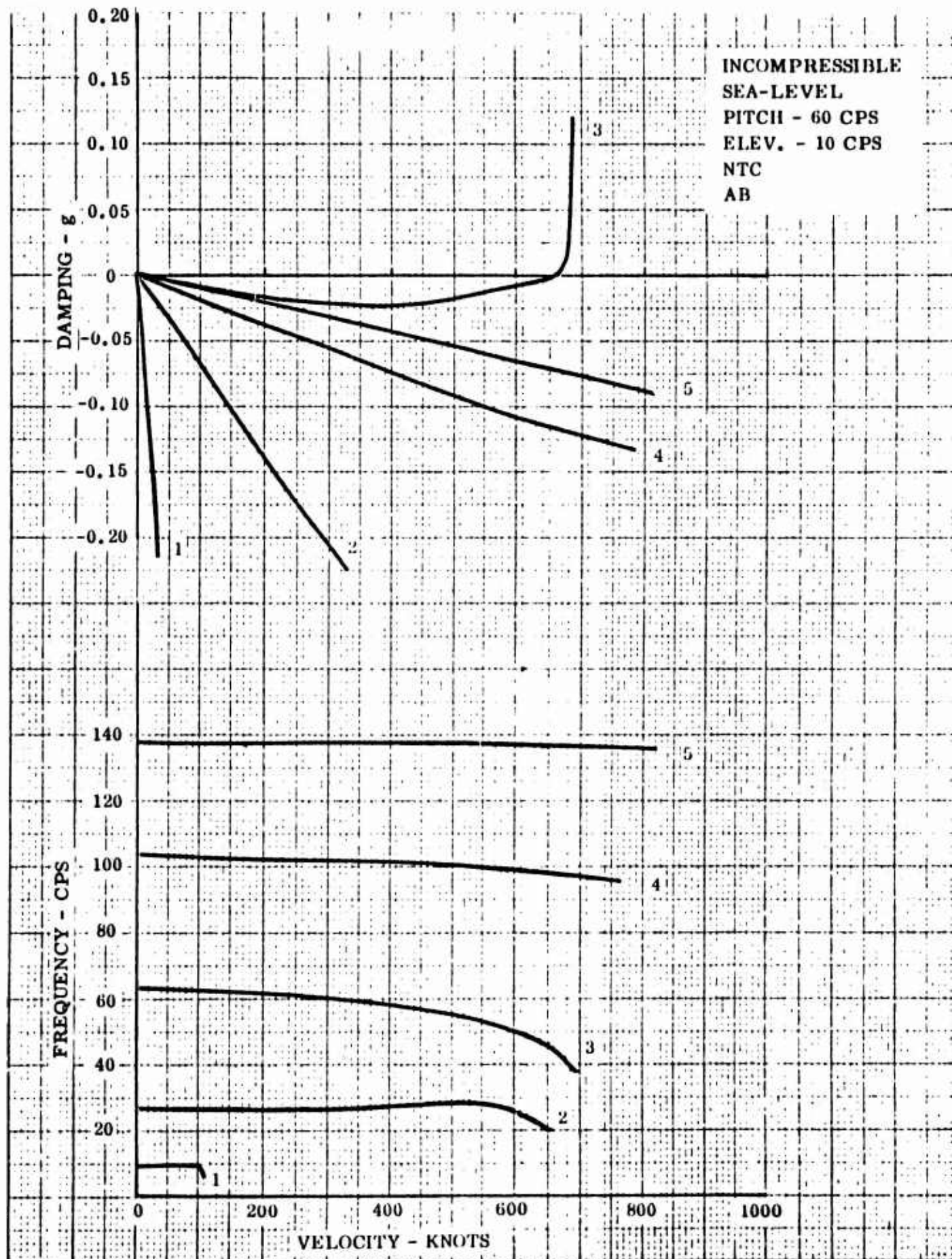


Figure 40 Symmetric Analysis - Cantilevered Condition

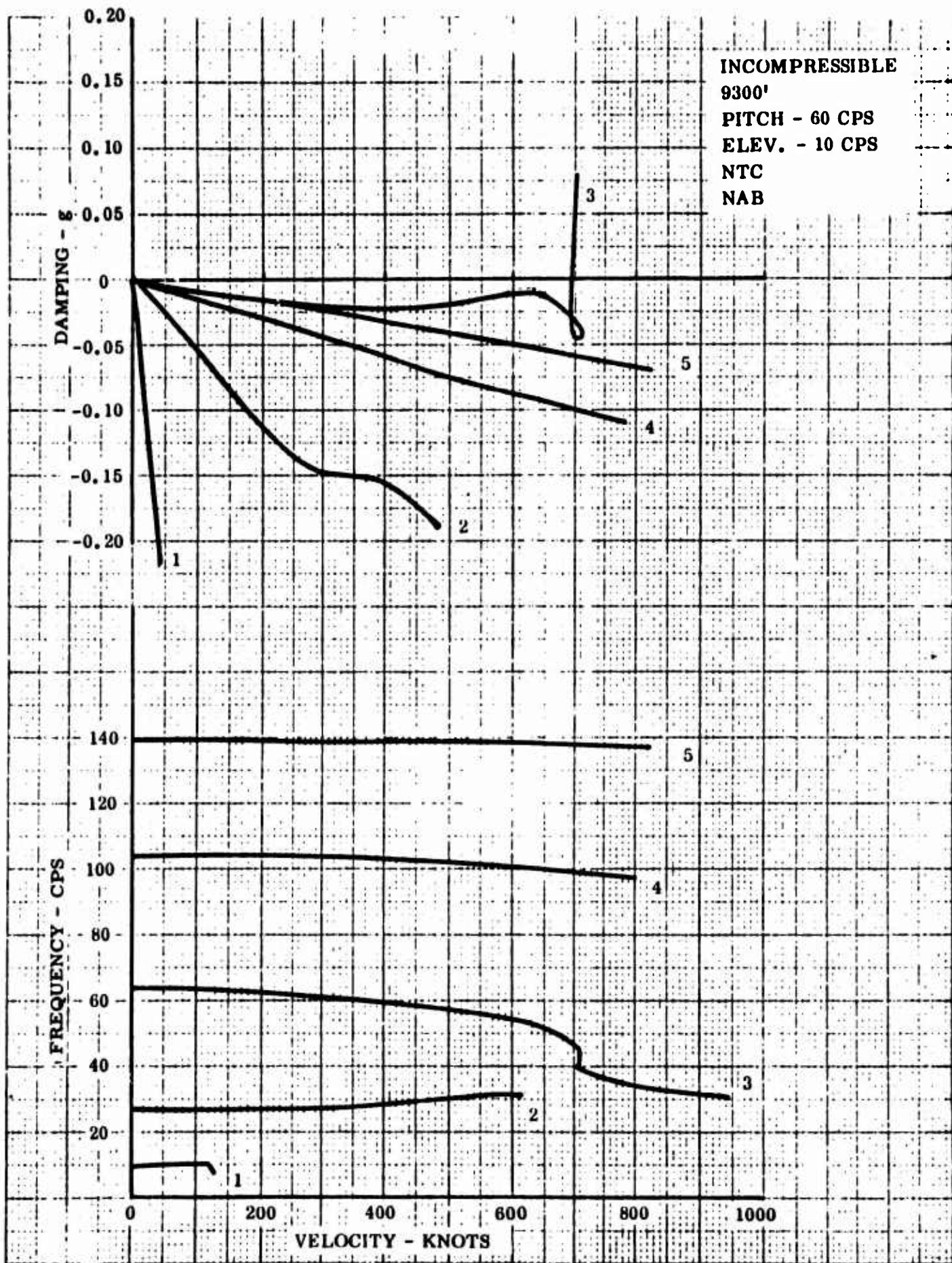


Figure 41 Symmetric Analysis - Cantilevered Condition

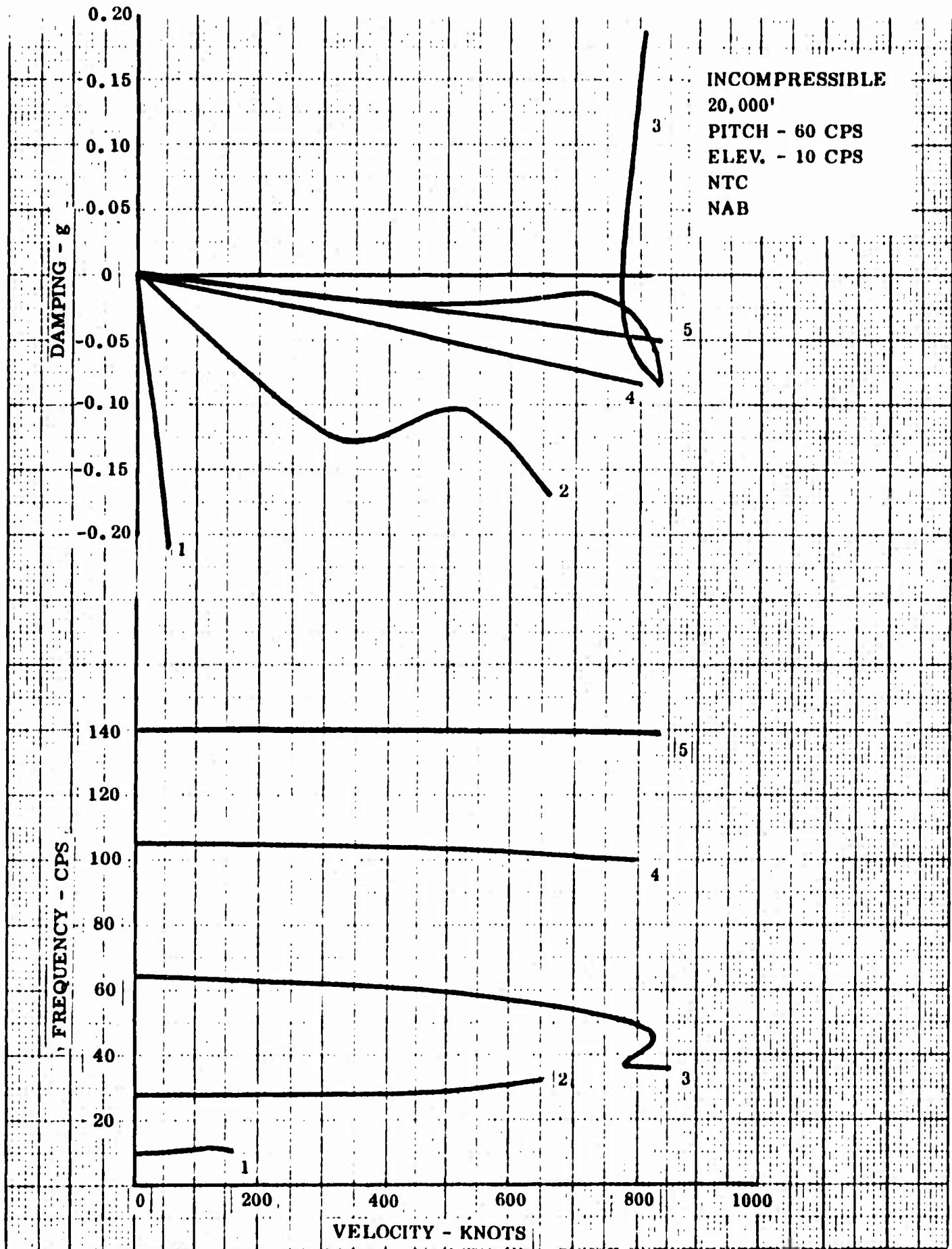


Figure 42 Symmetric Analysis - Cantilevered Condition

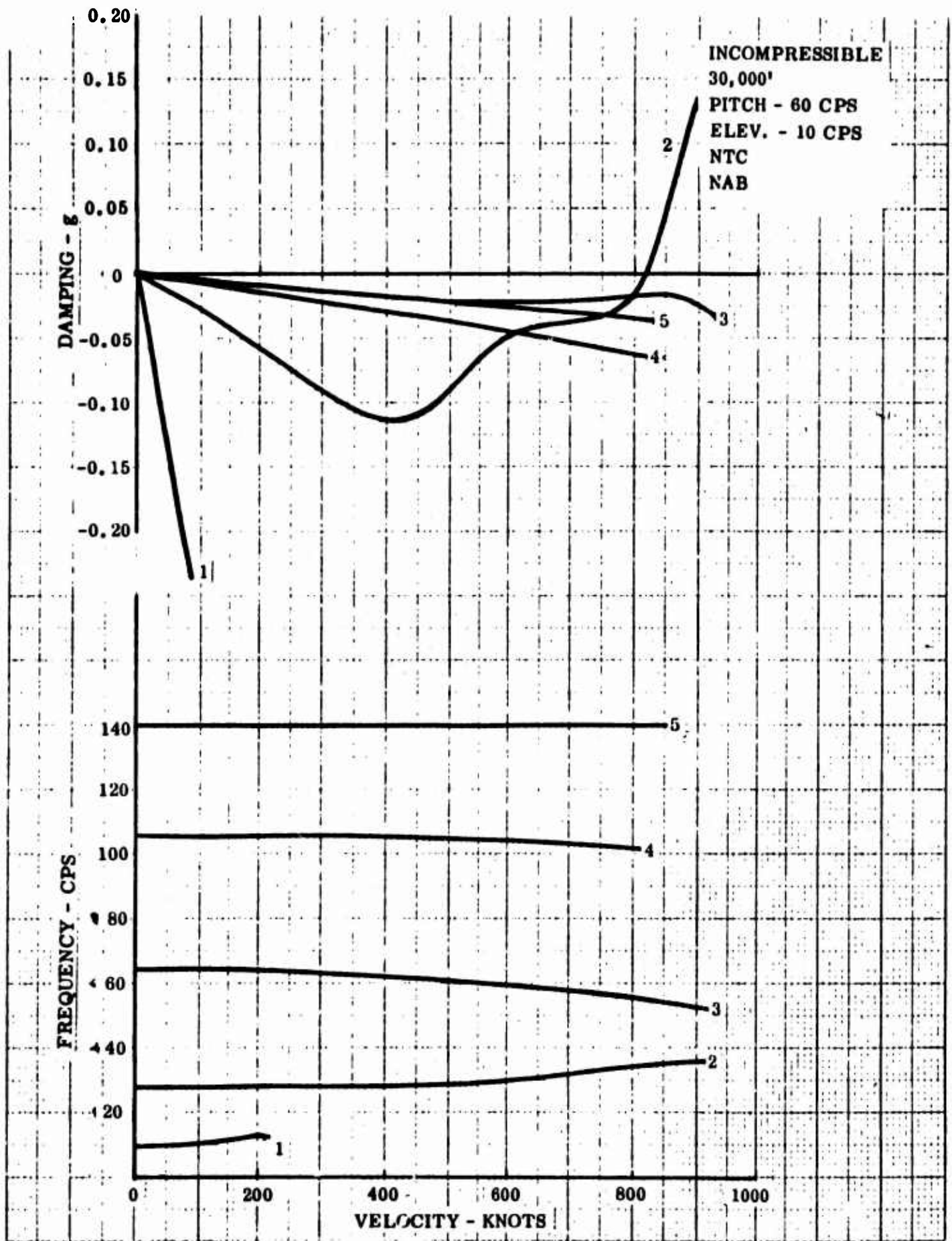


Figure 43 Symmetric Analysis - Cantilevered Condition

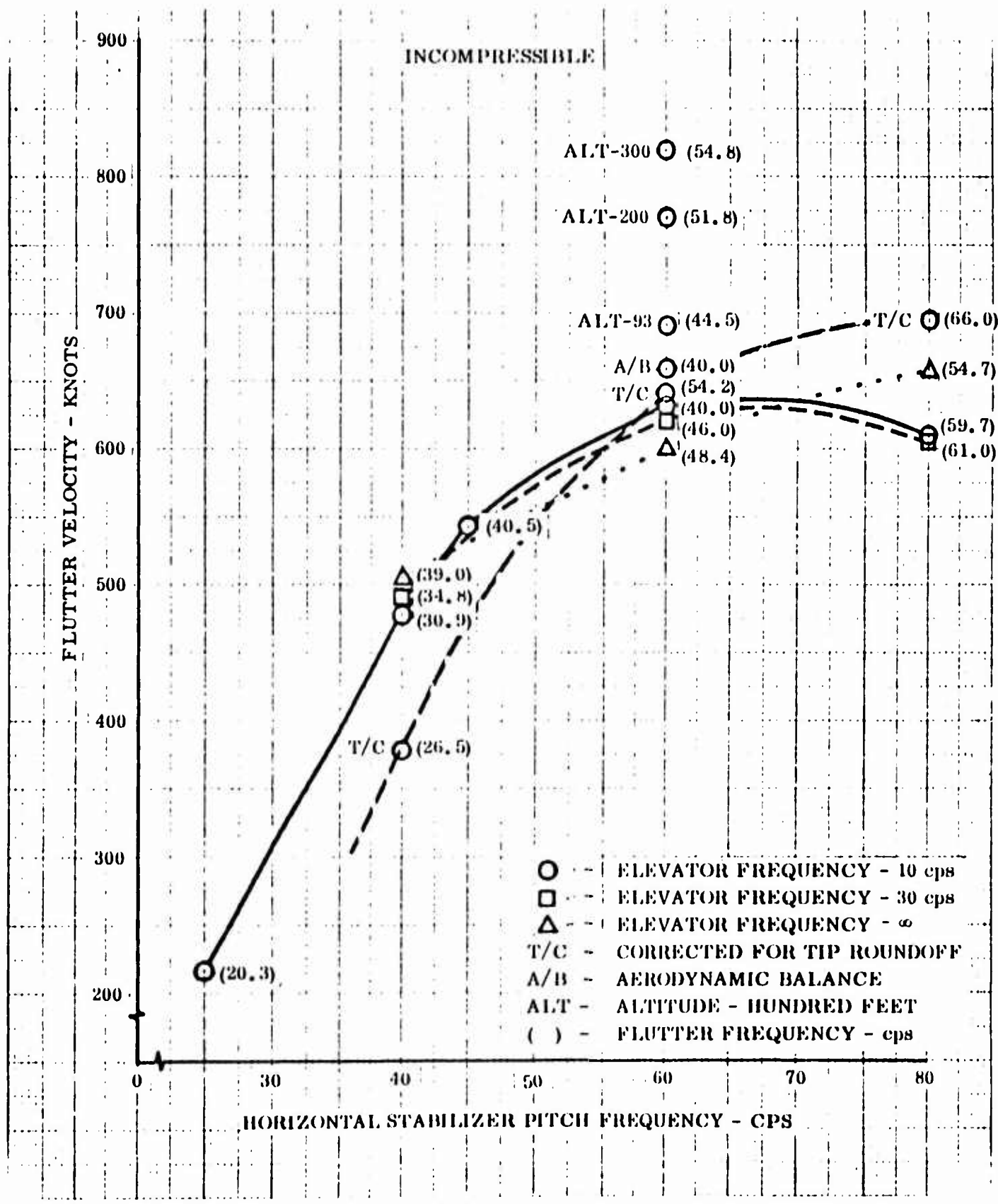


Figure 44 Symmetric Analysis - Cantilevered Condition - Parameter Effects

COUPLED MODES FROM SOLUTION
OF EQ. 6.0 WITH $\underline{A} = \underline{0}$

- - 1st
- △ - 2nd
- - 3rd
- ◇ - 4th
- ◊ - 5th

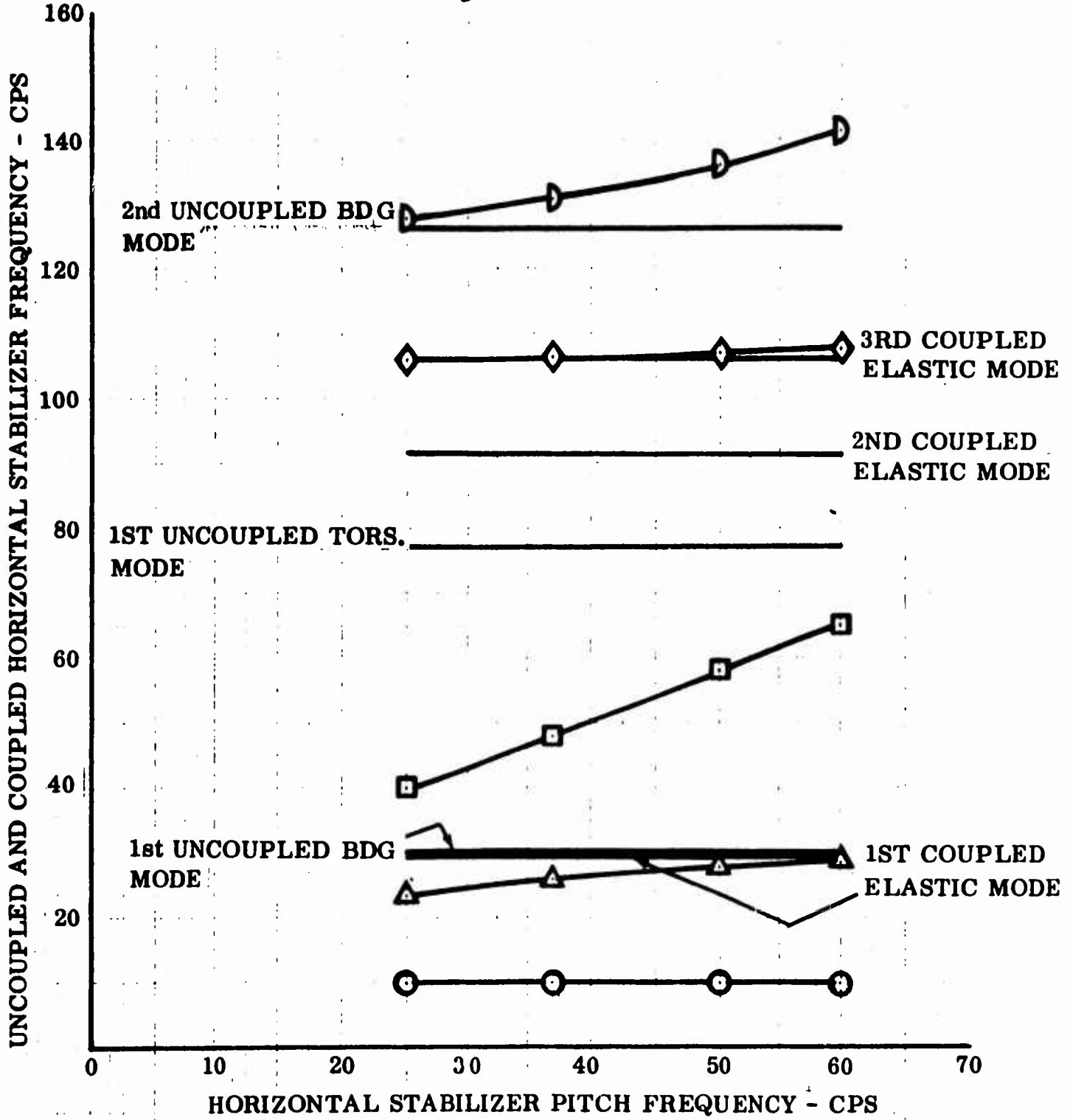


Figure 45 Symmetric Analysis - Cantilevered Condition - Modal Coupling

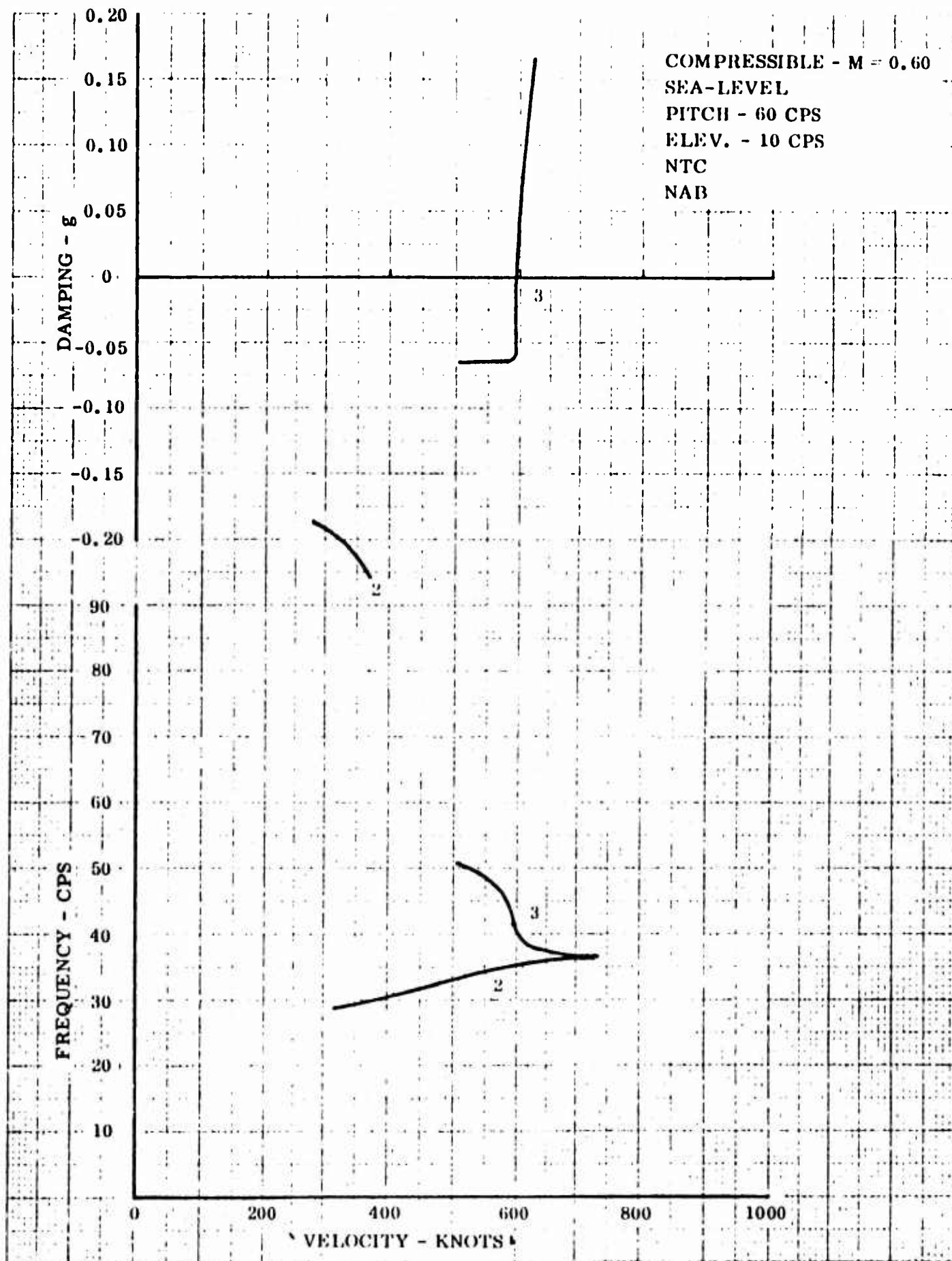


Figure 46 Symmetric Analysis - Cantilevered Condition

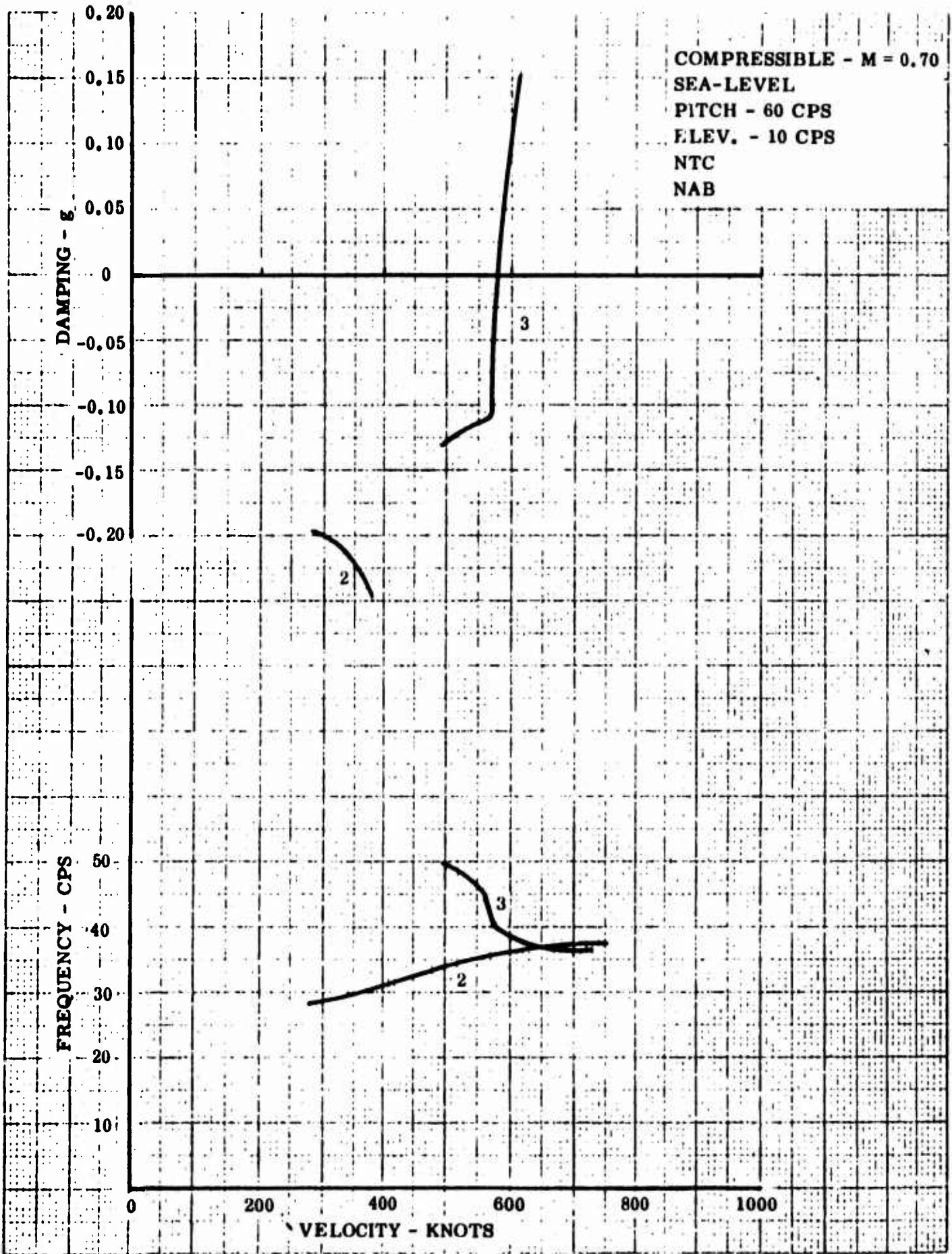


Figure 47 Symmetric Analysis - Cantilevered Condition

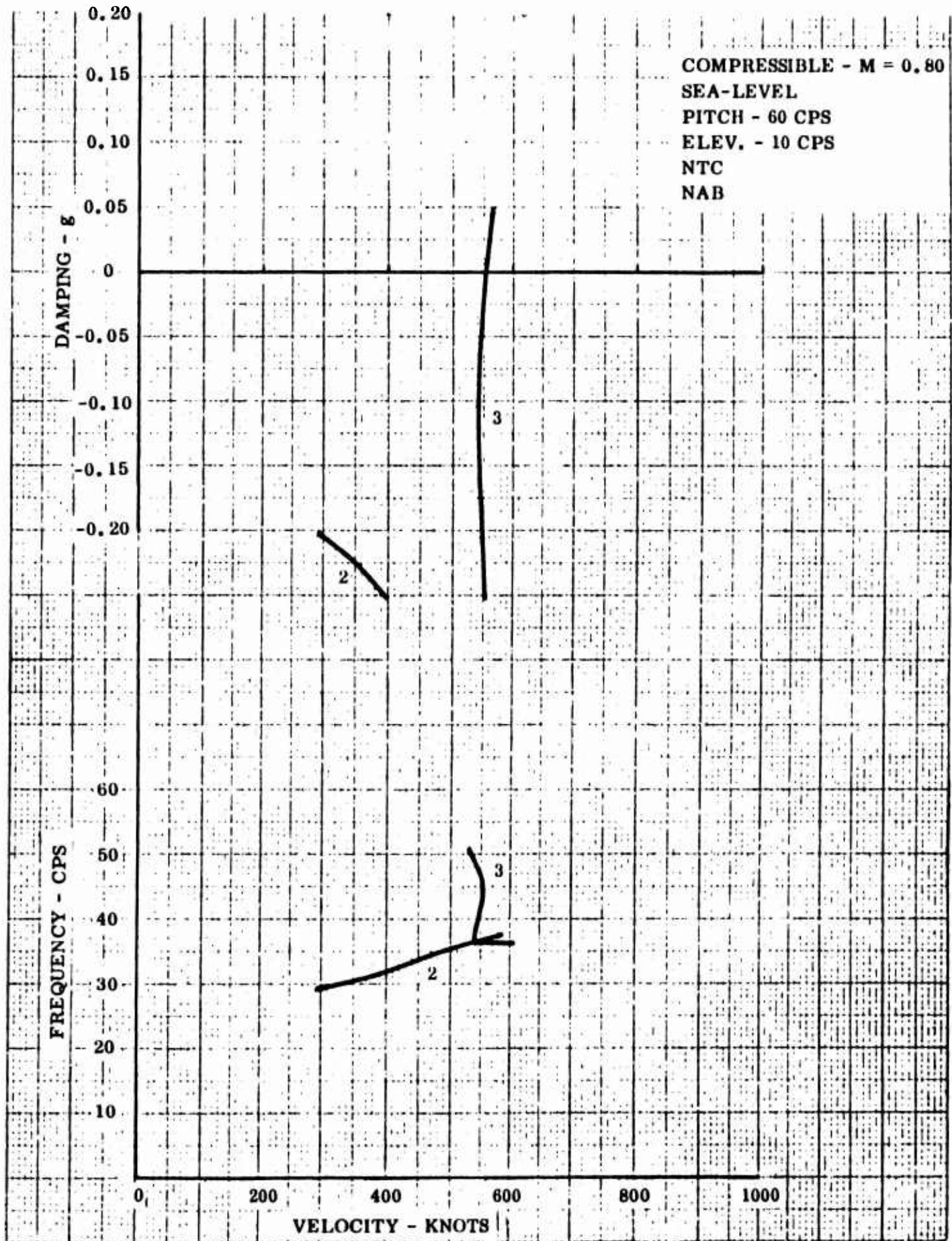


Figure 48 Symmetric Analysis - Cantilevered Condition

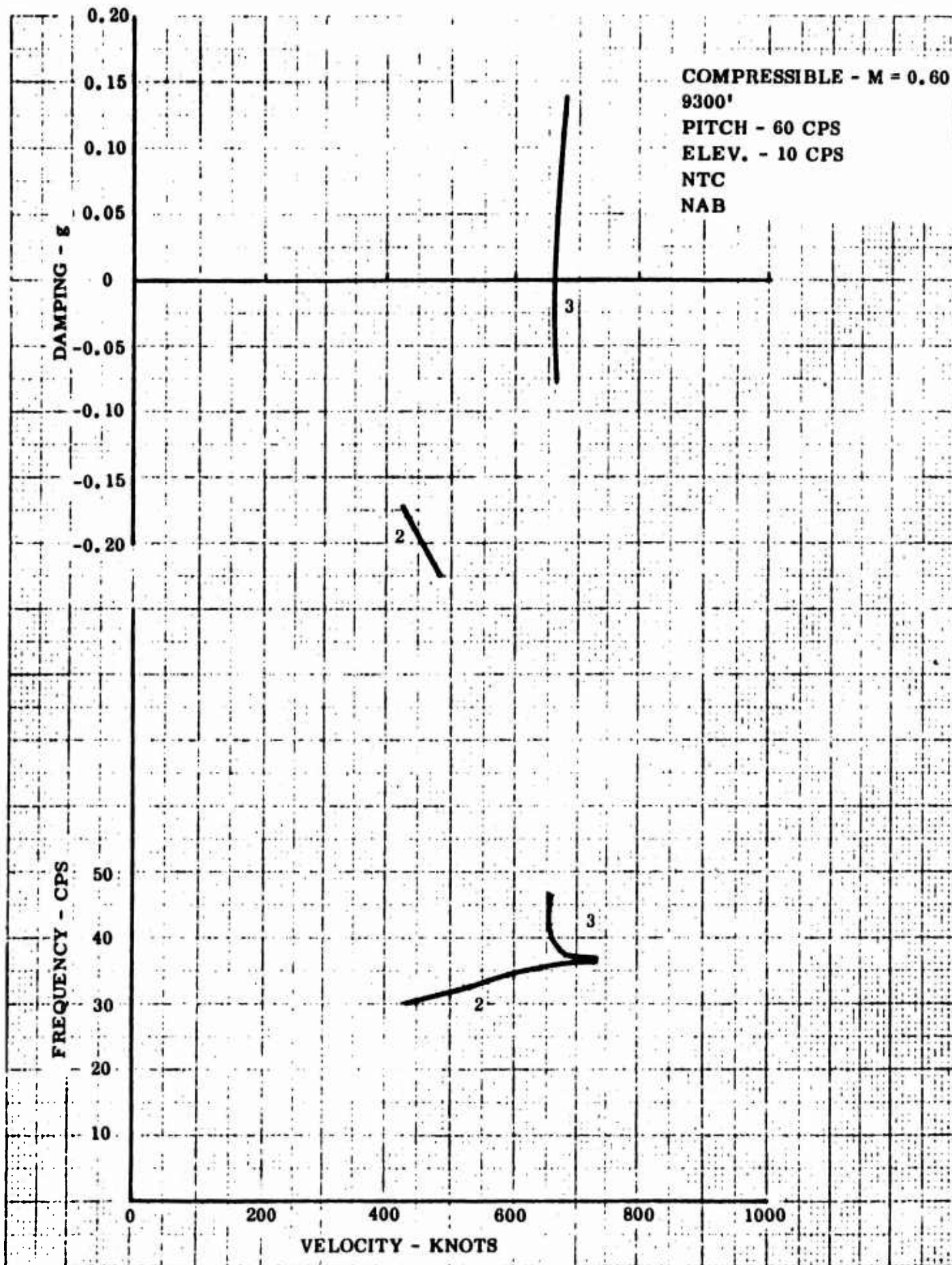


Figure 49 Symmetric Analysis - Cantilevered Condition

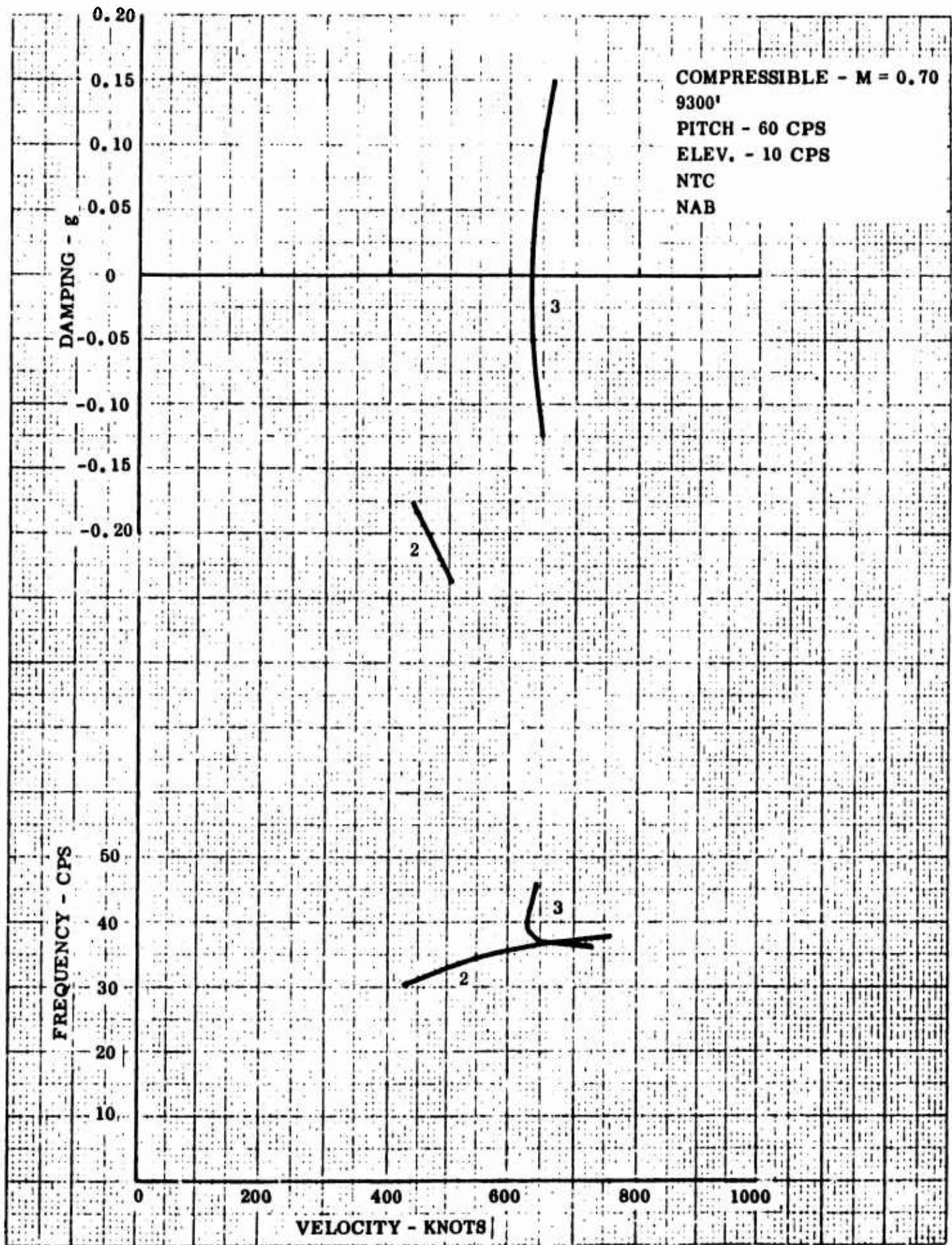


Figure 50 Symmetric Analysis - Cantilevered Condition

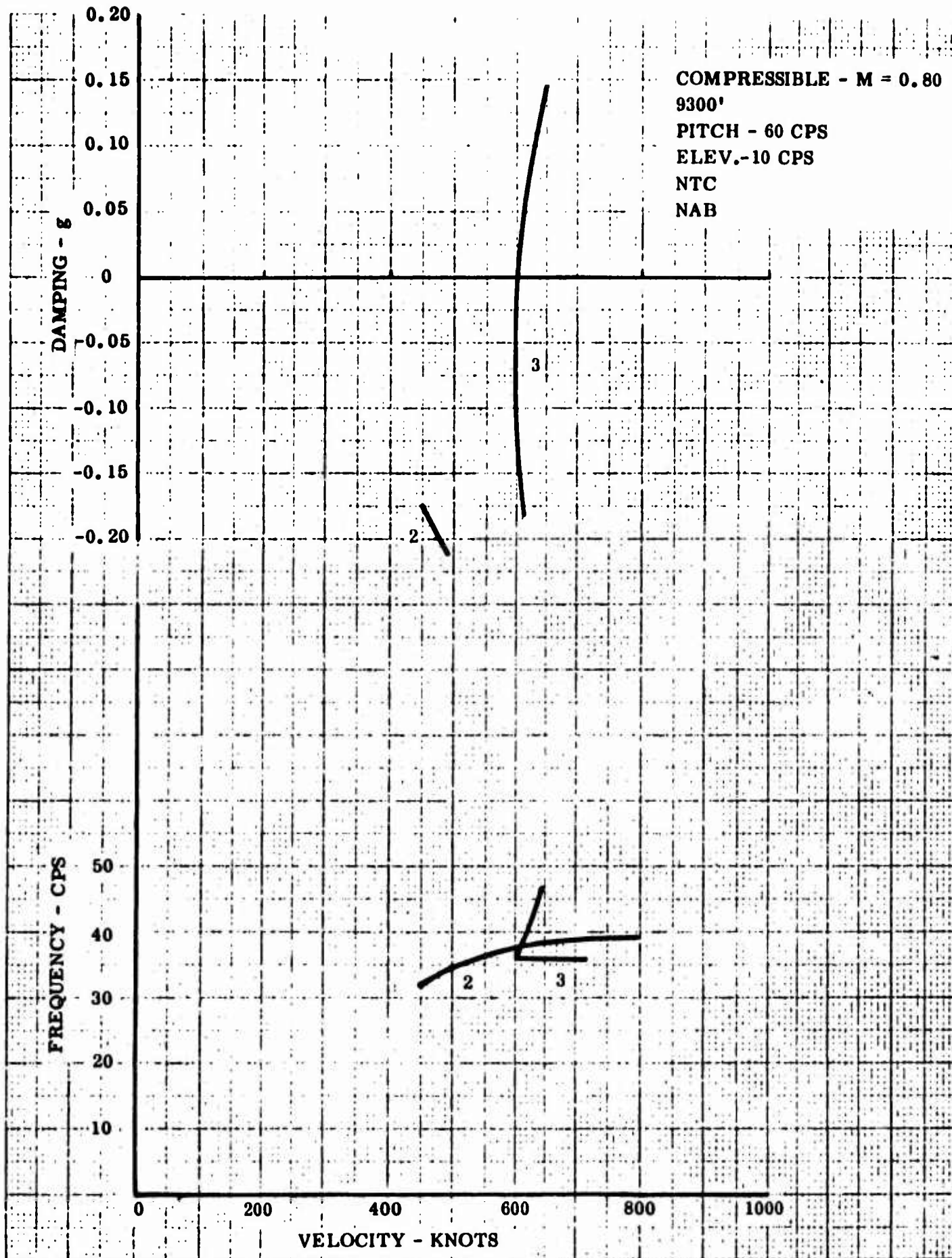


Figure 51 Symmetric Analysis - Cantilevered Condition

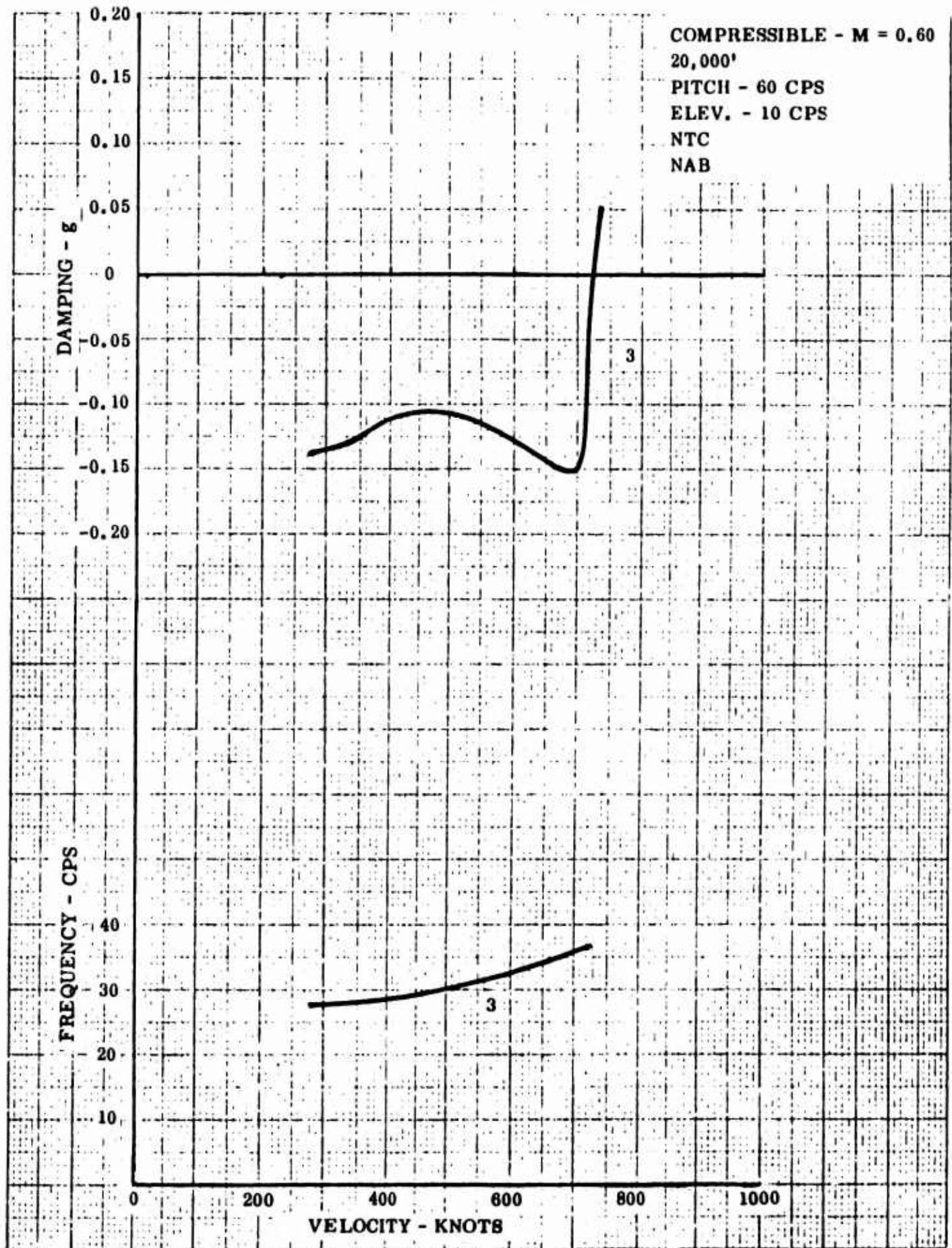


Figure 52 Symmetric Analysis - Cantilevered Condition

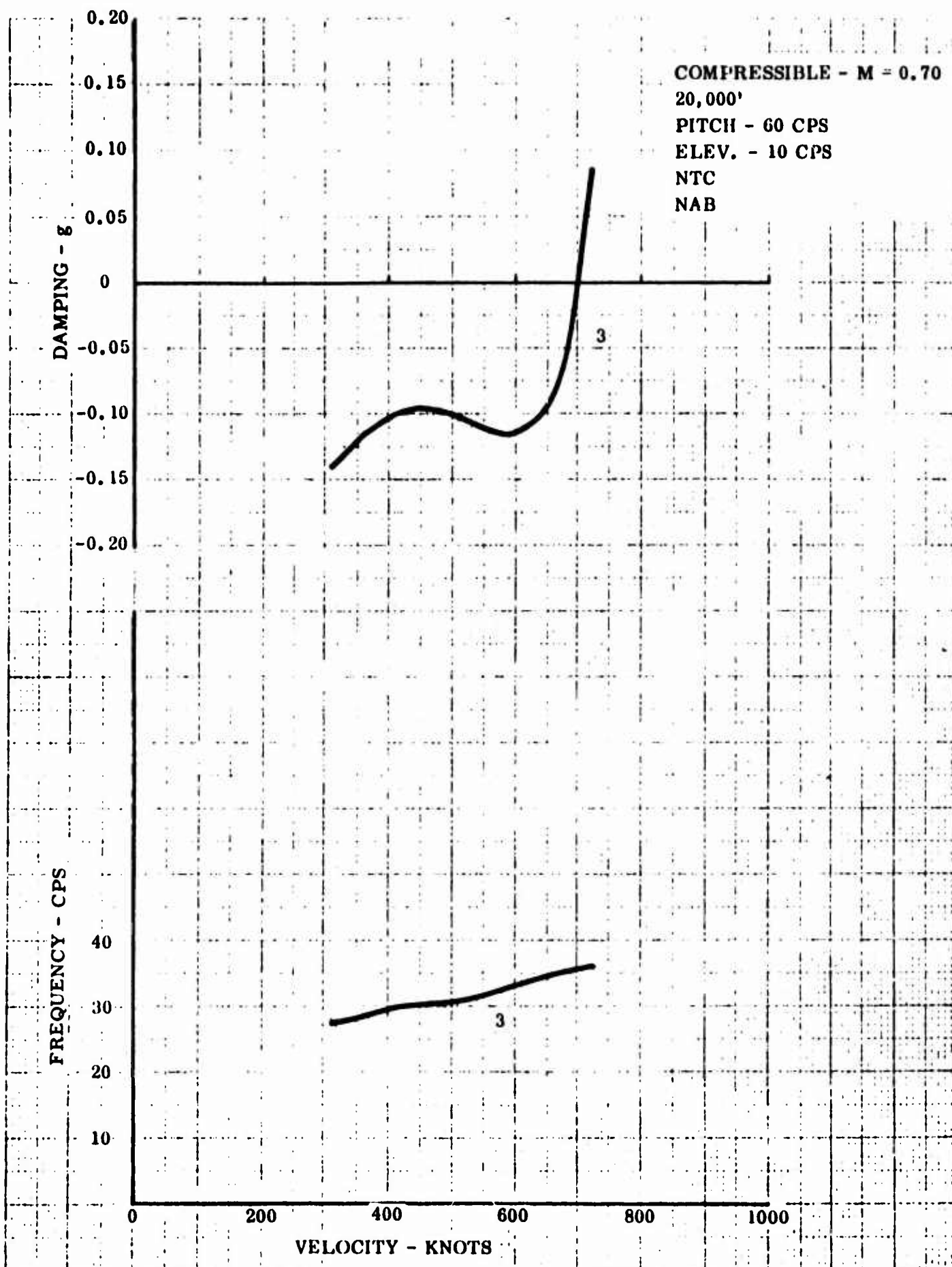


Figure 53 Symmetric Analysis - Cantilevered Condition

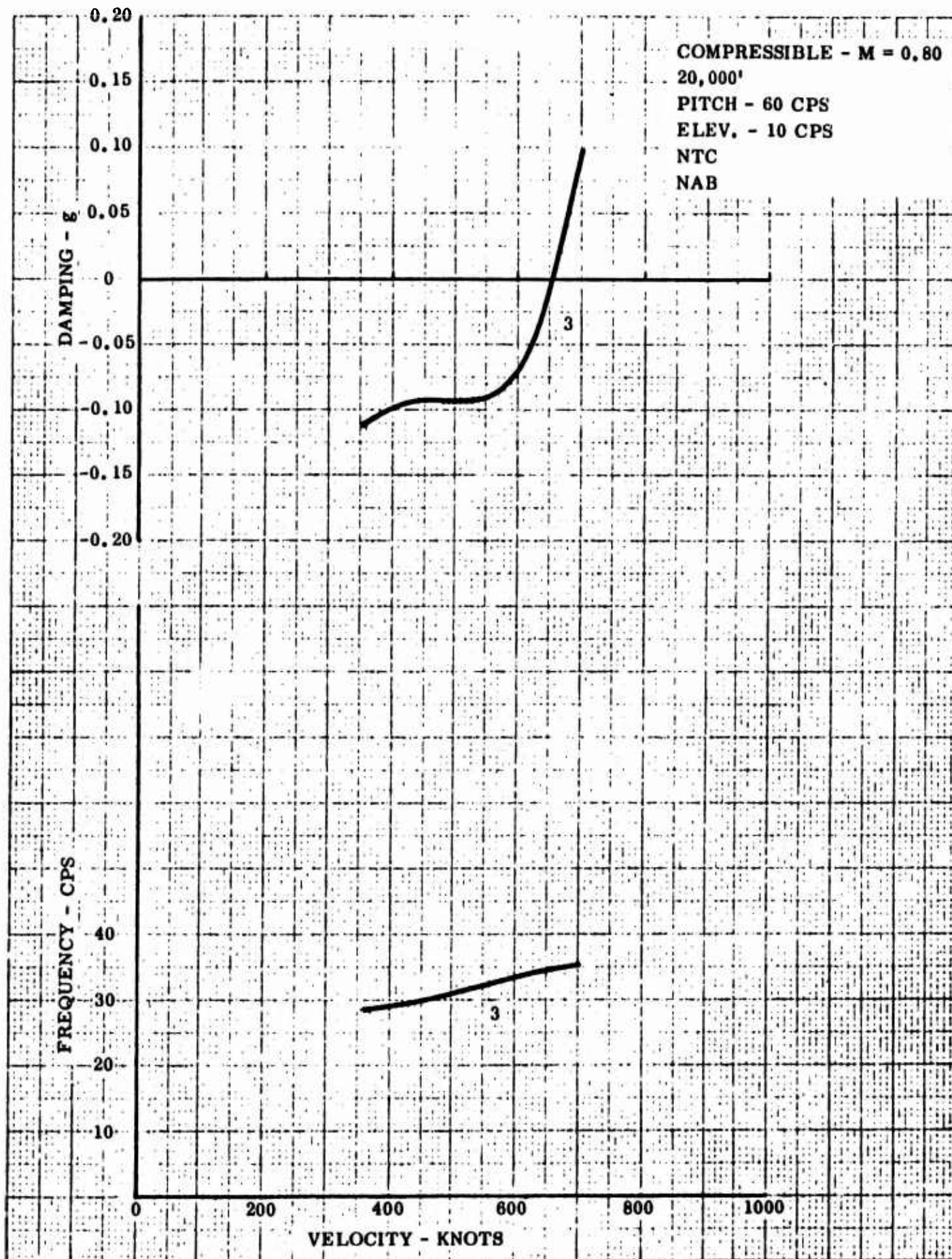


Figure 54 Symmetric Analysis - Cantilevered Condition

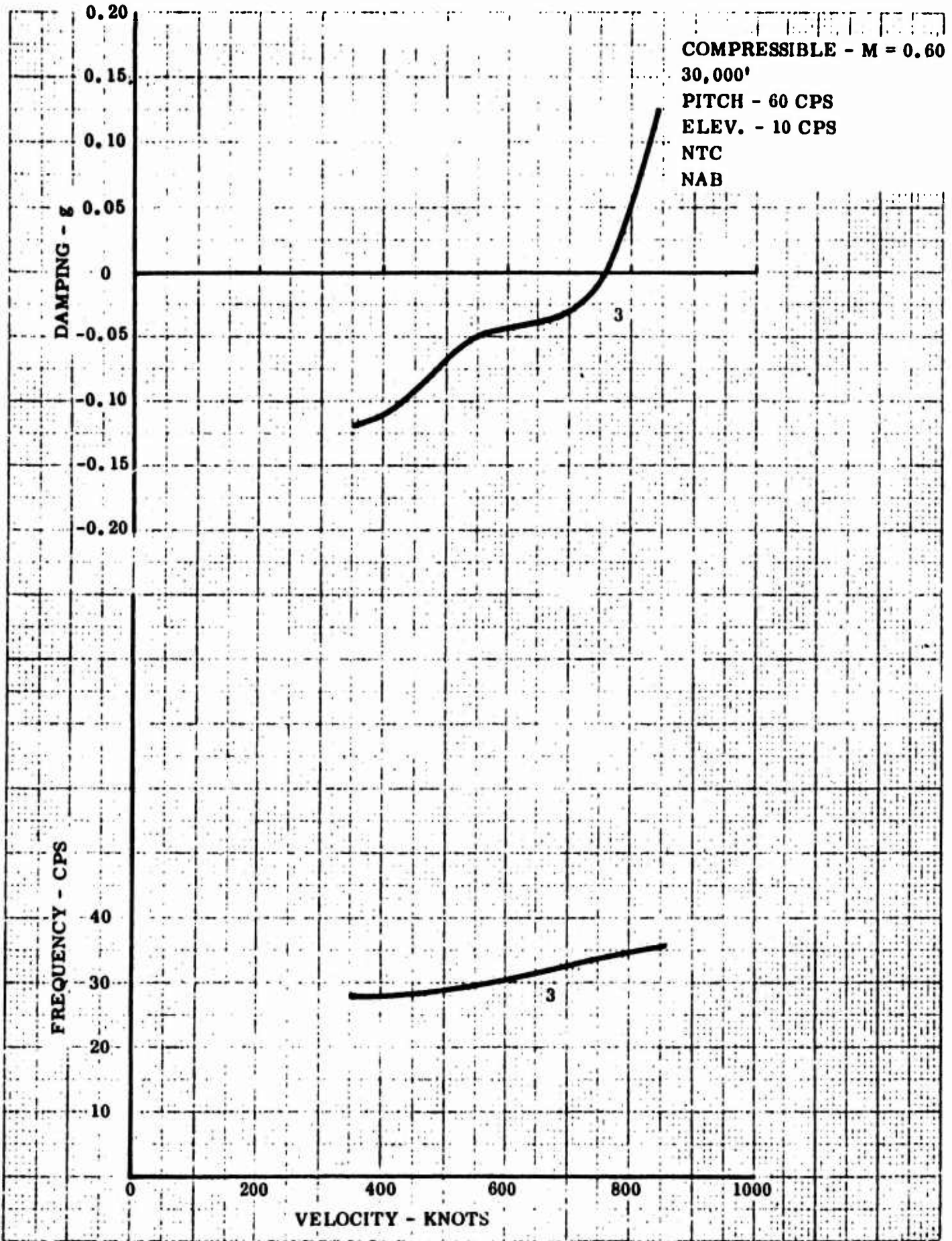


Figure 55 Symmetric Analysis - Cantilevered Condition

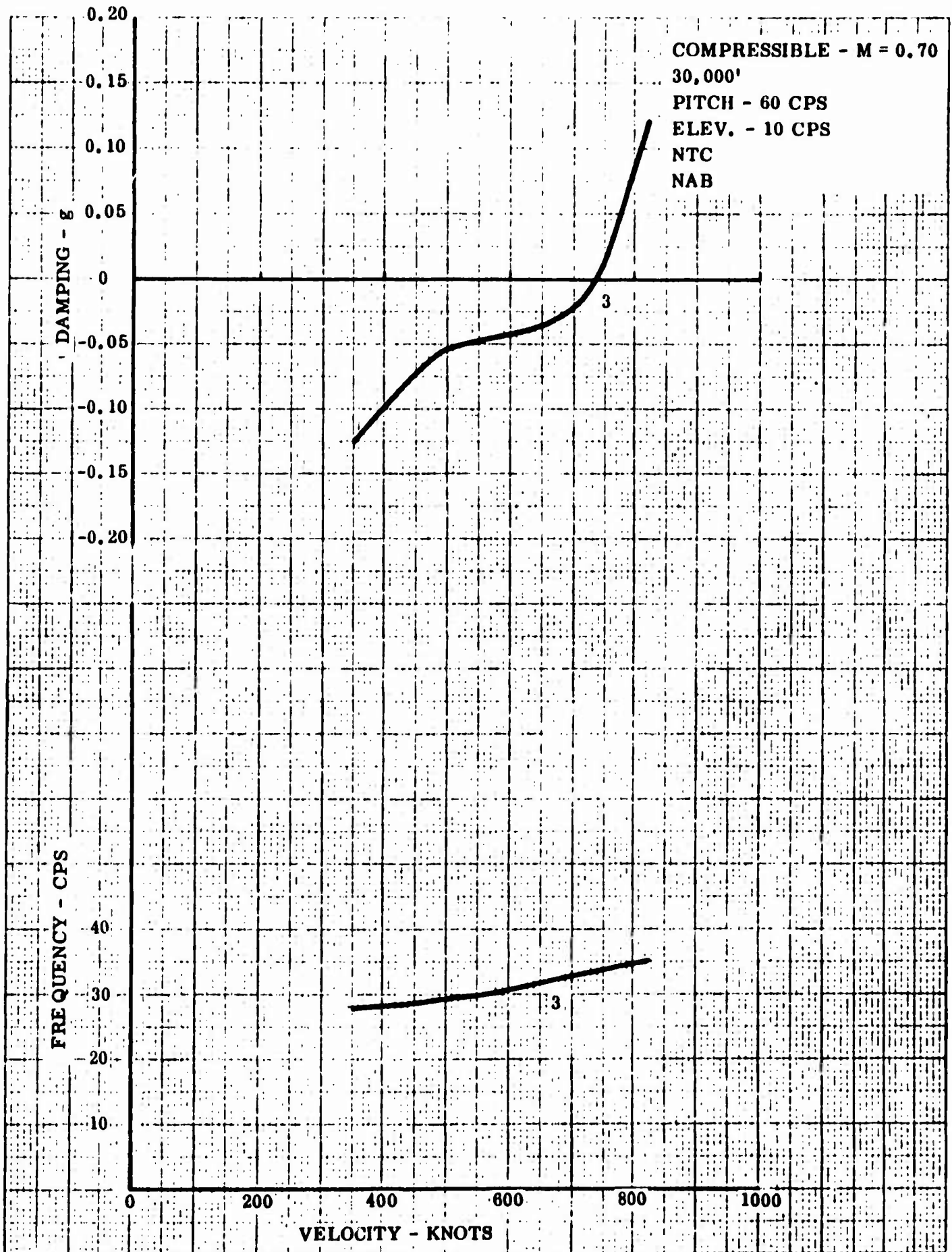


Figure 56 Symmetric Analysis - Cantilevered Condition

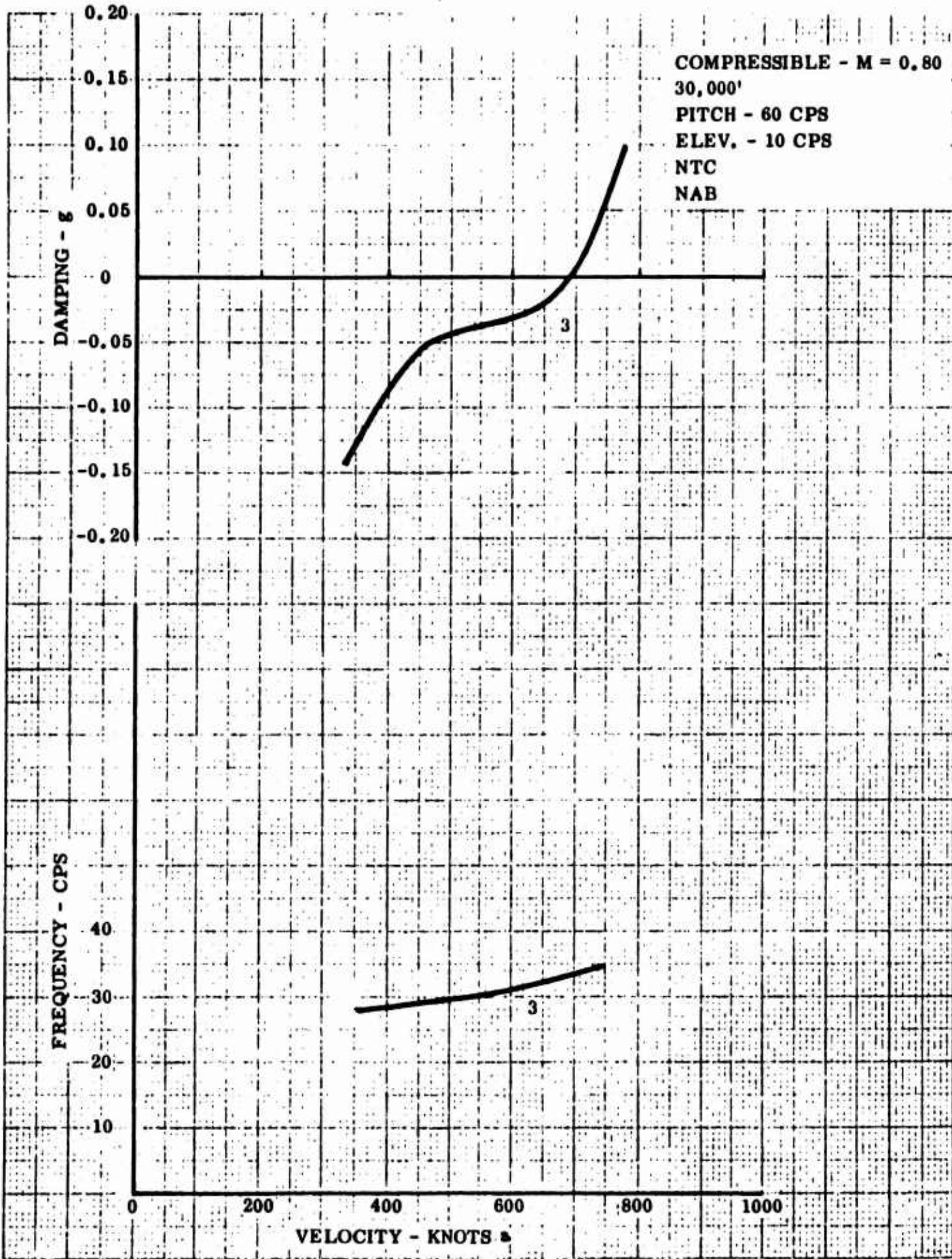


Figure 57 Symmetric Analysis - Cantilevered Condition

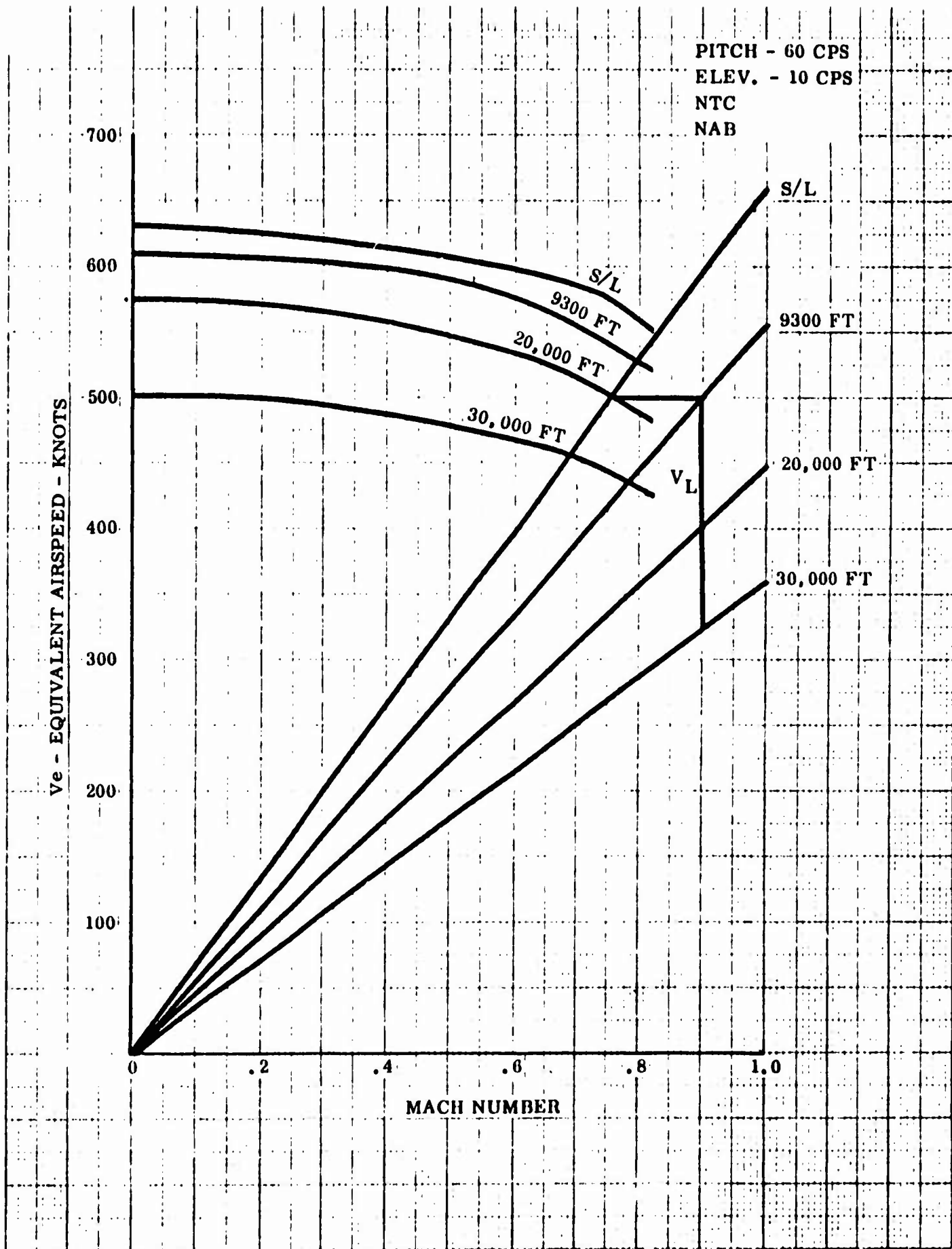


Figure 58 Symmetric Analysis - Cantilevered Condition - Mach Number Effects

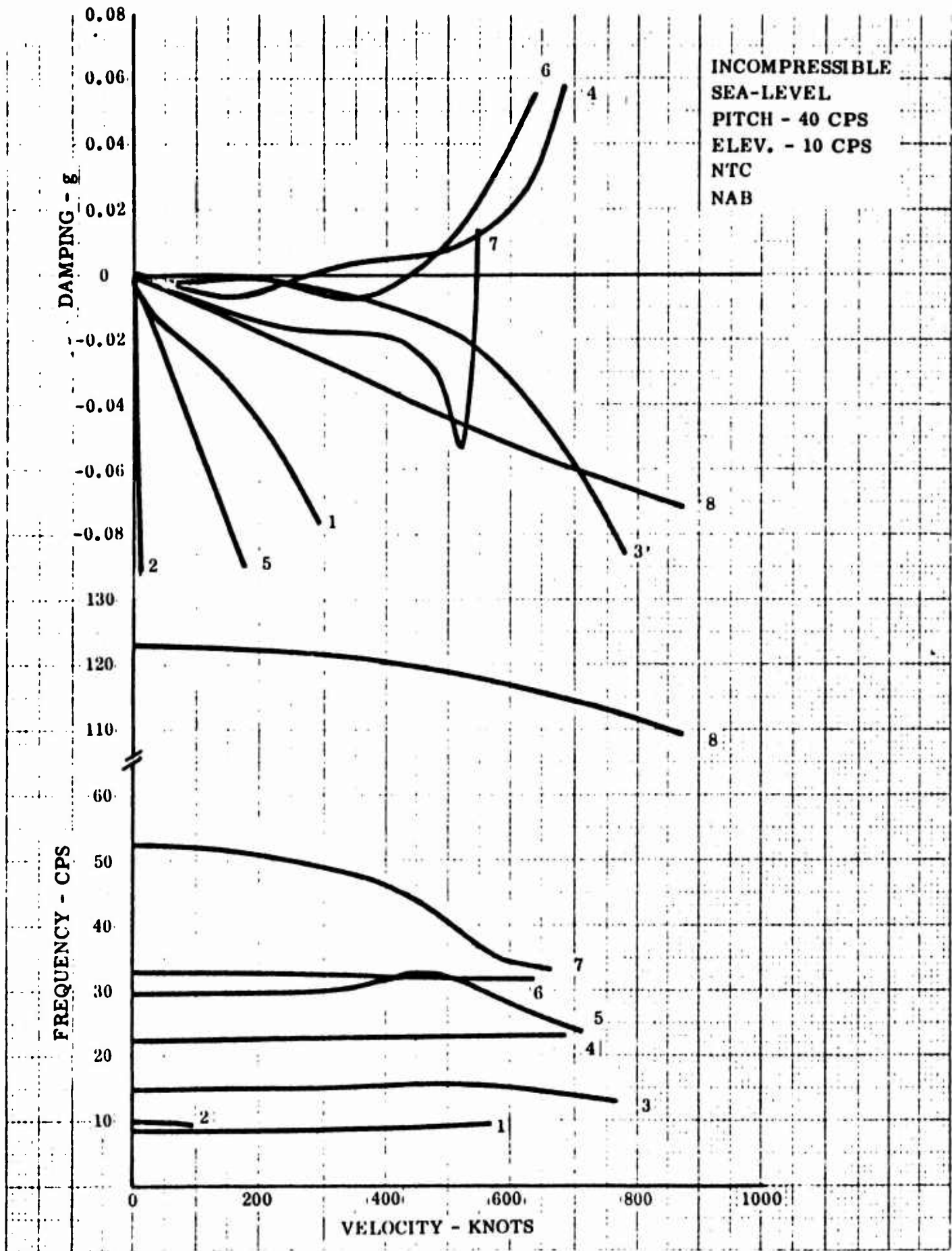


Figure 59 Symmetric Analysis - Free-Free Condition

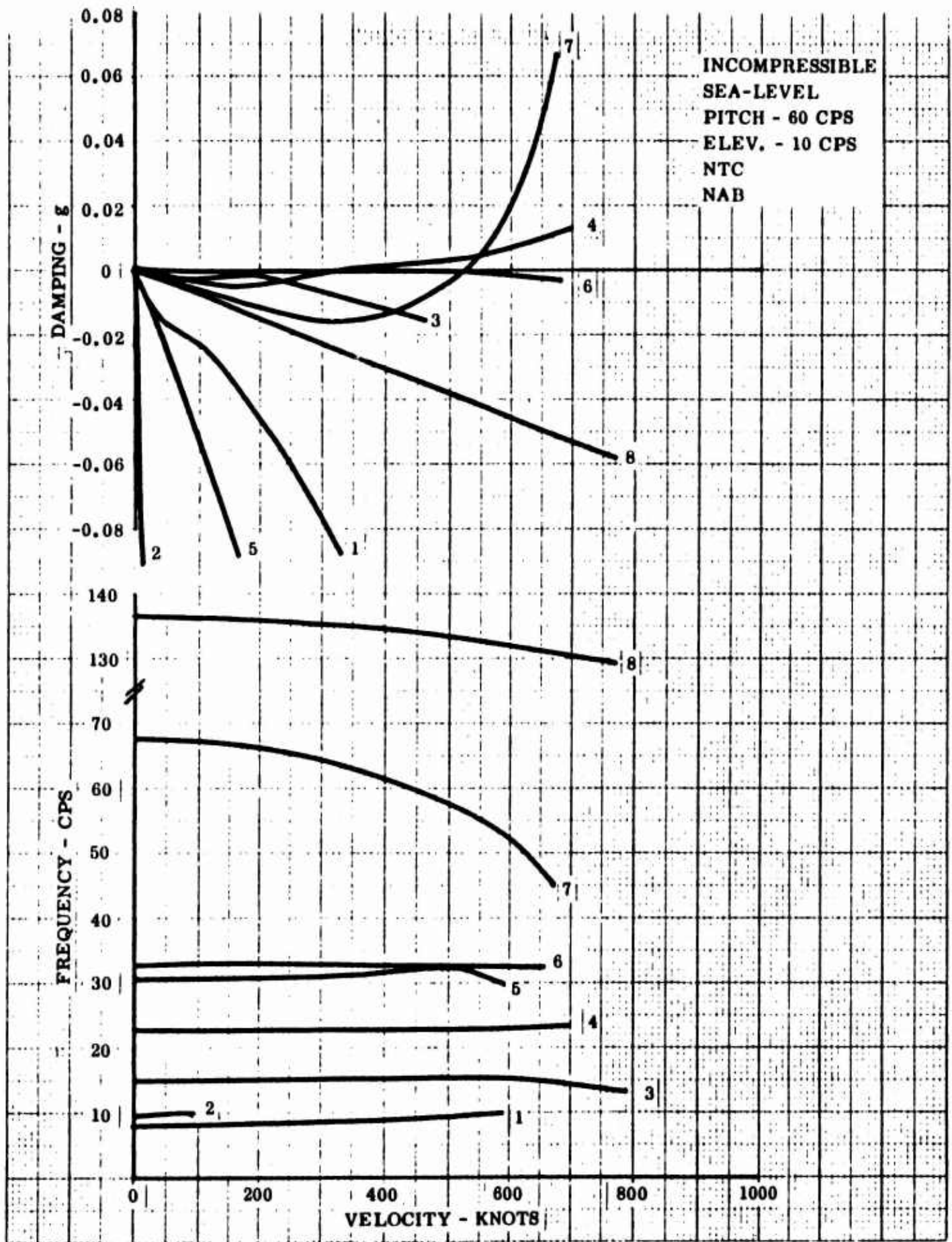


Figure 60 Symmetric Analysis - Free-Free Condition

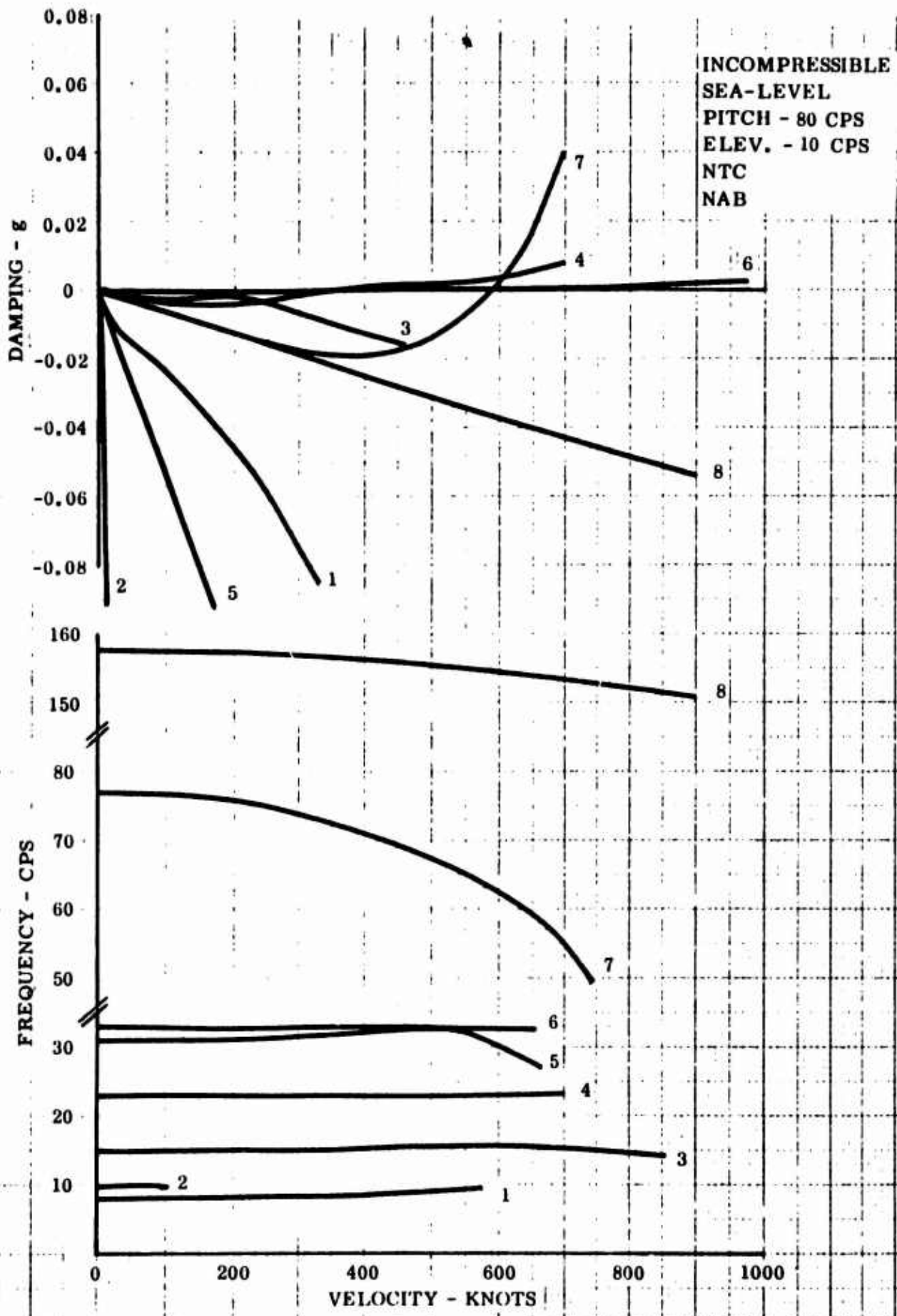


Figure 61 Symmetric Analysis - Free-Free Condition

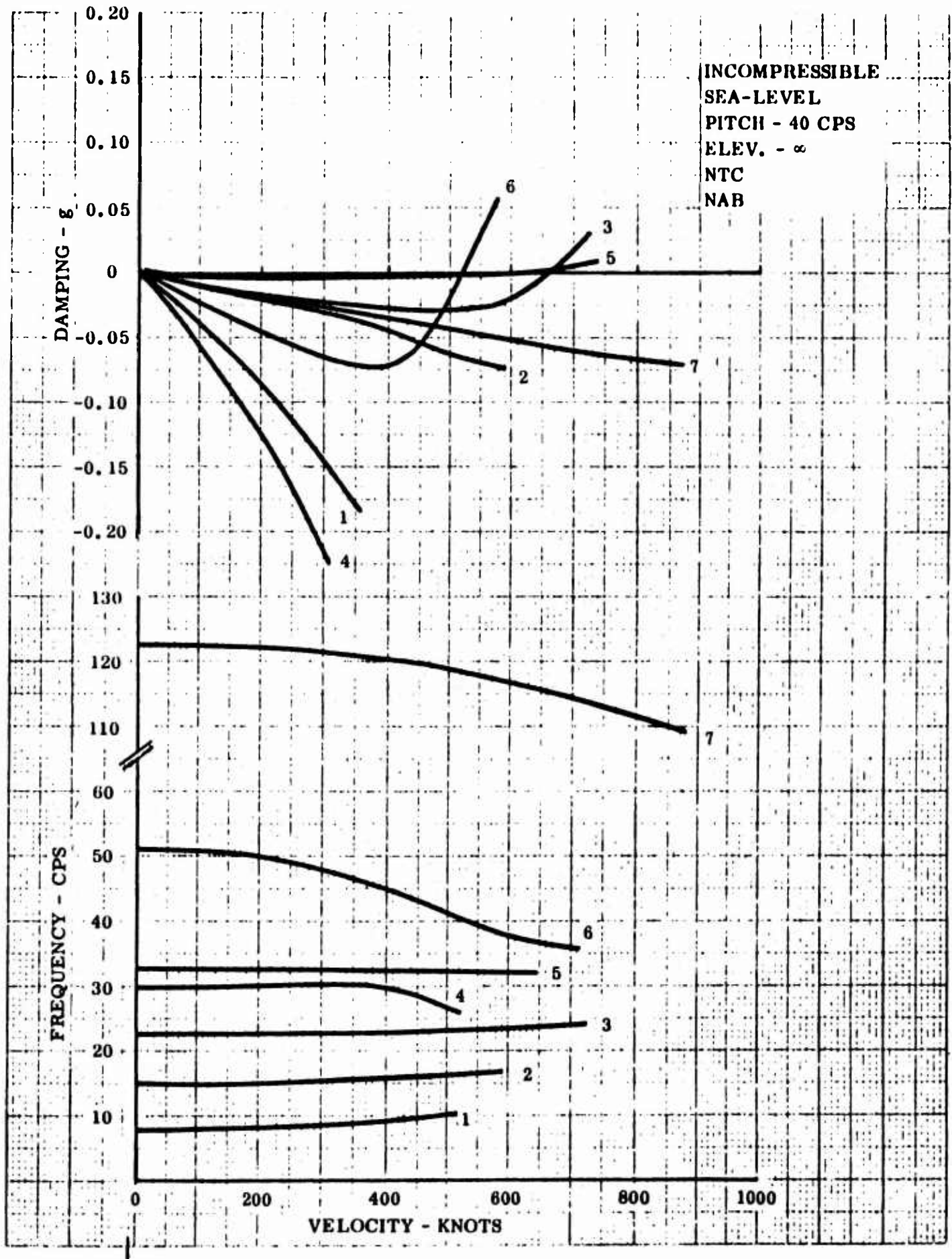


Figure 62 Symmetric Analysis - Free-Free Condition

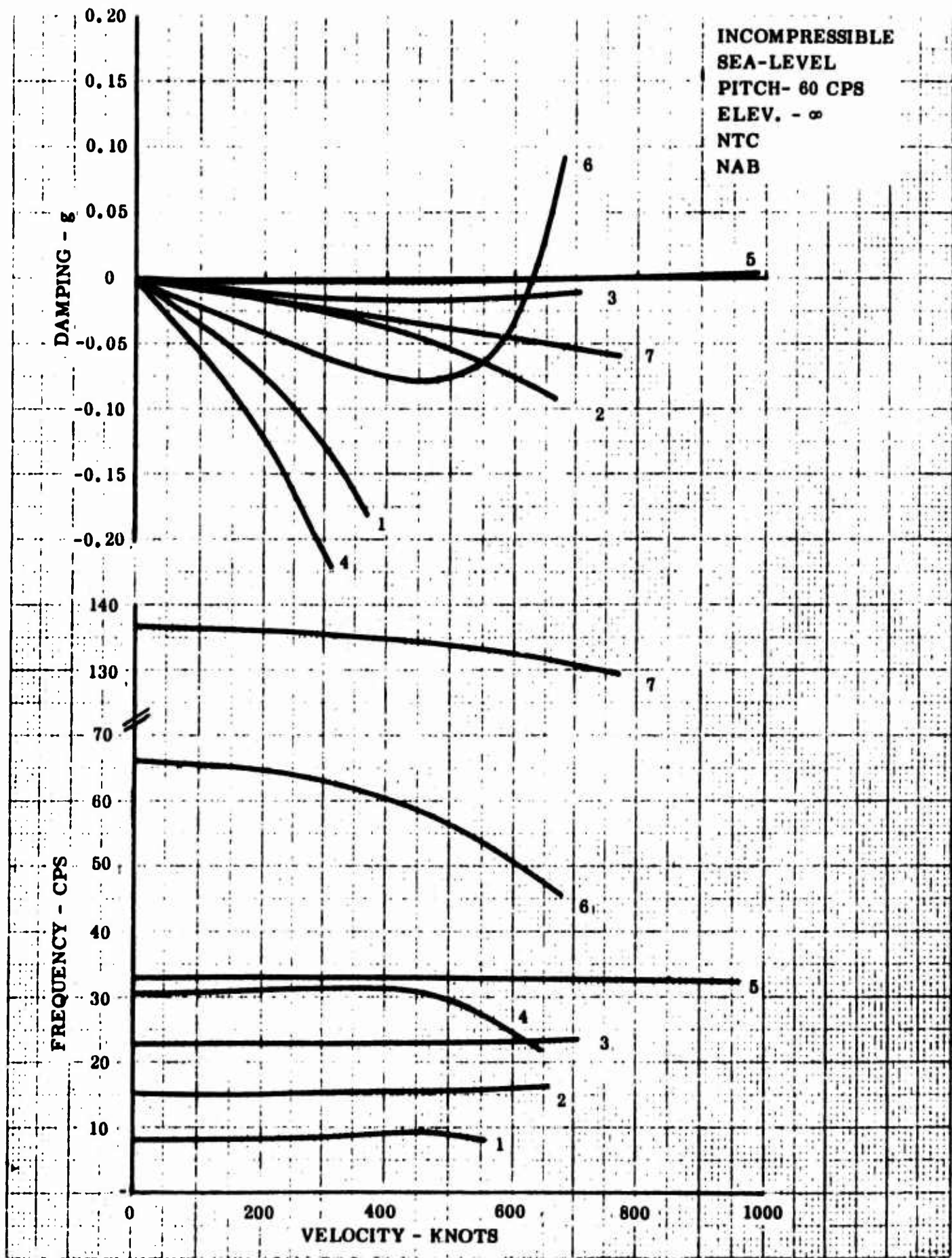


Figure 63 Symmetric Analysis - Free-Free Condition

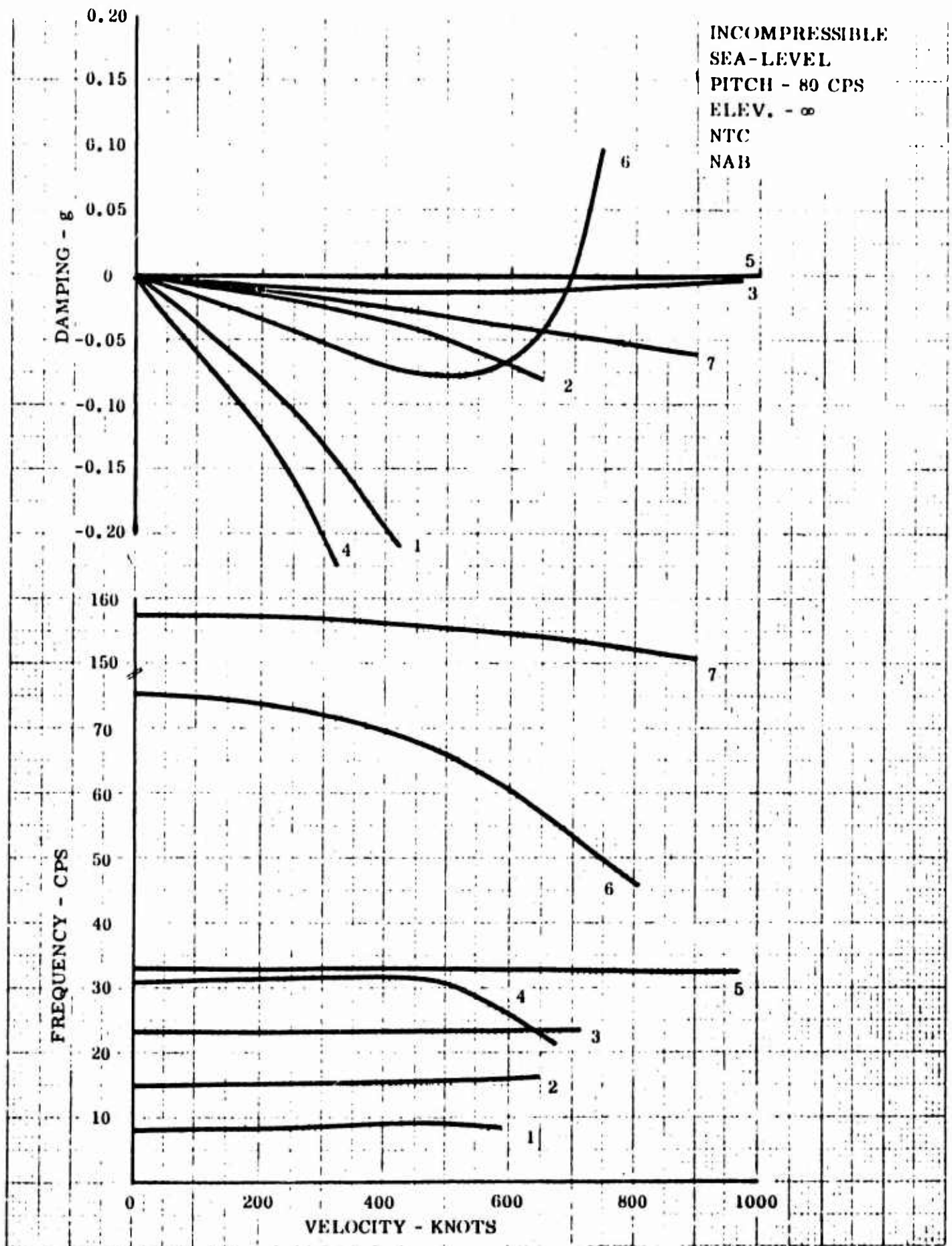


Figure 64 Symmetric Analysis - Free-Free Condition

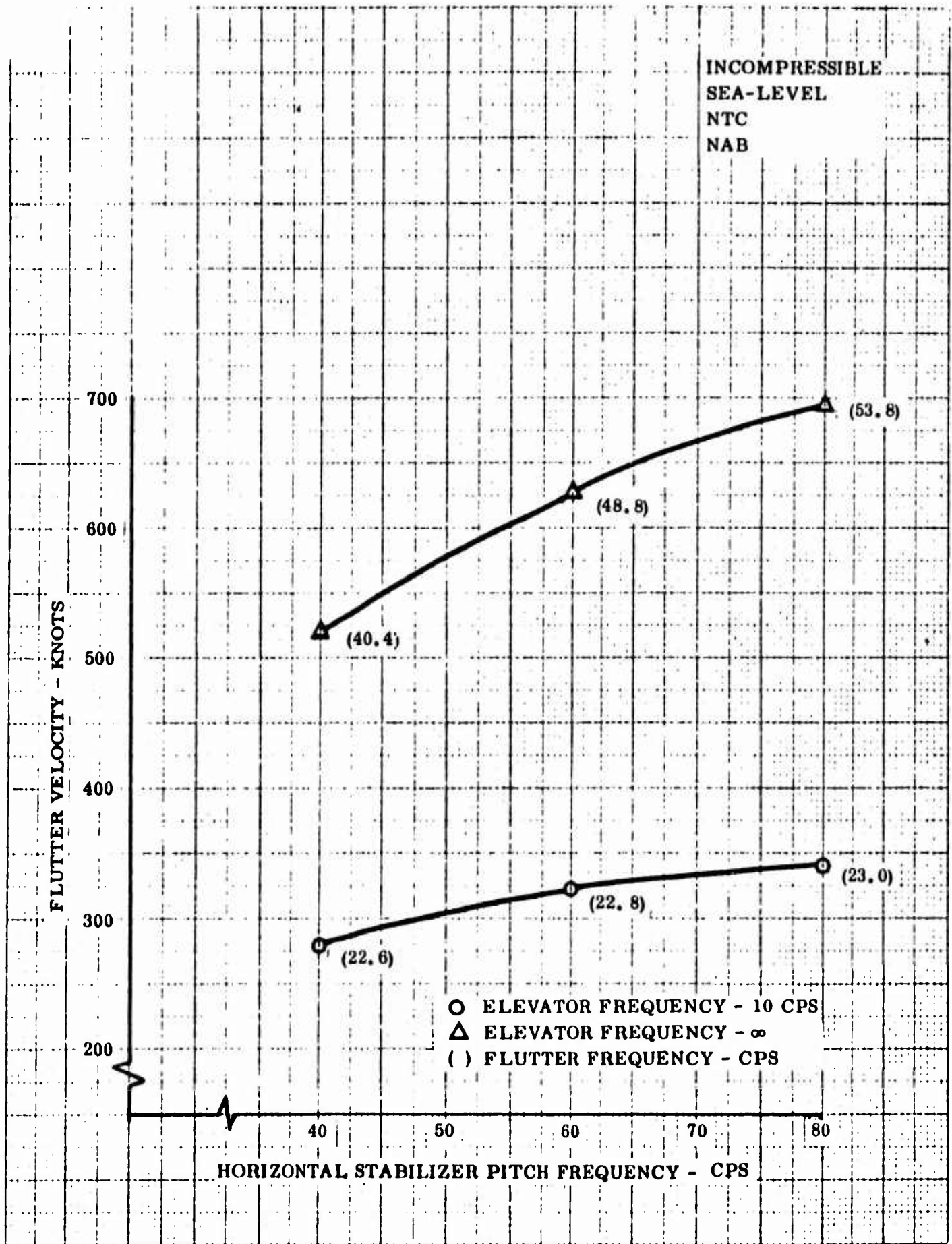


Figure 65 Symmetric Analysis - Free-Free Condition - Parameter Effects

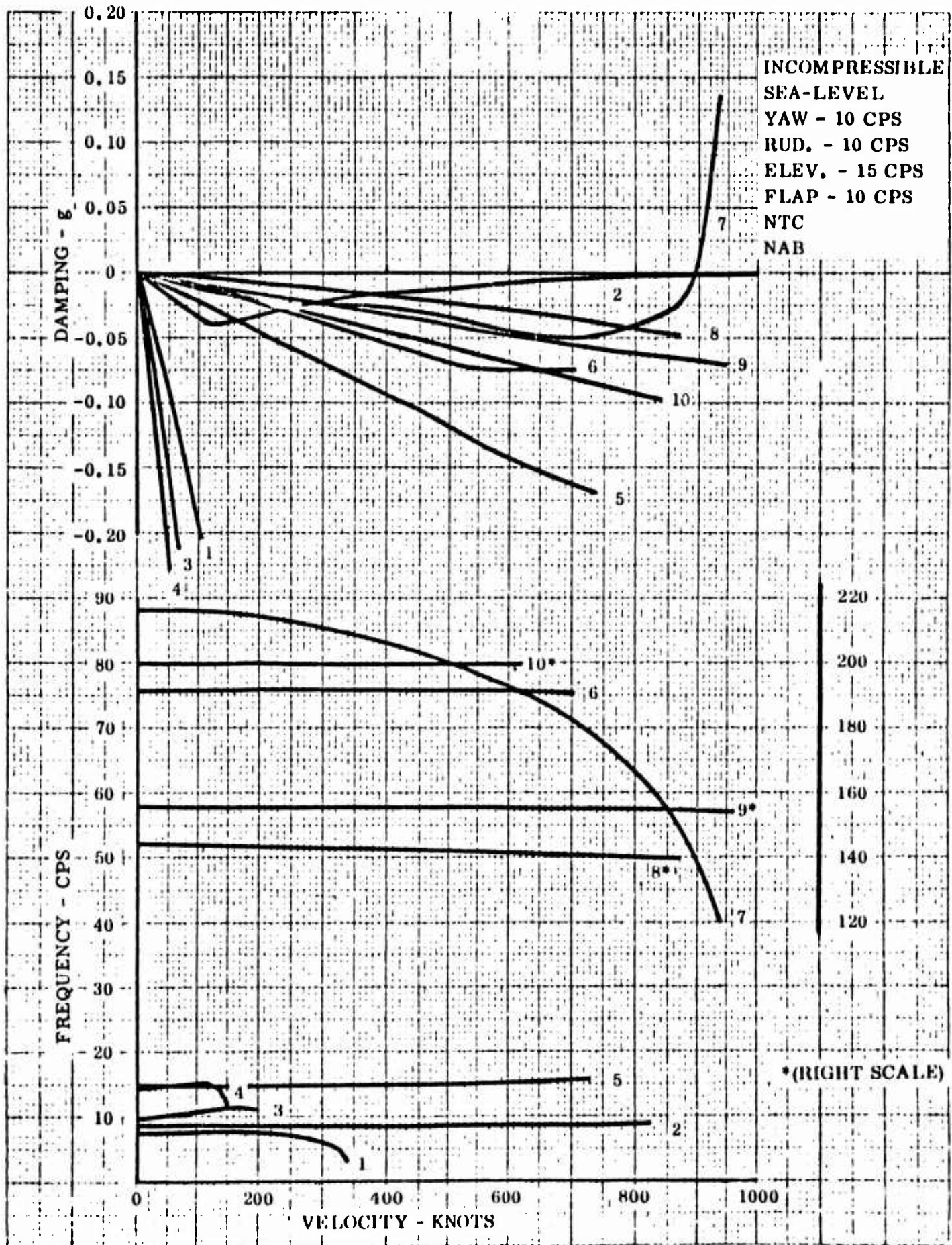


Figure 66 Antisymmetric Analysis - Cantilevered Condition

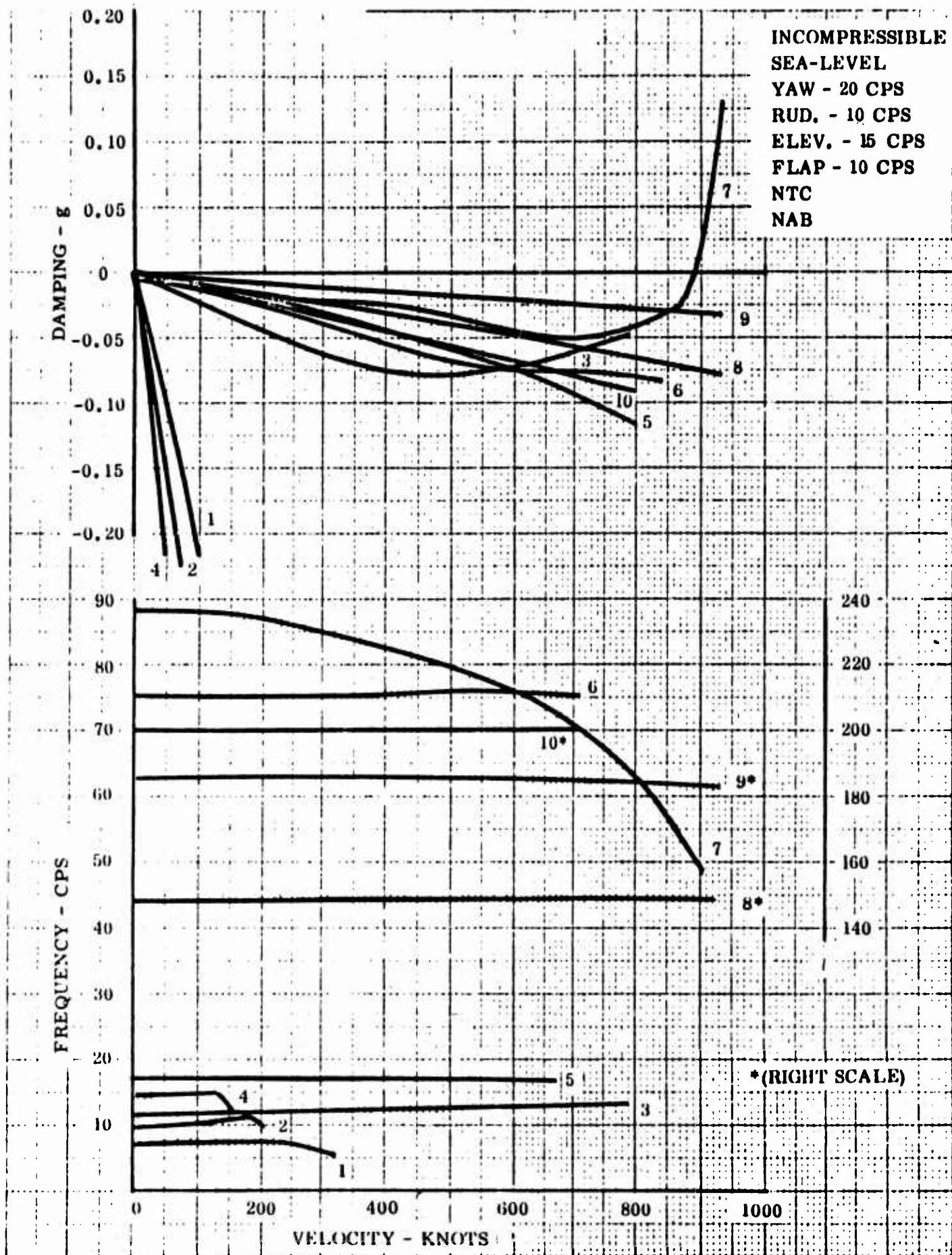


Figure 67 Antisymmetric Analysis - Cantilevered Condition

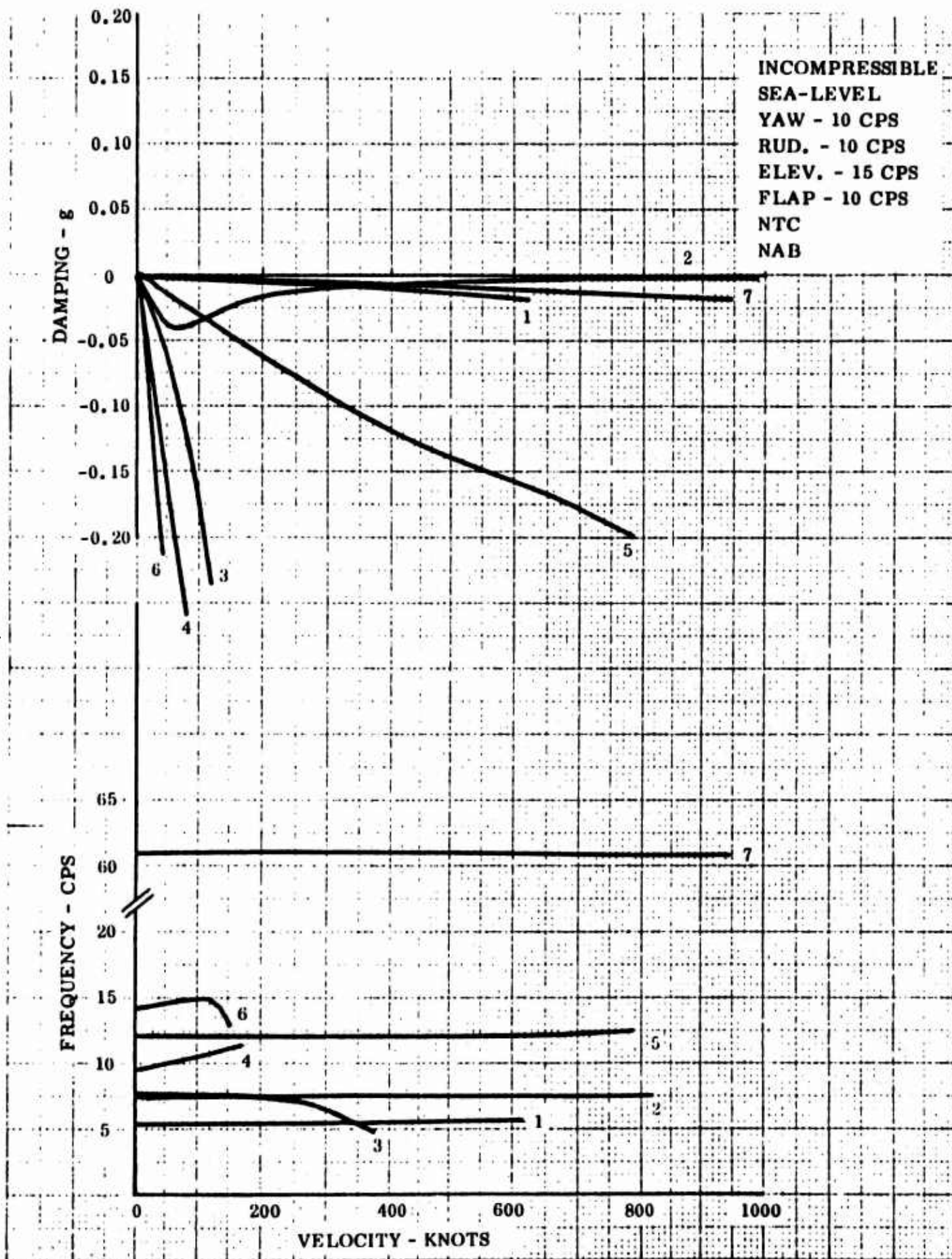


Figure 68 Antisymmetric Analysis - Free-Free Condition

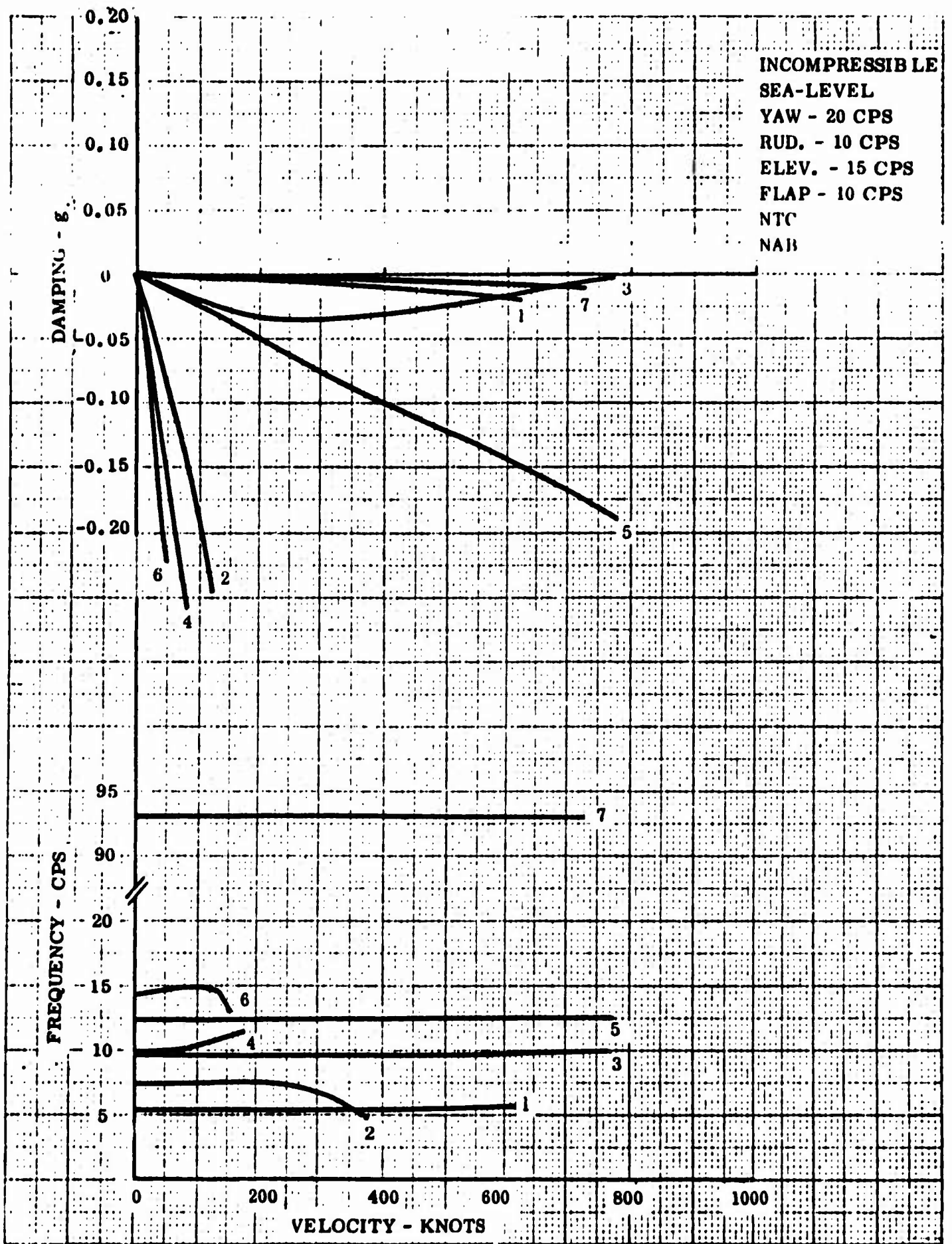


Figure 69 Antisymmetric Analysis - Free-Free Condition